Electrokinetic Removal of Sodium Dodecyl Sulfate from Proteins for Mass Spectrometry Analysis

by

Philip Jaroslav Jakubec

Submitted in partial fulfilment of the requirements
for the degree of Master of Science

at

Dalhousie University
Halifax, Nova Scotia
December 2021

Table of Contents

List of Tables

List of Figures

Abstract

Transmembrane electrophoresis (TME) is an electrokinetic method designed to remove sodium dodecyl sulfate (SDS) from protein samples prior to mass spectrometry analysis. Proteins in solution are stored behind dialysis membranes while the electromotive force of an applied electric field drives the charged surfactant off the proteins and across the membrane. For optimal MS analysis, SDS must be depleted below 10 ppm. Assuming 5000 ppm SDS in the original sample, this implies greater 99.8% detergent removal. An actively cooled TME (AC-TME) system is presented that employs water-circulating tubes to mitigate Joule heat build up and to maximize the rate of SDS depletion. The AC-TME device was operated in constant current mode (40-400 mA), while monitoring the applied voltage, system temperature, pH, and measuring the residual SDS in the sample and final protein recovery. The soluble supernatant of the SDS-depleted samples is easily recovered while an *in-situ* TME digestion protocol was developed to ensure recovery of hydrophobic proteins in a format amenable to MS analysis. LC-MS/MS of the resulting fractions was performed, with comparative analysis of the soluble and TME-retained proteins to identify trends in the numbers and types of proteins recovered in each of the obtained fractions. Compared to the conventional-TME system AC-TME provides superior protein recovery and a higher rate of SDS depletion. These favorable results are explained by the capacity to operate AC-TME at significantly higher voltages while maintaining a temperature that maximizes protein retention in the solution phase. To further remove the potential for protein loss through TME purification, an in-situ TME trypsin digestion protocol was also developed and demonstrated here. Thermally aggregated proteins are therefore retrieved and amenable to an optimized bottom-up MS workflow to identify purified proteins. LC-MS/MS characterized a significant number of proteins ranging in size, hydrophobicity, abundance across the soluble, supernatant, and residual protein pellet *in-situ* TME fractions. SDS was depleted below 10 ppm in under 10 minutes in a fully automated platform. The improved protein purification device and protocol presented removes one of the major bottlenecks in proteome analysis, enabling the use of SDS-based workflows in a robust and high throughput format, for proteomic LC-MS analysis.

List of Abbreviations

ABC	Ammonium bicarbonate
AC	Active cooling
ACN	Acetonitrile
AC-TME	Active-cooled transmembrane electrophoresis
ALS	Acid labile surfactant
ANOVA	Analysis of variance
BCA	Bicinchoninic acid
BSA	Bovine serum albumin
BUP	Bottom-up proteomics
CAD	Computer aid design
CMC	Critical micelle concentration
CSD	Charge state distribution
DS^-	Dodecyl sulfate anion
DTT	Dithiothreitol
EOF	Electroosmotic flow
ESI	Electrospray ionization
GELFrEE	Gel-eluted liquid fraction entrapment electrophoresis
GRAVY	Grand average of hydropathy
HPLC	High performance liquid chromatography
IAA	Iodoacetamide
ID	Inner diameter
kDa	kilodalton
LC	Liquid chromatography
LC-MS	Liquid chromatography mass spectrometry

LC-MS/MS	Liquid chromatography-tandem mass spectrometry
LC-UV	Liquid chromatography-ultraviolet absorbance
LTQ	Linear trap quadrupole
m/z	Mass-to-charge ratio
MaSDeS	MS-compatible degradable surfactant
MALDI	Matrix-assisted laser desorption/ionization
MBAS	Methylene blue active substances
mRNA	Messenger ribonucleic acid
MS	Mass spectrometry
MWCO	Molecular weight cut-off
OD	Outer diameter
PAGE	Polyacrylamide gel electrophoresis
pI	Isoelectric point
PTM	Post translational modification
QqQ	Triple quadrupole
SDS	Sodium dodecyl sulfate
TCA	Trichloroacetic acid
TDP	Top-down proteomics
TFA	Trifluoroacetic acid
TG	Tris glycine
TT	Tris Tricine
YPD	Yeast peptone dextrose

Acknowledgements

Thank you to my parents Dana and Jarek Jakubec and my sister Tessie Jakubec whose unconditional care allowed me to complete this graduate program along with the requisite bachelor's degree. Furthermore, their motivation and perseverance have been sources of inspiration.

I want to acknowledge that I completed this program with the encouragement and support from a community of fantastic human beings. Thank you to the following people, organizations, and places for the opportunities to learn via experiences and to have enriched my life. I strive to pass these lessons on with the joy I experienced them.

Thank you to my supervisor Dr. Alan A. Doucette for his mentoring and the opportunities to be challenged and to grow as a professional and scientist.

To my lab colleagues and peers from Dalhousie University: Jessica Nickerson, Venus Baghalabadi, Subin R.C.K. Rajendran, Hammam Said, Ziheng Dang, Nicole Unterlander, Kirsten Jones, Mallory Davis, and Dr. Justin Tom, I thank you for your comradery and for being inspiring scientists and innovators.

I wish to acknowledge my supervisory committee Dr. Heather Andreas and Dr. Michael Freund for your critical feedback of the research presented and to Graduate coordinator Dr. Peng Zhang for overseeing my program. Thank you graduate studies administrative assistant Lea Gawne for your aid in navigating me through the administrative requirements of the program.

I wish to further acknowledge and thank the faculty and staff at Dalhousie University's Chemistry Department for their aid and support during my conducting this research. Dr. Roderick Chisholm and Dr. Peter Wentzell provided consultation on research and stepped in for administrative duties. I thank machinist Mike Boutilier, and glass blower Todd Carter who contributed to manufacturing the AC-TME components. I also thank mass spectrometry technologist Xiao Feng, for providing instruction on the operation and analysis with mass spectrometry, as well as Dr. Alejandro Cohen from the Biological Mass Spectrometry Core Facility at the Life Sciences Research Institute for performing LC-MS/MS measurements.

My time at Dalhousie University changed my life for the better and I thank the people and places in Nova Scotia for doing so.

When the light shines the dimmest, and the darkness is all consuming, hold to that this too shall pass.

Chapter 1 Introduction

Proteomics is the large-scale analysis of proteins expressed by a specific biological system with a defined set of conditions.[1] The goals of proteomics extend to an understanding of the complex mixture of proteins in a proteome, including their functions, levels of expression, interactions, modifications, and their effects.[2,3] Mass spectrometry is currently the most frequently used platform for proteome characterization, being capable of sensitive, high throughput analysis. However, mass spectrometry (MS) is but one component in a complex analytical workflow employed for proteome analysis. Equally vital to the process are methods for protein isolation, purification, and separation ahead of MS.[4,5] These front-end sample preparation steps therefore dictate the success of an MS analysis. Considering the requirements of front-end protein manipulation ahead of MS, detergents such as sodium dodecyl sulfate (SDS) have played an integral part in multiple aspects of the proteomic experiments, including their extraction, enrichment, solubilization and mass-based separation. Unfortunately, detergents are rarely amenable to MS analysis. For this reason, detergent-depletion techniques are critical to facilitate the analysis of proteins in MS workflows. The optimization of a rapid and effective detergent depletion strategy is the topic of the current thesis.

1.1 Proteomics

The term ‘proteome’ was coined in the mid 1990’s by Marc Wilkins as a shorthand notation of, “*the PROTEin complement expressed by a genOME.”*[6] The proteome describes the total set of protein isoforms and modifications expressed by a genome, cell, tissue, organism, or system of interest.[6] These molecules are not only responsible for initiating a

large proportion of the chemical activity within cells, but also serve key structural roles. The field of proteomics arose to complement genomics and transcriptomics; while a gene is considered constant and even messenger RNA (mRNA) cannot disclose the differing functions of a given protein depending on post-translational processing, the proteome is a far more dynamic system.[7–14] The identification of specific post-translational modifications (PTMs) which can chemically alter the functional activity of a protein is a prominent goal of proteomics analysis, as PTMs are often implicated in disease and thus bear significant value to the pharmaceutical industry for drug target discovery,[15–19] characterising biomarkers,[20–24] elucidating biological mechanisms,[25,26] and finding new treatments for diseases such as cancer.[17,27–30]

The term 'proteoform' is used to describe any chemically distinct form of a protein, resulting from amino acid sequence manipulations or modifications.[31] During transcription, eukaryotic organisms can produce mRNA containing a rearranged sequence of codons *via* intron excision and exon splicing. Additionally, proteins amino acid sequences can be altered with a multitude of distinct chemical moieties including methylation, acetylation, phosphorylation, glycosylation along with over 200 other processes,[32] the net effect being a potential change in the physicochemical properties of the protein. Protein functions and interactions can be altered by PTMs and regulate cellular activity by changing the conformation, charge states, steric properties, and solubilities of protein molecules.[10,30,33,34] The complexity of the proteome relative to the genome is even greater when considering that PTMs can act in tandem to tailor the activity of a specific protein. For example, it has been shown that gene regulation is highly influenced by specific PTMs expressed on histones, which are an integral component of nucleosomes for

DNA packaging.[35] While gene-level analysis has already revolutionized our understanding of biological systems, proteomics has even greater potential to examine the dynamic nature of living systems.

Though proteome characterization can provide valuable information, it is considered a far more challenging analytical system than its genome counterpart. One of the surprising findings of the Human Genome Project was that the human proteome contains 'only' approximately 22,000 directly coded proteins. However, owing to PTMs, alternate splicing events, and allelic variations, the resulting proteome is estimated to be anywhere from 100,000 to over 1 million distinct components.[36,37] Furthermore, proteomic samples display a wide variation in concentration of individual proteins, with upwards of 10 orders of magnitude difference between the least and most abundant components of a plasma sample.[38,39] Naturally, the concentration of each sample component is not static; the proteome of a biological organism responds rapidly to changes in environment, stage of growth, or other factors. The chemical diversity, dynamic range and changing nature of the proteome all demand extremely sensitive, selective, and fast analytical instruments to profile such complex mixtures. Mass spectrometry has therefore revolutionized proteomics as a high-throughput and sensitivity sample analysis platform, noting that it is also reliant on quantitative sample extractions, separations, and purifications to ensure high quality measurements.[40,41]

1.1.1 Mass Spectrometry Workflow for Proteomics Analysis

A MS instrument measures the mass-to-charge ratio (*m/z*) of ionized analytes in the gas phase, providing the potential to not only identify but also quantify the various proteins present in a sample. Multiple types of mass spectrometers exist, tailored to the analysis of

different types of analytes depending on the specific combination of ion source and mass analyzer. The foundation and development of MS traces back to the early 20th century, though modern instruments are far more advanced and implemented in a variety of platforms. The history of MS began in 1912 at the University of Cambridge by Sir Joseph John Thomson, together with his research assistant, Francis William Aston when they constructed and recorded a parabola spectrograph to distinguish unique isotopes of neon. Ions were separated based on their differing parabolic trajectories manipulated by magnets on either side of an evacuated chamber and detected either using a fluorescent screen or photographic plates.[42] MS has expanded tremendously to encompass unique types of mass analyzers which impart separation of ions according to their mass to charge ratio (*m/z*), with considerably higher resolution, sensitivity, mass range and scan speed. These instrument developments permitted the application of MS to numerous compound classes.

An example of a typical MS-based proteomics experiment is outlined below, noting that there are now multiple unique approaches to proteome analysis which may omit one or more of the stages described. Prior to MS analysis of the sample, proteins must first be isolated. Therefore, the first stage of the workflow may involve cellular lysis, disrupting the membranes and solubilizing the proteins (often with the aid of chemical additives).[43] Following this, for what is known as the 'bottom up' approach to MS analysis,[44] proteins are digested, typically with an enzyme such as trypsin, into shorter (peptide) segments which are considered easier to solubilize, separate, and analyze by MS. Given the complexity of the sample, the peptide mixture is next separated ahead of MS, typically by liquid chromatography, which conveniently can be directly coupled to MS. The favored approach for coupling LC-MS is a soft ionization technique known as electrospray

ionization (ESI), which transitions the charged analytes to the gas phase for MS analysis.[45] MS analysis of a proteomic sample involves acquiring both the mass of the original (intact) peptide, as well as the formation and mass determination of fragment ions through a process known as tandem mass spectrometry.[46] Following data acquisition, various computational approaches are available to analyze the MS data, translating spectral files into amino acid sequence information indicative of the proteins present in the sample.[47] While improved mass spectrometry instrumentation has been expanding its capabilities for proteome characterization, it should be realized that many of the key stages of a proteomics workflow are not directly connected to the MS instrument. For example, ineffective cell lysis, or poor protein solubilization would lead to sample losses, while the presence of matrix interferences which suppress ESI ionization can bias the detection of analytes. Thus, regardless of the sensitivity or scan speed of today's state-of-the-art MS instrumentation, such limitations in front-end sample preparation will impact the quality of the resulting data.

1.1.2 Peptide Ionization and Mass Analysis

In 1989, John Fenn pioneered the application of electrospray ionization (ESI) to enable the analysis of extremely large molecular weight proteins by mass spectrometry.[45] ESI is considered a soft ionization process, meaning that analytes undergo minimal fragmentation during ionization, which permits MS analysis of larger, more thermally label molecules in their intact form. ESI is ideal for ionizing peptides and proteins, as it typically generates multiply charged ions to permit analysis of compounds with extremes in molecular weight. This was of particular benefit given the upper mass limit of early quadrupole mass analyzers (typically on the order of *m/z* 2000). ESI also facilitates high-

throughput analysis of mixtures, given its capacity to directly couple with the continuous elution of solvent from a liquid chromatographic separation. With ESI, the analytes of interest are typically present in an acidified, mixed aqueous and organic solvent (with acetonitrile / water / 0.1% formic acid being the most typical of a proteomics experiment). As such a solvent system is also typical of reversed phase separation, ESI therefore presents an ideal interface between chromatographic separation and mass spectrometry. Furthermore, ESI can be implemented at the nano-flow regime[48] (sub microliter per minute flow), enabling higher sensitivity analysis,[49] and becoming today's mainstay approach to proteome characterization.

A mechanistic description that outlines the transition of analytes from solution to gas-phase ions is described below and shown in Figure 1.1. An understanding of this process is essential to the larger goals of this thesis, which explores the elimination of matrix interferences (namely surfactants) which can suppress the ESI process when present in the sample.

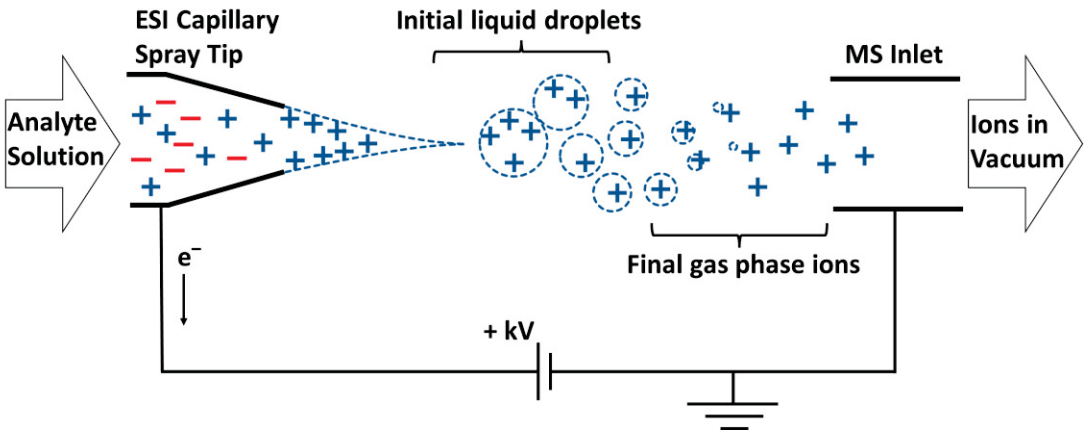

Figure 1.1 Schematic depiction of the general ESI source, operating in positive ion mode, ejecting analyte solution containing charged ions that yield gas phase ions entering the MS instrument.

Beginning from the perspective of a reversed phase separation, the eluting analytes are present in an acidified mobile phase (acetonitrile/ water) and are sprayed into open atmosphere from the end of a capillary where the solvent encounters a voltage potential difference of typically 1.5-5 kV that disperses the sample solution into an aerosol of highly charged droplets in atmosphere,[50] depicted in Figure 1.1. The solvent droplet repeatedly evaporates, aided by high temperature, disintegrating, and becoming smaller.[51] Charged analytes will electrostatically repel each other as the solvent is evaporated until the Rayleigh limit is reached and the surface tension of the droplet is overcome by the Coulombic force of repulsion and the droplet disintegrates into a smaller offspring of droplets, known as Coulombic fission. This process repeats and offspring droplets carry approximately 2% of the parent mass and 15% of the parent charge.[52] As the droplets shrink it loses approximately 90% of its mass increasing the mass to charge ratio until the ions are released from solution and enter the MS inlet as gas phase ions.[53] The mechanism that finally releases the analytes from solvent molecules is still debated and several theories have been developed to model the mechanism.[54] The ion evaporation model suggests droplets reach a given size and the electric field at the surface of the droplets generated by charged analytes becomes strong enough to emit the solvated ions out of the droplet. Alternatively, the charge residue model implies that droplets become so small they essentially contain a single charge analyte molecule until all solvent evaporates leaving the residual ion.[50] It is suspected that unfolded, hydrophobic proteins are ejected from droplets sequentially as one chain terminus gets expelled into the gas phase, known as the chain ejection model.

The composition of the sample including the type of solvent used are critical for successful ESI process. The pH of the solution will impact the conformation of proteins and peptides in solution, which directly impacts the charge state distribution on these molecules.[55] Importantly, a low pH will lead to the protonation of N-terminus of basic residues, such as lysine and arginine). The type of solvent is known to impact the ionization of proteins and peptides in ESI-MS. The polarity, gas-phase basicity, and surface tension of the solvent impact the Rayleigh- limit charge of droplets in ESI, directly impacting the maximum charge states and charge state distributions (CSD) of peptide fragments. Other additives aim to increase the CSD of peptides and proteins termed charge-enhancing or "supercharging" additives, like dimethyl sulphoxide (DMSO) or *m*-nitrobenzyl alcohol.[56]

Detergents are commonly used reagents in protein chemistry. Membrane proteins for example will commonly require detergent treatment to aid in their solubilization in aqueous solvents (membrane protein isolation is discussed in Section 1.3.1). It is well reported that detergents will interfere with ESI-MS (the impacts of residual detergents on other aspects of the proteomics workflow are expanded in Section 1.4).[57] With respect to ESI, coulombic interactions between surfactants and oppositely charged analytes results in surfactant-peptide ion adducts that do not transfer to gas phase.[58] Surfactants will alter the surface tension of nanodroplets in ESI, impact the charge envelope of peptides, and generate adducts and background ions, all of which result in suppressing the analyte signals. While MS analysis is pivotal to high-throughput proteome characterization, residual surfactants present in the sample have the potential to severely impact the detection process, unless appropriate sample purification is available.

1.1.3 Bottom-Up, and Top-Down Proteomics Approaches

The typical proteomics workflow described in the previous section is generally referred to as bottom-up proteomics (BUP), referring to the analysis of peptide fragments following enzyme (or chemical) digestion. Bottom-up proteomics is currently the more common approach.[59–61]Alternatively, MS analysis can be conducted on intact protein sequences, either as denatured molecules or in their native conformation. Analysis of intact proteins is known as top-down proteomics (TDP).[62] The value in TDP is the potential to detect complete proteoforms including PTM's as opposed to fragments of amino acids to infer a given protein molecule. Regardless of method (BUP or TDP), the amino acid sequence of the protein is ionized and characterized by way of MS fragmentation and analysis (i.e., tandem mass spectrometry). However, the greater complexity of chemical structure for intact proteins, their wide dynamic range, and potentially limited solubility implies that the manipulation of intact proteins is more challenging than that of their peptide counterparts.[63,64]

1.2 Protein Solubility

Maximizing a protein's solubility is one of the most vital conditions enabling MS characterization. Protein solubility is a function of its molecular structure, which is closely dictated by its cellular localization, which in turn relates to its function. Proteins can be described through their primary structure, namely the order of amino acids in a polymerized chain. In their native environment, proteins will adopt higher order, three dimensional structures which not only maximize their solubility but lend the protein their functional characteristics. Secondary protein structures are classified as interactions in the

primary chain resulting in local folds, most common types known as α-helices and β-sheets shaped by hydrogen bonding between carbonyl and amino groups. The tertiary structure of proteins arises from the interactions of amino acid functional R groups. These have a variety of interaction types depending on the characteristics of the amino acid. The combination of amino acid residues, resulting α-helices and β-sheets, R group interactions, and disulfide covalent linkages that contribute to a proteins tertiary structure.

In aqueous solution proteins will adopt a conformation such that their polar regions envelope and shield the bulk of the hydrophobic regions. In doing so, the polar amino acid groups are exposed and allowed to interact with the aqueous environment through hydrogen bonding, ionic-, and protein-solvent interactions. These interactions increase the proteins overall solubility by forming an ordered layer surrounding the protein called a hydration sphere.[65–67] A protein's higher order structure can be disrupted (denatured) where the hydrogen bonds maintaining the proteins' tertiary structure are broken. Protein denaturation is a dynamic process and can be reversible but can also lead to irreversible and insoluble aggregation. Changes to a protein's conformation can directly impact its solubility. Factors that will influence a proteins conformation include pH, temperature, ionic strength, and the presence of additives such as surfactants.[68–72] Discussion of SDS-protein denaturation is described in Section 1.2.2. To quantitatively prepare samples it is important that the physicochemical properties of the solvent favor protein solubility.

1.2.1 Thermal Denaturation and Protein Aggregation

High temperatures are known to impact protein structure and solubility *via* thermal denaturation. The partial unfolding of the protein's native structure can expose hydrophobic protein residues that form intermolecular structures leading to aggregates.

These protein aggregates are dominated by hydrophobic sites of the amino acid sequence creating intermolecular interactions. Protein aggregates are still partially susceptible to proteolysis reactions and can generate sufficient digested peptide fragments to permit MS identification. However, accurate quantitative analysis may be compromised.[73]

Yan et al. (2004) investigated the heat-induced unfolding and aggregation of hemoglobin molecule using FTIR spectra to monitor hemoglobin's thermal transitions. They reported a sequence of temperature-dependent protein denaturing events over a range of 30-70°C.[74] Hemoglobin denaturation below 44°C was dominated by conformational changes of α-helices warping tertiary structure.[74] This study also showed that heat-induced structural changes were extended to protein chain structures as temperatures reached 60°C and above that β-sheet structures became denatured. Of interest is that the formation of protein aggregates was found to start occurring in the range of 44-54°C indicating it may be specific regions of the proteins sequence that influence formation of aggregates.

Thermal denaturation has also been shown to change protein profiles and generate polydisperse protein bands and spots in SDS-PAGE gels and heavily interferes with MS analysis.[74–77] The temperature of 60 °C is considered the upper limit that a proteomic sample can be exposed to before thermal aggregation becomes significant.[74,77,78]

1.2.2 Sodium Dodecyl Sulfate

The anionic detergent sodium dodecyl sulfate (SDS) is popular in proteomics research, as seen for example through its role in sodium dodecyl sulphate-polyacrylamide gel electrophoresis (SDS-PAGE) separation.[79] SDS, commonly found in household and cosmetic cleaners and as an emulsifying agent, is a favored solubilising agent in biological and crystallography studies involving proteins.[80–84] SDS is a synthetic organosulfate

molecule and an anionic surfactant consisting of a sulfate group attached to a dodecane chain with a sodium counterion, see Figure 1.2. At low concentrations, SDS molecules exist as free monomers in solution. The critical micelle concentration (CMC) is the concentration of detergent at which point the individual molecules start to self-associate and aggregate, forming larger structures known as micelles.[85] The CMC for SDS in pure water at 25°C is 0.0082 M with each micelle containing ~62 SDS molecules (approximately 18 kDa)[86]

SDS is commonly used as an amphiphilic detergent in proteomics to denature, solubilise, and separate proteins via ionic and hydrophobic interactions. SDS binds to proteins with high affinity in a concentration-dependent manner where different interaction and binding types exist over a wide concentration range.[72,87–89] The anionic sulfate group binds positively charged amino acids such as lysine and arginine, while the alkyl chain binds to hydrophobic side chains.[72,90–92] In 2009, Bhuyan examined protein-SDS binding isotherms and reported three effective concentrations where SDS interacts with proteins.[93] At submicellar concentrations, monomeric detergent molecules bind to high-energy, hydrophobic regions on proteins. Leucine, isoleucine, and valine are reported to form hydrophobic clusters that block solvent from penetrating into these clusters. Secondly, SDS begins to cooperatively bind on the proteins surface leading to denaturation and changes in proteins tertiary and secondary structure. Above the critical micelle concentration (CMC) detergent molecules aggregate into micelles that dominate the SDS-protein interactions. The denatured protein covered in micellar SDS rosettes is termed the "necklace model."[94] The dynamic and varying interaction of SDS with proteins yields two discrete protein structural changes. The binding ratio of SDS to proteins is impacted by the sequence of

amino acids, temperature, and buffer matrix composition.[66,95] The SDS-protein binding ratio varies in the published literature from approximately 0.5-2 gram of SDS per gram of protein.[91] However, the most commonly reported study of SDS to protein binding (Reynolds, 1970) describes an approximately constant mass ratio of 1.4 g SDS per gram of protein.[93] This results in a near constant (negative) charge to mass ratio of SDS-bound proteins, and is the basis for SDS-PAGE and GELFrEE separations where proteins denatured by SDS are separated in a gel membrane based on their relative masses.[93,96]

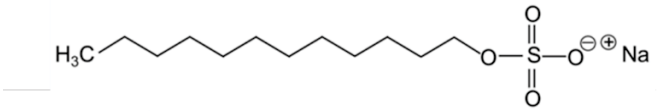

Figure 1.2 Structure of sodium dodecyl sulfate with the hydrophobic 12 carbon alkyl chain and hydrophilic organosulfate headgroup with monoisotopic mass 288.1371 Da.

1.3 Sample Preparation Strategies for MS Based Workflows

Following cellular lysis and extraction, protein solubility of the most hydrophilic components in the sample can typically be maintained by the protein's structural conformation. However, detergents are frequently employed to augment protein solubility, particularly for hydrophobic proteins. Membrane proteins are of low abundance relative to the size of a full proteome, however their impact in biology is far reaching. Detergent-based workflows can make these proteins preparation and manipulation simple procedure. They play roles in the organization and localization of a cell's components and organelles and importantly in the cell's interactions with its environments via signal transduction, cell recognition, and intercellular joining and are commonly implicated in disease.[97–100] In 2020, Lu et al. used the application of MS based genomics and proteomics to detect

abnormal membrane protein and microRNA expressions as lung cancer metastasis biomarkers.[101] The short non-coding RNA molecule, has-miR-137, was detected as a biomarker from MS proteomics experiments, as several of its indirect protein targets were isolated in membrane protein enriched high-metastasis cell lines.[101,102]

Classed into ionic, non-ionic, and zwitterionic detergents ionic detergents such as SDS, sodium deoxycholate, and sarkosyl are regularly used for complete protein denaturation. SDS has shown to improve whole proteome and membrane protein studies.[103] Non-ionic detergents are characterized by their uncharged headgroups and are considered milder as they disrupt protein-lipid interactions but do not denature proteins as strongly, a common example is Triton X-100. MS-compatible detergents are typically a non-ionic variety like MS-compatible degradable surfactant (MaSDeS) that Chang et al. (2015) reported successfully solubilized a variety of complex proteome samples from swine tissues and improved the detection of membrane and nuclear proteins compared to controls.[104] Zwitterionic detergents, like 3-[(3-cholamidopropyl)dimethylammonio]-1-propanesulfonate (CHAPS) have headgroups containing equal negative and positively charged species leading to a net neutral charge.[105] Thus, they lack conductivity and cannot be used for electrophoretic mobility, like SDS, but they will disrupt protein-protein interactions and can be used to denature proteins, commonly applied for isoelectric focusing.

1.4 SDS Incompatibilities and Limitations with LC-MS

Detergents play key roles for extracting, isolating, and preserving protein samples, but typically will interfere with near all other aspects of proteomic workflows including

both LC and MS platforms, deteriorating chromatography and signal quality and proteolytic digestions.[106,107] The common anionic surfactant SDS has a maximum concentration threshold of 0.01% (100 ppm) SDS above which the surfactant is incompatible with proteomic workflows.[106] SDS also interferes with trypsin digestion as it denatures proteins, including enzymes, disrupting their structural conformation and subsequently activity.[108–111] Ghosh (2008) reported that concentrations as low as 0.08% SDS are sufficient to denature trypsin and decrease its proteolytic activity.[112]

Kawasaki and Suzuki (1990) showed that increasing concentrations of SDS from 0 to 0.1% slowed the elution of peptides from reverse phase (RPLC) columns, reducing the separation of peptides and broadening their signal peaks.[113] SDS binding to positively charged residues on the proteins, like arginine and lysine residues, yields the proteins with greater net hydrophobicity.[114] At higher concentrations, SDS will adsorb onto the surface of alkyl-bonded stationary phases of RPLC columns and subsequently yield a net negative charge that further impacts retention times.[115] In 2015, Ortiz-Bolsico et al. determined that adsorbed SDS remained constant (~2.6 $\mu mol \times m^{-2}$) through the acetonitrile concentrations of 5-20% above which SDS-column interaction slightly decreases.[115]

Perhaps the most significant impact of SDS on the proteomics workflow is seen through the electrospray ionization process, by altering the surface tension of microdroplets.[106,116,117] This therefore interferes with the normal generation of ions through Coulombic fission of ESI droplets. Surface active agents like SDS, at concentrations above 0.01%, have been shown to fully suppress MS signals.[107,109,118,119] For example, in 2015, Kim et al. showed MS signal deterioration at 0.01% SDS noting the formation of adducts in the MS spectrum which was also reproduced by Kachuk et al. in 2016.[107,120] The main

impacts of SDS on MS analysis includes the lowering of analyte signal intensities, the formation of adducts structures, and the increased presence of background ions that may obscure and even suppress sample signals and potential shifts in the expected charge envelopes. Mass spectral data becomes cluttered by detergent adducts rendering it difficult to interpret with multiple studies publishing confirming these detriments.[118,121,122]

In summary, SDS is considered an ideal additive for improving protein manipulation during front-end preparations, but unfortunately is also detrimental to multiple downstream aspects of the proteomics workflow, including digestion, separation, and detection. This therefore presents the proteomics researcher with three options: avoid using SDS altogether, employ a very low concentration of SDS and dilute the solution if necessary, or employ SDS at appropriately high concentrations for the early stages of the proteomics workflow, followed by an effective protein purification strategy to eliminate SDS and avoid the detrimental impacts it causes during MS analysis.

1.4.1 Sample Cleanup Strategies to Remove Residual SDS

SDS removal is challenging, without impacting the recovery of proteins due to the strong interactions between protein and detergent. Removing SDS from hydrophobic (membrane) proteins also increases the risk of sample loss as the proteins may no longer remain soluble without the detergent.[123–125] The interest in separating detergents from protein and biological samples has existed even before the formalization of the field of proteomics.[103,126–129]

Column-based methods for SDS removal are popular for their simple design and user interface whereby SDS contaminated samples are passed through the column, which ultimately has the goal of separating protein from SDS. Numerous mechanisms of

separation have been developed and commercialized. Reverse phase (RP) LC separates protein according to their relative hydrophobicity.[130,131] While RP columns have been reported to isolate proteins from SDS, the success of depletion is limited as the surfactant can continue to interact with proteins.[132,133] Membrane protein separation is challenging with RP since hydrophobic proteins are susceptible to self-aggregate and can precipitate once the detergent concentration is lowered.[133] Hydrophilic interaction liquid chromatography (HILIC) uses an ionic resin that interacts with water becoming hydrophilic that separates polar compounds. In 1993, Jenö et al. published an SDS removal based on HILIC using trace enrichment before sample proteolysis.[134] Some HILIC applications have been published that target PTM analysis.[135,136] Ion exchange chromatography techniques rely on differences in the net charges between proteins and surfactant micelles. Sze et al. (2018) report a weak cation exchange online removal system that permits in-solution digestion of protein samples containing SDS, whereas other methods must deplete SDS prior to proteolysis.[137] Size exclusion chromatography (SEC) can only deplete free SDS (in solution). Protein-bound SDS molecules, as well as larger micelles, depending on the column's pore size, and will not be removed, making SEC unsuitable for MS-based workflows.

Numerous column-based protein purification kits are available commercially. Typically, these make use of an affinity resin packaged into a small spin cartridge that operates in a centrifuge. These cartridges retain proteins while the detergents are washed away. Commercial spin columns have been compared, whereby the Pierce Detergent Removal Spin-Column appears to generate the most favorable results.[127,138]

A variety of additives have been reported to adsorb detergent molecules. Metal-organic-frameworks are a nanotechnology attracting attention for its favorable chemical properties suited to removing detergent contaminants on mass.[139] Dolochar has been used as an adsorbent additive to remove SDS.[140] Polystyrene adsorbents are rapid and efficient at removing N-Lauryl sarcosine detergent, but has not been applied to SDS.[141,142] Cyclodextrin has been applied by Quirino in 2018 to bind SDS forming CD-SDS inclusion complexes that are funneled to waste prior to MS and as a result reduce the amount of SDS monomers and multimers signals.[128,143]

Membrane filtration techniques are effective at removing SDS while retaining larger proteins. Dialysis is only effective to remove free (unbound) SDS and generally takes a long time.[144] For MS analysis, protein-bound SDS must also be removed. Commercial products including Slide-A-Lyzer®, Pierce™ 96-well microdialysis plates, SnakeSkin™ Dialysis Tubing, with various specified MWCO's can be employed, but the result will be an incomplete purification.

As an evolution of simple membrane filtration, Filter Aided Sample Preparation, or FASP[145,146] is a popular protocol published by Wisniewski et al. in 2009 that also highlighted the benefits of using SDS in proteomics workflows. FASP retains proteins above a MWCO filter, but also disrupts SDS-protein interactions with inclusion of 8 M urea. Following multiple lengthy centrifugation steps, the SDS can be successfully removed.[147] Since the advent of FASP, several competing strategies for SDS removal have been reported, most of whom achieve the required purity for MS analysis. Examples include single-pot, solid-phase-enhanced sample preparation, or SP3 for short, and suspension trapping (STrap).[148–151]

The solubility of SDS is diminished by inclusion of potassium salts causing it to precipitate. KCl precipitation is reported to deplete >99.9% SDS from peptide samples by ion substitution-mediated precipitation whereby potassium binds DS^- forming KDS leaving peptide samples free of SDS.[152–154] The approach is however ultimately limited by the solubility of KDS. Alternatively, a long-standing practice, solvent-based protein precipitation is used to isolate, purify, and concentrate samples.[41,70,155] Several techniques exist for precipitating proteins and isolating from contaminants and there are many comparative studies in the literature.[155–158] Protein precipitation has been demonstrated to remove, reliably and rapidly, both free- and protein bound detergent yielding pure proteins but is criticized for being susceptible to variance from one lab to the next.

Acetone precipitation can overcome the binding energy of the protein-bound SDS and purify to a high level. A rapid and consistent precipitation protocol is reported by Nickerson (2020) with high purity and recovery of 98 ± 1%. They report improved precipitation efficiency with near-homogeneous recovery of all the proteins by using a combination of 80% acetone with high salt concentration and temperature.[41] The ProTrap XG was developed by Crowell et al. in 2015 to facilitate acetone precipitation whereby aggregated proteins are centrifuged and retained on a polytetrafluoroethylene membrane as SDS and acetone pass through, leaving pure sample with 99.75% detergent removed.[159,160]

Electrophoresis-based SDS depletion methods use an applied electric field to influence and move the negatively charged detergent molecules. SDS-PAGE is a gel-based electrophoretic technique that uses SDS to denature and confer negative charges to then separate protein mixtures under an applied electric field in a polyacrylamide matrix. This

traps the proteins in the gel allowing for the removal of SDS through a series of organic solvent washes. The trapped proteins can then be digested after which the smaller peptides are extracted.[161] Of the physico-chemical techniques that have contributed to the study of proteins, and expanded the field of proteomics, electrophoresis has been of primary importance. In 1975, Tuszynksi and Warren used the application of electrophoretic dialysis to drive off protein-bound SDS. They modified an electrophoresis gel destainer with dialysis tubing to retain proteins while charged detergent molecules (SDS) were stripped from the samples. Detergent contaminated cytochrome c and BSA after 11 hours achieved much higher purity than dialysis would offer by applying 20 mA of constant current to the samples. More recently, Quirino et al. (2020) have also developed an electro-kinetic based platform for rapid SDS removal focused on peptide purification. Utilizing an agarose gel filled micropipette tip with cathodic electrode and the apparatus is suspended in electrolyte that holds an anode. Samples are loaded on top of the gel, where they are retained for easy recovery, while the smaller detergent molecules are pulled off the samples by the force of an electric field producing pure peptides.[162–164]

1.5 Transmembrane Electrophoresis

Transmembrane electrophoresis is an instrumental approach for SDS depletion developed in this laboratory[165,166] to provide a reliable method for depleting protein-bound SDS without compromising sample yield. Analogous to electrodialysis, an electric potential is applied across a MWCO membrane directing charged analytes to pass through the membrane while retaining the larger MW proteins, a schematic depiction is shown in Figure 1.3. The conventional TME platform was originally described by Kachuk and

colleagues (2016) and then modified by Unterlander and Doucette (2018) to better control Joule heating and understand how the theory behind TME,[165,166] TME has since been applied to both BUP and TDP workflows.[167] TME has previously shown to reliably remove protein-bound SDS to below 10 ppm while maintaining yields of 90 -99.9% depending on the sample composition.[165,166] However, one of the significant limitations of TME is the excess Joule heat which limits the magnitude of the applied electric field. Recall (Section 1.2.1) that higher temperatures (>60°C) have a direct impact on protein aggregation, thus potentially lowering sample yield.

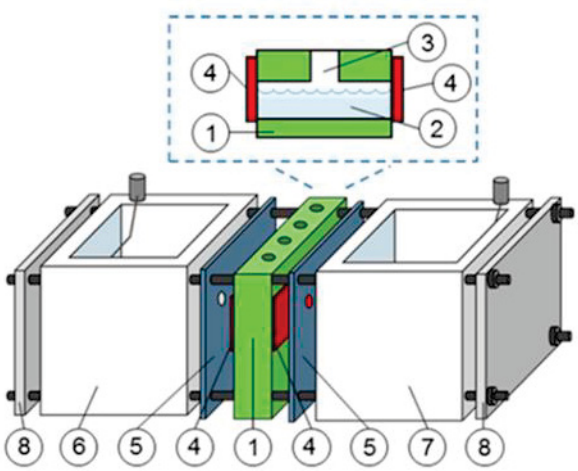

Figure 1.3 Depiction of the TME device with buffer chambers (1), sample cell (2), SDS-protein sample solution, (3) sample inlet (4), MWCO membranes, (5) silicon gaskets, (6 and 7) cathode and anode buffer chambers, (8) and system retaining clamps that hold the TME device together and maintain the water-tight seals. This figure was used with permission from Kachuk et al. (2016).[165]

Unterlander (2018) improved the original TME design by first investigating the theory and mechanism governing how TME functions.[166] The original version of TME required one hour of run time to deplete samples to 100 ppm of SDS and efforts to expedite this by increasing the strength of the electric field were unfruitful. Specifically, Joule heating, caused by the high application of constant currents resulted in thermal aggregation

of proteins causing lower yields and thus limited the performance of TME. Efforts to overcome the high temperatures initially required that the TME applied voltage was periodically paused, and that the sample was mixed via pipetting to disperse the Joule heat being formed during electrophoresis. This was not only laborious but added significantly to the total time required for SDS depletion. Further attempts to mitigate the formation of high temperatures were made by chilling the TME device to -20°C and using pre-cooled electrolyte solution (4°C). Finally, implementing stir bars inside the sample wells to continuously stir the sample aided in dispersing heat.

A theoretical model describing the relation between the applied electric field and SDS depletion rate is provided here. The movement of an ion in an electric field and passing across a membrane is the sum of the diffusion, electromigration, and convection forces that govern mass transport in electrophoretic systems described from the Nernst-Plank (NP) equation:

$$J_{total} = -D\frac{dc}{dx} + D\frac{ze}{k_B T}cE + v_s c \qquad \text{Equation 1.1}$$

Where J is the diffusion flux, D is the diffusivity of the analyte ($\frac{cm^2}{s}$), c is the concentration of the analyte, x is the position, z is the valence of the ionic species, e is the elementary charge, k_B is the Boltzmann constant, E the electric field ($\frac{V}{m}$), v_s is the velocity of the solvent, and T is the temperature (K). A novel way to describe the residual SDS remaining in the TME solution was first described by Unterlander in 2018 to model the residual SDS inside the TME sample cell. Although, not synonymous with the flux of SDS the two are related via NP equation. The flux of SDS is related to the strength of the applied electric field using an exponential decay function derived from the NP equation:

$$SDS_t = SDS_0 \cdot e^{-\lambda t} \qquad \text{Equation 1.2}$$

where SDS_t is the concentration of SDS at time t (ppm) and SDS_0 is the initial concentration (typically 5000 ppm), t is time (s), and λ is the decay constant. This decay constant (λ) is a function of several parameters shown below:

$$\lambda = \frac{DzFE}{LRT} \qquad \text{Equation 1.3}$$

Where F is Faraday's constant ($\frac{c}{mol}$), L is the length of the sample cell including the membranes (cm), and R is the gas constant ($\frac{J}{K \cdot mol}$). The simplified equation modeling residual SDS is based two major assumptions: both the temperature and the voltage throughout a TME run are constant. While these factors remain relatively stable at lower applied currents the assumptions do not hold for higher applied currents, resulting in higher Joule heating. As temperature changes, the rate of SDS depletion no longer follows the predicted exponential function. The decay constant (λ) is related to the half-lives ($t_{½}$) of SDS decay as per the equation below:

$$t_{½} = \frac{\ln(2)}{\lambda} \qquad \text{Equation 1.4}$$

The half-lives provide a quantitative approach to discuss TME system optimization. For example, with the original TME reported by Kachuk, the SDS depletion rate was described through a minimum half-life of 5.9 min while Unterlander reported a half-life of 1.1 min.[165,166]

Updates to the design of TME were made to further reduce the limitations of the TME system, by mitigating the impacts of Joule heat formation. Stir bars inside the sample wells allowed for improved heat dissipation to the adjacent buffers, allowing continuous operation at higher electric fields without the need to pause the power supply and prevent sample overheating. Given that TME is the central topic of this thesis, a detailed description of the underlying electrophoretic process is described in the next section.

1.5.1 Mechanisms Underlying Electric-Field Based Methods

Electrophoresis is a powerful tool for the separation of mixtures, the determination of purity, and can be applied for small as well as large scale preparations.[168–170] Electrophoresis is the movement of charged particles under the influence of an applied electric field.[171] An electrophoretic system consists of two electrodes of opposing charge that are immersed in and connected to a conducting medium. An electric potential can be generated between the two electrodes and charged ions migrate from the anode to the cathode and ions in the electrolyte will maintain the current. Reduction occurs at the cathode, with water reducing to form hydrogen gas and hydroxide ions. Oxidation at the anode results in forming protons that react with water to form hydronium, together with oxygen gas, and electrons. Charged species within the solution will also migrate to either the anode or cathode depending on their charge state (anions migrate to the positively charged anode; cations to the cathode) expressed by the parameter electrophoretic mobility, ($\frac{m^2}{Vs}$). This is expressed in terms of the Coulomb force, F_e ($\frac{J}{cm}$), being exerted onto the analyte that is driving it to migrate towards electrode per Equation 1.5:

$$F_e = q \times E = zeE \qquad \text{Equation 1.5}$$

Here, q (units in *Coulombs, C*) represents the product of the charge number, z, and the elementary charge, e, multiplied with the electric field, E. The opposing force to Coulomb's force is the drag force, F_{drag} ($\frac{kg \cdot m}{s^2}$), exerted onto the particle which is expressed by Stoke's law (Equation 1.6) and is a product of the analyte's velocity, v ($\frac{m}{s}$), and the frictional coefficient, f ($\frac{kg}{s}$).

$$F_{drag} = f \times v = 6\pi\eta r \times v \qquad \text{Equation 1.6}$$

The frictional coefficient, *f*, accounts for the molecules size, shape, and viscosity of the medium being used for electrophoresis and is more specifically expressed as $6\pi\eta r$, where η is the dynamic viscosity of the solution ($\frac{kg \cdot m}{s^2}$) and r is the ionic radius (m) of the analyte. Ions migrate at different rates according to their charge, size, the magnitude of the electric field, and the viscosity of the matrix. The velocity, termed drift velocity, v_{drift} ($\frac{m}{s}$), that a particle reaches during electrophoresis occurs when the Coulomb force, F_e ($\frac{J}{cm}$), exerted by the electric field is greater than the drag force, F_{drag} ($\frac{kg \cdot m}{s^2}$), that molecule experiences provided by Equation 1.7 below:

$$v_{drift} = \frac{zeE}{6\pi\eta r} \qquad \text{Equation 1.7}$$

The speed at which particles of different and varying sizes in a specific medium migrate towards an electrode depends on their sizes and charges and the specific medium and electric potential being used.

1.5.2 Joule Heat

Under the influence of an applied electric field, charged molecules in solution will migrate and subsequently generate heat through frictional forces. This production of heat is also known as Ohmic or resistive heating, described below:

$$H = VIt \qquad \text{Equation 1.8}$$

where, *H* is the heat produced (*J*), *V* is the applied voltage, *I* is the applied current (*A*), and *t* is time (*s*). This equation can be expressed to reflect the relationship between Joule heat and resistance:

$$H = I^2Rt \qquad \text{Equation 1.9}$$

where, R is the resistance (Ω). Joule heating leads to an increase in temperature in the sample chamber in the transverse and longitudinal directions. Excess Joule heating can have several negative impacts within the sample channel, with the extreme case resulting in boiling of the solution, result in bubble formation which most likely will cause a short in the system and terminate the experiment. At lower temperatures, heat-induced protein aggregating is also a concern. Resistive heating cannot be eliminated; it is a consequence of high applied electric fields together with the resistance of the sample. Rather, the management of Joule heating is crucial for efficient, and importantly, reproducible electrokinetically driven separation systems.

1.6 Research Objectives

MS technology has advanced to a point where the front-end sample preparation can be considered the major bottleneck in a proteomic workflow. This is particularly true for TDP applications but is still an important concern in BUP workflows. SDS is a favored additive in membrane protein analysis but compromises downstream analysis if not effectively eliminated from the sample. Several SDS depletion protocols are available, through to varying degrees of success. Some are ineffective at removing SDS below critical levels (0.01%). Others result in considerable protein loss. Still others are lengthy, difficult to automate and cause concerns in terms of reproducibility.

TME is capable of high protein purity together with high recovery, in a reproducible, fully automated fashion.[159,160,161] Since its initial disclosure, improvements have been made allowing TME to operate at higher electric fields (typically the current is maintained at a constant value, with 70-90 mA being the upper limit). Higher electric fields

imply faster SDS depletion, although protein recovery due to high temperature aggregation became an increasing concern. Herein, a modified TME device is described, and is referred to as active-cooled transmembrane electrophoresis (AC-TME).

Chapter 3 introduces active-cooled transmembrane electrophoresis (AC-TME). This approach is designed to mitigate the impact of Joule heat and facilitate higher operating currents for faster rates of SDS depletion. The design parameters, buffer systems, and operating characteristics are tested on their impacts on the speed of purification compared to protein yield are discussed. The performance of AC-TME at purifying membrane proteins is correlated to the mathematical expressions presented with conventional TME. The limits of AC-TME are tested at high applied current and evaluated using LC-MS/MS. A novel AC-TME trypsin proteolysis protocol is presented, designed to eliminate loss of protein aggregates that adhere to the inside of the sample-wells during operation. The sample recoveries after AC-TME runs are compared with cytosolic and membrane enriched protein fractions, purified at high operating currents.

Chapter 4 is conclusions and provides summary of the results and their implications is presented alongside recommendations for future directions and continuation of this research with perspective on recent advances in the field of proteomics.

Chapter 2 Materials and Methods

2.1 Chemicals and Reagents

Bovine serum albumin (BSA) protein standard, N-p-tosyl-L phenylalanine chloromethyl ketone (TPCK)-treated trypsin (T8802) were purchased from Sigma (Oakville, ON). Yeast (*Saccharomyces cerevisiae*) were propagated from a sample of Fleischmann's® traditional dry active yeast and Atlantic salmon (*Salmo salar*) proteome extract was sourced from fillets muscle, and both were purchased at a local grocery store. Milli-Q water was purified to 18.2 MΩ-cm from a Sartorius Arium Mini Water Purification System (Goettingen, Germany). YPD growth medium was purchased from Thermo Fisher Scientific (Ottawa, ON). HPLC grade solvents (acetone, methanol, ethanol, acetonitrile, chloroform), as well as methylene blue, and the Pierce™ BCA protein assay were purchased from Thermo Fisher Scientific (Ottawa, ON). SDS-PAGE gel casting and staining reagents, urea, dithiothreitol (DTT), and iodoacetamide (IAA) were from Bio-Rad (Mississauga, ON). Sodium dodecyl Sulfate (SDS) and formic acid were sourced from Fluka (Mississauga, ON). Trichloroacetic acid (TCA), trifluoroacetic acid (TFA), and all other chemicals used were sourced from Sigma.

2.2 AC-TME Device Design and Assembly

The AC-TME design was based on the previously published TME systems and was constructed in house.[165,166] The device consists of a central sample cartridge that holds the proteins with a top inlet to load samples into the cartridge cells, as shown in Figure 2.1 (labelled 9). The five holes in the sample cartridge each form a sample cell by placing

Spectra/Por® RC 3.5 kDa MWCO dialysis tubing (Fisher Scientific, Ottawa, ON) on either side of the sample cartridge and using four silicon gaskets cast from a Sylgard 184 silicone elastomer kit (Dow Corning) for a watertight seal. A 0.5 cm PTFE-coated magnetic stir bar (Fisher) was placed in each sample cell before assembling.

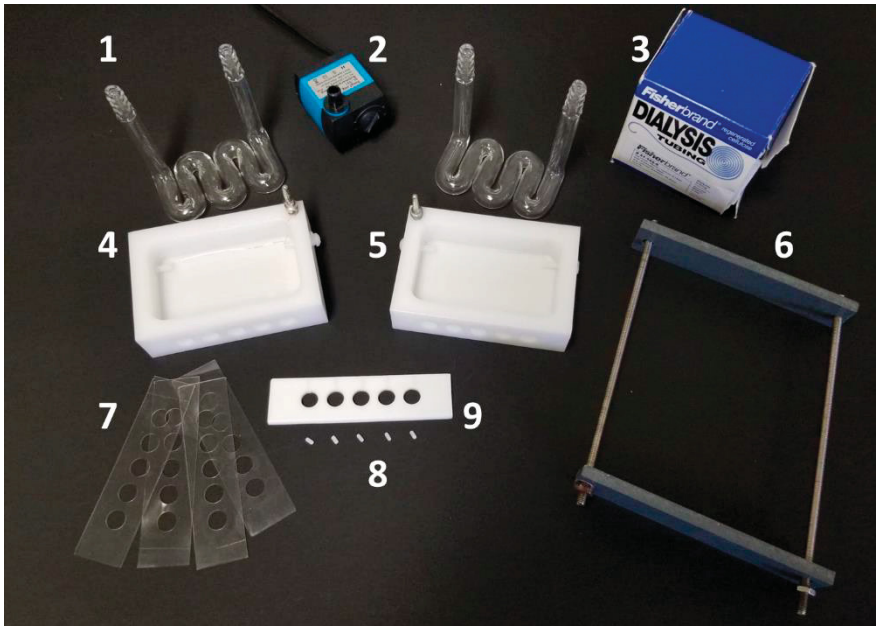

Figure 2.1: Photo displaying the parts required to assemble the AC-TME device. (1) Active-cooling buffer chamber tubes, (2) submersible water pump, (3) roll of 3.5 kDa dialysis tubing, (4,5) cathode and anode buffer chambers, (6) brackets to hold the assembly together, (7) silicone gaskets, (8) magnetic stir bars, and (9) sample cartridge. Components not shown here are the power supply and stir plate, clear ½ inch vinyl tubing connecting the active-cooling buffer chamber tubes (1) to the submersible pump (2), and the safety box that holds the AC-TME unit during operation.

The anode and cathode buffer chambers were machined from polyoxymethylene (Delrin®) and the sample cartridges from PTFE (Teflon™) to the specifications and dimensions presented in Figure 2.2A, B. Holes (0.5 cm) to mount the 5 mm standard pin electrode leads (the same used provided with the Bio-Rad Mini-Protean® SDS PAGE system) were drilled into the top outer corner of each buffer chamber and two small prongs were inserted

at the base of the chambers to fit Teflon™ plugs to attach platinum wire (7.6 cm long, 0.127 mm diameter, Sigma Aldrich) electrodes, which span the length of the buffer chamber, and connecting the Pt electrode to the leads. The silicone gaskets were cast by mixing 10 parts of the Sylgard 184 kits elastomer base with 1 part curing agent and poured over a glass plate to an approximate thickness of 0.8 mm and allowed to cure for 48 hours at 25°C. Once solidified, the gaskets were cut out and holes punched to match the shape of the sample cartridge and buffer chambers, seen in Figure 2.2B.

Active-cooling tubes, consisting of ½ inch glass tubing bent to shape, were designed, and fitted to maximize its surface area inside the buffer chambers to expedite heat exchange. The inner volume of each buffer chamber was approximately 48 mL depending on the size of the sample cartridge used (3-, 6-, or 10-mm thickness, termed small, medium, and large sample cartridges). The inside of the sample cells are cylindrical chambers with 1 cm diameters and lengths the same as the cartridge size used (3-, 6-, or 10-mm) with volumes of approximately 220, 440, or 730 µL, respectively. The MWCO membrane used on either side of the sample cartridge was soaked in Milli-Q water for 10-minutes before assembly.

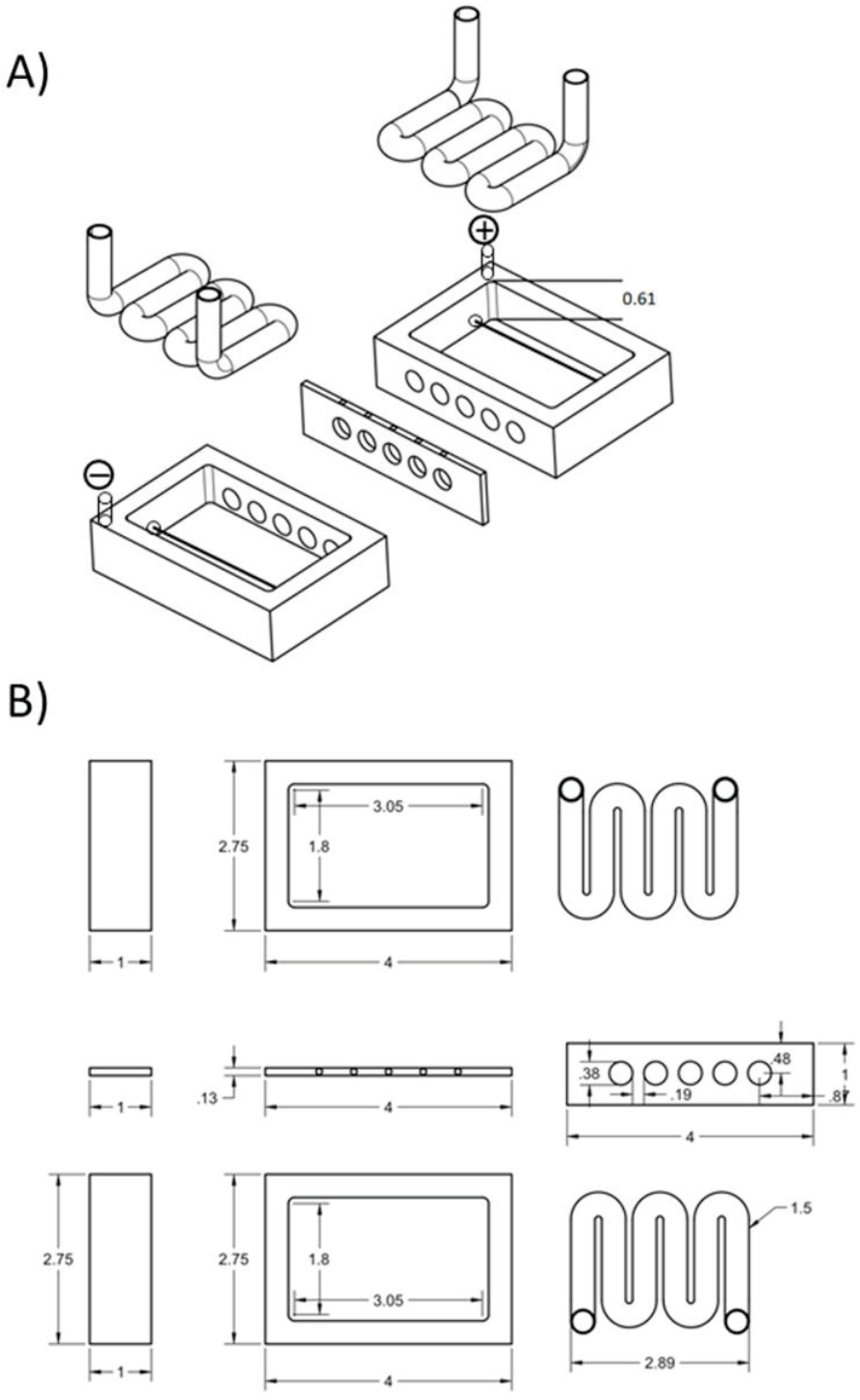

Figure 2.2 A) The CAD design sheet showing the AC-TME component's dimensions and relative size to each other. B) The sample cartridge comprises five sample wells of cylindrical shape with MWCO membranes at either end connecting the sample wells to both buffer chambers and thus creating the circuit for ions to flow from anode to cathode.

The components of the AC-TME were assembled beginning with a buffer chamber and stacking each layer on the benchtop in the following order: cathode buffer chamber, silicone gasket, pre-soaked MWCO membrane, silicone gasket, sample cartridge, one stir bar into each well (0.5 cm PTFE magnetic stir bar, Fisher), silicone gasket, pre-soaked MWCO membrane, silicone gasket, anode buffer chamber, and finally it was clamped together and tightened with two m3 nuts. The assembled AC-TME system and its components laid out in order are shown in Figure 2.3A, B.

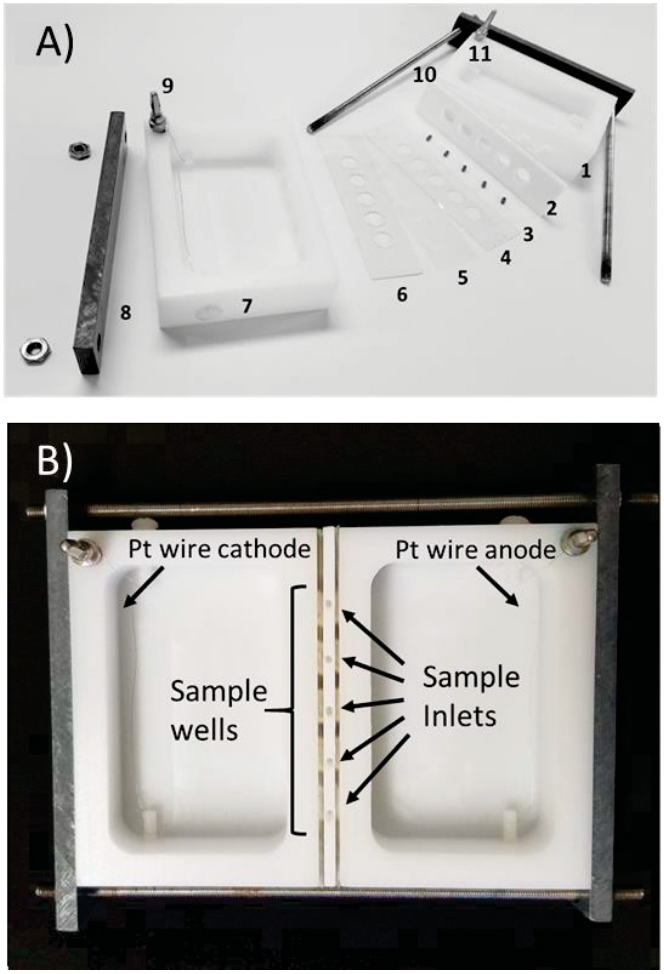

Figure 2.3: A) A close-up photo of the components required to assemble the TME device without active-cooling system, pump, nor power supply. (1) anode and (7) cathode buffer chambers, (2) sample cartridge, (3) stir bars, (4 & 6, 10) four silicon gaskets (note the image only shows two of the four), (5, 10) two 3 kDa MWCO membranes, (8) clamp to hold the components together and watertight, (9 & 11) electrode leads to connect to the power supply. B) Assembled, but empty, AC-TME device.

The device was placed into the safety box, which in turn was positioned above a stir plate. Once ready to load samples into the device, 25 mL of pre-chilled (4°C), tris Tricine (pH 8.3) was added to each buffer chamber. TT buffer was prepared at two different concentrations: 25 mM or 100 mM of each component (pH 8.3). Additionally, tris glycine was prepared and employed in the TME system at a concentration of 25 mM tris and 192 mM glycine (pH 8.3).[173] Protein samples were loaded by pipette (200, 400, or 700 μL depending on sample cartridge thickness of 3-, 6-, or 10-mm) with a gel loading tip to fit through the narrow sample inlet. These volumes were calibrated to fill the sample cells to maximize the contact area between sample solution and the MWCO membranes through which the current passes. Larger contact of sample solution with the MWCO allows for greater flux of ions. Lastly, the lid of the AC-TME safety box, with active-cooling tubes fitted connected to the ice bath, and electrodes was placed on top of the device, connecting it to the power supply, and to the active-cooling system. Temperature readings were recorded by an infrared thermometer or a temperature probe. The fully assembled AC-TME platform is seen in Figure 2.4.

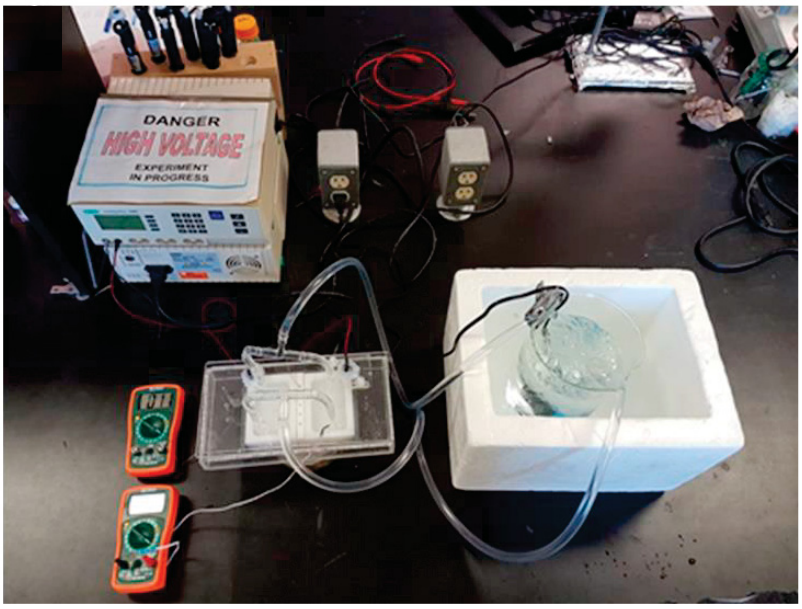

Figure 2.4: Overhead photo of the AC-TME as seen during an experiment with cold water (1.0 ± 0.5°C) circulating through active-cooling tubes inside the buffer chambers and an ice bath. The power supply and leads are connected to the electrodes and two temperature sensors are seen measuring the temperatures with the buffer chambers and sample wells.

2.3 AC-TME Operating Instructions

The operation of TME can be summarized into four steps: 1) samples were loaded into the AC-TME system, 2) power is turned on and the applied electric field and subsequent electromotive force drive the detergent off the protein molecules, generating heat as a by-product, 3) active-cooling tubes withdraws heat from the buffers as it is produced, 4) lastly, SDS depleted proteins are retrieved via micropipette, as depicted in Figure 2.5. The AC water flow (1.0 ± 0.5°C) was initiated from the pump allowing water to circulate through the tubes before operating the TME system. Once assembled, and samples are loaded, the TME device was connected to a PowerPac™ 3000 electrophoresis power supply (Bio-Rad, Mississauga, Canada). The device was operated in constant

current mode with applied currents ranging from 0-400 mA with time course experiments ranging from 1-60 minutes. Prior to removing sample aliquots from the TME system, the power supply was temporarily stopped, by either disconnecting one electrode from the power supply or turning the power supply off. The sampled aliquots could be removed for residual SDS and protein yield measurements throughout the duration of the run. The pH of the anodic and cathodic buffer chambers was measured before and after TME purifications. The temperature of the buffer chambers, and of the samples contained within one of the TME cartridge cells, were recorded using a thin thermocouple probe inserted directly into the system during TME operation.

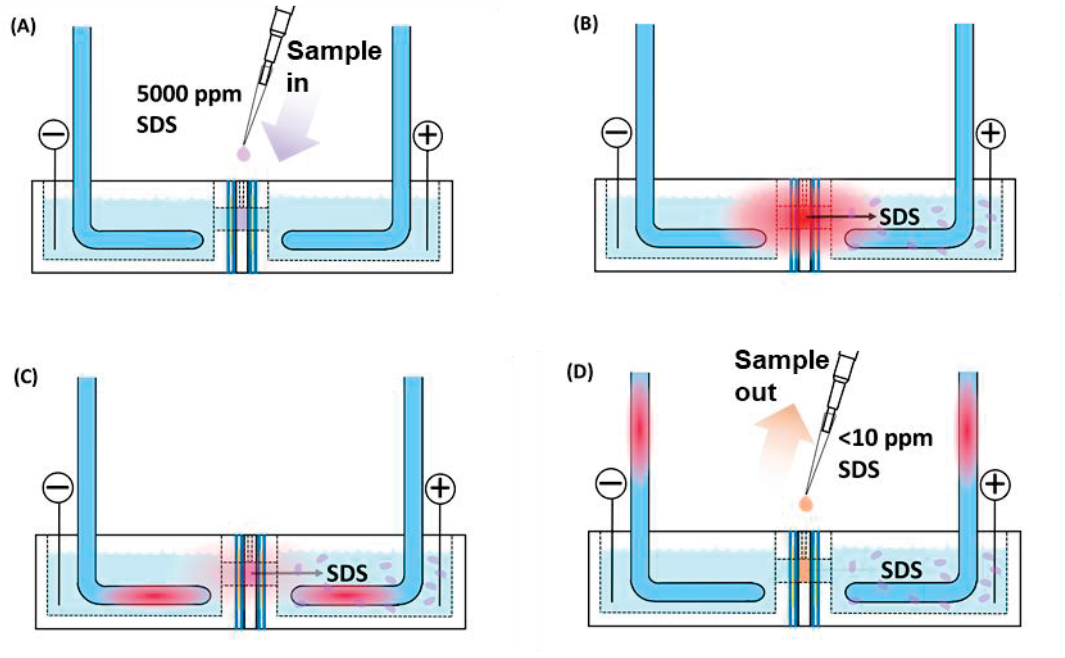

Figure 2.5. (A) SDS contaminated samples are loaded into the TME sample cartridge wells from the top via micropipette. (B) Power is applied and SDS is driven from the samples via the electric field while Joule heating is also being generated. (C) The active-cooling system withdraws heat (represented by red colour) from the samples and removes it out of the system and into an ice bath. (D) Pure proteins are retrieved from the TME device with micropipette and SDS is discarded with the buffer.

2.4 Sample Proteome Preparation and Isolation

2.4.1 Bovine Serum Albumin and Whole Proteome Sample Preparation

BSA was dissolved to 0.1 and 1.0 $g \times L^{-1}$ in Milli-Q grade water, together with 5000 ppm SDS (0.5% w/v). A total proteome extract was obtained from yeast (*Saccharomyces cerevisiae*) propagated in YPD broth growth medium consisting of 12.5 g of dry YPD broth dissolved in 250 mL water and autoclaved to be sterile. Three granules of active dry yeast (Fleishmann's®) were suspended in 5 mL of YPD broth in a sterilized 25 mL test tube (Millipore Sigma) and incubated at 32°C on a shaker until an OD_{600} of 1. The 5 mL aliquot was then added to the 250 mL stock of YPD growth medium and grown again to an OD_{600} of 1. Yeast cells were collected after growth by centrifugation and twice washed with water. Cells were lysed either by French press (three passes at 16,000 psi) or by grinding (approximately 20 min) to a fine powder in liquid nitrogen in a mortar with a pestle followed by extraction in water or tris 50 mM, pH 8.0 and 1% SDS.[174] Atlantic Salmon (*Salmo salar*) muscle proteome extract was made by homogenizing fillet meat in a blender, grinding the blended meat under liquid nitrogen temperatures, and extracting in water or tris 50 mM, pH 8.0. Lysed cell extracts were centrifuged to remove debris at 16,000 × g (13,000 rpm, Fisher Scientific accuSpin microcentrifuge, cat. No. 75003241, rotor No. 75003243) for 10 minutes to achieve a whole proteome protein extract.[175] The protein concentrations were quantitated with Pierce bicinchoninic acid (BCA) protein assay. The total yeast proteome extracts were diluted with Milli-Q grade water and spiked with SDS (Bio-Rad, Mississauga, Canada) to a final concentration of 1.0 or 0.1 $g \times L^{-1}$ protein and 0.5% SDS (v/v).

2.4.2 Membrane and Cytosolic Protein Enrichment from *S. cerevisiae*

The membrane and cytosolic enriched protein fractions were produced using an ultracentrifugation method described by Wu et al. (2011) with modification.[123,124] The whole proteome protein extract was ultracentrifuged at 118 000 ×*g* (55 min, 4˚C, 3 mL of protein extract ×6 vials total) and the supernatant was collected and labeled as the cytosolic protein fraction. The pellet was then resuspended in 50 mM ammonium bicarbonate and centrifuged at 168 000×*g* (40 min, 4˚C). The resulting membranous pellet, pale beige in color, was dissolved in 250 µL 1% SDS with vortexing and sonication (alternating 1 min sonication and 5 min vortexing until dissolved) and was labelled as the membrane protein fraction. The concentration of whole proteome, cytosolic, and membrane fractions was measured by BCA assay (Section 2.7) as well as by LC-UV (see section 2.8) and samples were diluted to final concentrations of 1.0 or 0.1 $g \times L^{-1}$ protein and 0.5% SDS (v/v).

2.5 Methylene Blue Active Substances Assay

The level of SDS remaining in the samples following AC-TME was determined using methylene blue active substances (MBAS) assay and measured on an Agilent 8453 spectrophotometer (Mississauga, Canada) as described by Arand et al.[176,177] The sample aliquots removed from the AC-TME run were diluted such that their concentration would fall in the linear dynamic range for their respective assays. The MBAS assay has a relatively narrow linear dynamic range of 2-15 ppm. Furthermore, a minimum volume of sample was aliquoted so that maximum sample recovery was ensured, as both assays are sample destructive. Regardless of the volume removed, they were factored into final sample recovery calculations to account for sample loss from the aliquots removed.

Methylene blue active substance (MBAS) reagent (50 mg methylene blue, 10 g sodium sulfate, 2 mL sulfuric acid diluted to 200 mL) was combined with SDS-containing sample in a 1:1 (v/v) ratio, vortexed at low speed, and then combined with 4 parts chloroform (v/v). The lowest volume of MBAS and solution that can be used were 40 µL of MBAS solution mixed with 40 µL of sample solution for a total of 80 µL once mixed to provide enough volume of solution to be measured accurately. The aqueous layer was removed by pipette and the absorbance of the chloroform layer was measured at 651 nm and compared to a SDS calibration curve spanning 0-25 ppm SDS.

2.6 Bicinchoninic Assay

The final sample protein concentration was measured using the Pierce™ BCA protein assay kit.[178,179] Protein extract solutions were combined with the BCA working reagent in a 1:20 ratio of sample to reagent, vortexed to mix, and then incubated at 57˚C for 30 min. Working reagent was made fresh before each use by combining the reagent A and reagent B of the assay kit in a 50:1 ratio and kept in darkness before combining with protein extract solutions. After incubating, the absorbance was measured at 562 nm against a calibration curve of BSA ranging in concentration from 0.01-0.5 $g \times L^{-1}$ or 0.5-3 $g \times L^{-1}$. The calibration standards were buffer matched. For example, if the samples were in tris Tricine buffer with SDS the calibration curve would also be made with the same concentration of buffer and detergent. Changes in volume can occur and so dilution factors must be used when calculating the concentrations of sample solutions.

2.7 Trypsin Proteolysis

Trypsin enzyme was prepared to 1 $g \times L^{-1}$ in 1 mM HCl. Protein samples purified of SDS (200 µL of 0.1 and 1.0 $g \times L^{-1}$) were reduced and alkylated prior to digestion. Because these samples have just finished a TME run they are buffered in the same TME buffer (TT buffer, pH = 8.3). For this, 10 µL of DTT (200 mM) was first added to the sample and incubated (60°C, 30 min), followed by 22 µL IAA (400 mM) and this time incubated in darkness (room temperature, 30 min). TPCK-trypsin enzyme was added at an enzyme to protein mass ratio of 1:50 (w/w) and incubated in a heat bath (37°C, 12 hours). The digestion reaction was stopped by mixing 10% TFA to a final acid concentration of 1%.[180] The pH of samples was tested using litmus paper.

2.7.1 *In-situ* AC-TME Trypsin digestion of the Residual TME Sample Pellet

The samples originally loaded into the AC-TME device were retrieved by pipetting out of the device. Residual proteins remaining inside the sample cell that could not be retrieved by pipette were instead digested inside the AC-TME sample cell. To the empty sample cartridge, 20 µL of 8 M urea (pH 8.3) was added to each well. The TME unit was placed on a stir plate to mix the solution for 10 minutes and then 80 µL of 100 mM tris (pH 8.3) was added to increase the volume of solution in the sample cell to cover any residual proteins and mixed for another 5 minutes. For digestion, 5 µL of DTT (200 mM) was added to each well and the unit was incubated (60°C, 30 min) then 11 µL IAA (400 mM) was added and again incubated (room temperature, 30 min, dark). TPCK-trypsin enzyme was added at a mass ratio of 1:50 and the unit was again incubated (37°C, 12 hours). The trypsin

proteolysis reaction was stopped by mixing in 10% TFA to a final 1% and the samples were retrieved with a micropipette.

2.7.2 In-Gel Trypsin Hydrolysis

Membrane protein samples were trypsin in-gel digested after SDS-PAGE using a protocol described by Shevchenko et al.[181] Briefly, the gel containing the protein bands was dissected as a 5 mm band, placed into microcentrifuge tubes, and incubated for 10 min in 500 µL ACN. The samples were centrifuged, and all supernatant removed and replaced with 10 mM DTT and incubated at 56°C for 30 minutes, after they were cooled to room temp and incubated with 500 µL ACN. Again, all supernatant was removed, and the gel pieces were alkylated 55 mM IAA, enough to fully cover the pieces, and incubated in darkness for 20 minutes. Another 500 µL ACN aliquot was added, and the sample was incubated 10 minutes and again the supernatant was removed. The samples were then digested by adding 13 ng×µL^{-1} trypsin to cover the pieces and incubated at 4°C for 90 min and then topped off with additional trypsin and incubated another 90 min. Lastly, enough 100 mM ABC was added to fully cover the gel pieces and the samples were incubated at 37°C for 12 hours. The peptides from the samples were then extracted with two times 200 µL washes of 2:1 ACN and 5% formic acid in water. The extracts were combined and evaporated to dryness by Speedvac.

2.8 LC-UV Assay and LC Peptide Desalting Protocol

After trypsin digestion, peptides were quantified using a universal high-recovery protein quantitation assay by LC-UV, previously described by Orton and Doucette in 2013.[182] Approximately 5-10 µg of peptides were injected into a self-packed 1 mm × 10

μm C18 column (5μm octadecylsilyl beads, Waters, MA, USA) connected to an Agilent 1200 HPLC series instrument using a 5% ACN, 0.1% TFA/ water solvent. The HPLC contained an autosampler with a 100 μl loop, a diode array detector (λ_{abs} = 214 nm) and was connected to a fraction collector. Peptides elute from the column as a single fraction through a stepped gradient from 5% to 90% ACN and the fraction was collected over a 2 min interval between 10 and 12 minutes. The ACN concentration was then increased to 95% and after 17.5 minutes reduced to 5% for the duration of the 45 min run. The sample peak area was integrated, and the peptide yield was compared to a calibration curve of digested BSA protein ranging from 0.5–20 μg. Samples were desalted and collected for LC-MS analysis using the same protocol with the exception that the entire TME-purified sample was loaded onto the column and collected. If samples contained more than 100 μL they would be loaded in series *via* two injections which then eluted off the column as a single fraction. Desalted peptides were then dried under vacuum with a Speedvac and stored at -20 °C.

2.9 SDS-PAGE

Gels were cast for sodium dodecyl sulfate polyacrylamide gel electrophoresis (SDS-PAGE) using either 12 or 15 % total acrylamide (4% T stacking, 1 mm thick), and resolved on a Bio-Rad Mini-Protean® system.[79] Protein sample solutions were combined with sample buffer (0.25 M tris-HCl (pH 6.8), 10% SDS, 50% glycerol, 5% β-mercaptoethanol, 62.5 mM EDTA, and 0.05% bromophenol blue) in a 5:1 ratio and boiled on a heating block at 95°C for 5 min. Gels were resolved at 200 V for as long as it took the gel front to migrate to the end of the resolving gel without eluting out of the gel and into

the buffer solution. The gels were stained with silver[183] or by Coomassie blue[184] and imaged using a digital camera.

2.10 Gel Eluted Liquid Fraction Entrapment Electrophoresis

A custom 8-channel GELFrEE system was used on the whole yeast protein extracts and Atlantic salmon.[185] A 12% T polyacrylamide resolving gel column was cast in 4 cm long × 0.6 mm ID tubes to a height of 1 cm (127 µL) and then stacking gel (300 µL) was cast on top to a height of 3 cm. The system was run at 200 V with a PowerPac™ Basic Power Supply and 100 µL fractions were collected after the dye front as follows: 3×1 min, 3×2 min, 3×5 min, 3×15 min. Fractions from the same collection intervals were pooled together and visualized by SDS-PAGE and silver staining. Samples of low, medium, and high MW were made by pooling GELFrEE fractions together to create samples with relatively low, medium, and high ranges of molecular weights (details provided in Section 3.10 and shown in Figure 3.18).

2.11 Acetone Precipitation of Proteins

Acetone precipitation was conducted during the in-gel digestion of proteins from SDS-PAGE gels to deplete any residual SDS detergent. SDS-contaminated protein samples (100 µL) were combined with 400 µL of acetone (-20 °C) and incubated at 4 °C for 20 minutes.[41,186] The vials were centrifuged (9460×*g*, 5 min) to pellet the sample, supernatant was decanted leaving approximately 5 µL of residual solution, and this was further removed with air drying leaving behind the dried proteins.[41] The protein pellet underwent

two washing steps with 400 µL acetone and the supernatant was again discarded and any residual organic solvent was allowed to evaporate.

2.12 Tandem MS of Tryptic Peptides

Experimental and control AC-TME samples were analyzed on a LTQ linear ion trap mass spectrometer (Thermo Fisher, San Jose, CA) coupled to an Agilent 1200 HPLC. Each run consisted of 2 µg digested protein loaded onto a 75 µm × 30 cm self-packed Nanospray Tip (New Objective, Woburn, MA) containing 3 µm C18 Jupiter beads (Phenomenex, Torrance, CA). Peptides were resolved using a 1 hr gradient from solvent A (water/0.1% formic acid) to solvent B (acetonitrile/0.1% formic acid) as follows: 0 min, 5% B; 0.1 min, 7.5% B; 45 min, 20.0% B; 57.5 min, 25% B; 60 min, 35% B; 61 min, 80% B; 64.9 min, 80% B; and 65 min, 5% B. The flow rate was 280 µL/min but was split to the column to provide an approximate flow of 0.2 $\mu L \times min^{-1}$. LTQ was operated in data dependent mode, scanning *m/z* range was 400-1200 with zoom scan, and MS2 of top 5 ions.

TME-purified yeast and controls that did not undergo TME were further analyzed on an Orbitrap Velos Pro MS (Thermo Fischer) set to data dependent mode (MS followed by MS/MS of the top ten peaks) and using a Dionex Ultimate 3000 LC nanosystem (Bannockburn, IL), in MS mode at a resolution of 30 000 FWHM, scanning in rapid mode for MS^2 (66 666 $Da \times s^{-1}$, at <0.6 Da FWHM). The LC used a self-packed C18 (0.1×150 mm, Torrance, CA), coupled to a 10 µm New Objective PicoTip non-coated Emitter Tip (Woburn, MA) and used an 80-minute linear ramp from 5 to 35% acetonitrile in water and 0.1% formic acid.

2.13 Proteomic Data Analysis

Peptides were identified using the Proteome Discoverer software (version 1.4.1), searching the SEQUEST *S. cerevisiae* database (9000 entries, downloaded February 20, 2020), with allowed modifications of oxidized methionine or carbamidomethylation at cysteine. For MS analysis on the LTQ linear ion trap, the mass tolerance was set to 1.5 Da (MS mode) and 0.8 Da (MS/MS mode) and for the Orbitrap Velos 20 ppm (MS mode) and 0.8 Da (MS/MS) was employed. In each case, searching allowed up to two missed cleavages, and a peptide false positive rate of 1%, and 2 peptides per protein. Statistical analysis was done with Microsoft Excel using ANOVA and t-tests with results being significant if $p < 0.05$. An online software tool, Venny, was used to generate Venn diagrams and sort data lists.[187]

2.14 Safety Considerations

AC-TME is a research device and should only be operated with extreme caution; it uses high voltages without any automated safety shut off interlocks. It should be assumed that if there was human contact during operation, and an accidental shock occurred, that the user could be seriously harmed. The electrodes should be disconnected from the power supply before handling the device or pipetting samples. Because of exposed electrodes and electrolytes while operating TME, a safety box was designed to house the device while in operation, (see Section 2.2 Figure 2.4).

Chapter 3 Active-Cooled Transmembrane Electrophoresis[ǂ]

3.1 Introduction

Since the initial publication of TME by Kachuk et al. (2016), improvements have been presented to minimize the impacts of Joule heating, allowing application of stronger electric fields (Unterlander, 2018). This enabled a higher rate of SDS depletion while maximizing sample recovery.[165,166] However, the limitations of protein purification because of the effects of Joule heating in TME were still evident. This chapter provides an assessment and optimization of an alternative approach to overcome the shortcomings of resistive heating in the TME device, namely through active cooling. The goal of this technology is to withdraw heat from the sample well containing proteins, thus permitting higher operating conditions and faster purification times.

From prior work, the rate of SDS depletion was modelled mathematically on the assumption that the voltage remained constant throughout a "constant current" TME run (implying that resistance must be constant). However, it is shown here that temperature changes during the TME run result in a significant change in resistance, over the course of a constant current run. The net effect is a deceleration of SDS depletion over the course of the run. By contrast, AC-TME reverses this trend, and greatly improves the rate of SDS depletion. The newly constructed device (AC-TME) is applied to the manipulation of proteins isolated from cellular membranes for rapid purification of SDS ahead of LC-MS characterization of the resulting proteomic system.[188]

ǂ Portions of this chapter have been published in: Jakubec, P.J.; Doucette, A. A.; Automated Electrokinetic Platform for High-Throughput Sodium Dodecyl Sulfate Depletion Ahead of Proteome Analysis by Mass Spectrometry. *Analytical Chemistry.* (2021). DOI: 10.1021/acs.analchem.1c03549. Copyright (2021) American Chemical Society.

Previous TME research has focused on maximizing the sample recovery by mitigating any loss during TME process; thus, limiting the performance of the TME SDS removal platform. High temperatures lead to thermal denaturation of proteins native structures. Hydrophobic proteins, like membrane proteins, are especially prone to aggregating in aqueous solutions. Considering their structures, membrane proteins are more susceptible to thermal aggregation. These protein aggregates have previously been counted as a loss in the sample recovery, traded for the benefit of maximizing sample purity. Herein, an *in-situ* TME trypsin digestion was developed to target the thermally denatured proteins that aggregate and accumulate in the sample cell; thus, allowing for TME to be run at its maximum detergent depleting efficiency with near total retrieval of proteins samples.[188] AC-TME can purify proteins, with the capacity to accommodate samples of varying classes and sample matrix compositions, while maximizing the total recovery of samples with high process throughput for BUP experiments.

3.2 Experimental Protocol in Brief

The conventional TME system refers to that described by Unterlander, 2018, and was compared to the newly constructed AC-TME device, both with and without operating the active-cooling water radiator pump. Model proteins including BSA, whole yeast extract, cytosolic and membrane fractions of the yeast proteome, and Atlantic salmon (*Salmo salar*) muscle tissue were employed. A new tris Tricine (TT) background electrolyte was compared to the conventional tris Glycine (TG) TME buffer, and the amount of buffer required to run the device was also assessed. The performance of AC-TME was assessed in terms of SDS depletion rate, protein recovery, and system

temperature. The validity of an AC-TME purification protocol for membrane proteins was analysed with an enriched membrane proteins fraction, preparation from yeast protein extract for LC-MS characterisation and the data stored as XLSX files is shown in Appendix 1. An approach to recover proteins for bottom-up MS analysis through the direct addition of trypsin to the sample cells for *in-situ* TME trypsin digestion is presented. After an AC-TME run is completed and the sample solution is removed from the device, 8 M urea is added and allowed to mix inside the sample cells. Followed by TT buffer to dilute the urea and increase the volume of sample solution in the sample cells to cover the residual protein pellets in solution. The residual proteins are then trypsin digested by adding DTT, IAA, and trypsin enzyme, as described in Section 2.7.1.

3.3 TME with Tris Tricine Compared to Conventional Tris Glycine

The original TME system operated with a TG buffer system directly adapted from the Laemmli SDS PAGE method. While this buffer is ideally suited for protein focusing in SDS PAGE through isotachophoresis, these characteristics are not applicable in TME and therefore the TG buffer may not be optimal for TME performance. Differences in the TG buffer components pKa's, relative to the pH and the ratio of charged to uncharged ions, do not lend themselves favorably to TME. The ratio of buffer species that are in the charged state is very low relative to the total concentration of buffer species in solution. These uncharged buffer components increase friction without adding ions.

The incorporation of TT with SDS PAGE was originally done in the 1980's when Schagger and von Jagow aimed at separating smaller mass proteins (1 to 30 kDa) by SDS PAGE.[80] The requirements of a TME electrolyte are to simultaneously supply cations and

anions for the electrophoretic system, while buffering a near constant system pH. From the Henderson-Hasselbalch equation shown below the ratio of acid and base species were calculated for each of the buffer components (tris, glycine, and Tricine).

$$10^{(pH-pKa)} = \frac{[A^-]}{[HA]} \qquad \text{Equation 3.1}$$

The previously published TME versions used 25 mM tris and 192 mM glycine at pH 8.3. This compares to the new TT that consists of 100 mM tris with 100 mM Tricine. The glycine and Tricine buffer systems adopted for TME share the same pH (8.3), though they yield different concentrations of ionic species in solution. The structures of each of these four buffer components is shown in Figure 3.1, in their respective charge states over the full pH range. Glycine and Tricine are zwitterionic molecules and both species can exist with either a net neutral, or a negative charge of -1. Both components of the respective TG and TT buffers, can serve to buffer the solution pH. However, the pKa of Tricine (8.15) is significantly closer to pH 8.3 compared to glycine (9.6), resulting in a larger portion of Tricine ions that are in a negatively charged state (~58% Tricine *vs.* ~5% glycine *vs.* ~37% tris).

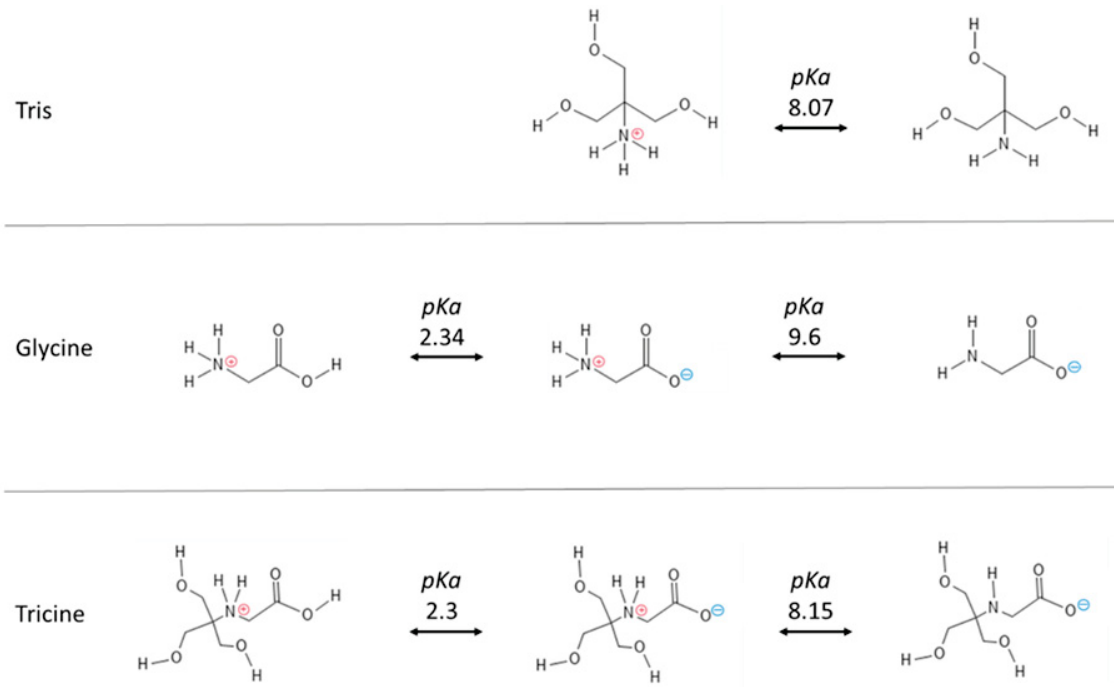

Figure 3.1 Chemical structures for buffer species, tris, glycine, or Tricine, used in TME buffers and their respective *pKa* values and charge states. Both glycine and Tricine are zwitterionic and yield a ratio of anionic and net neutral species, compared to cationic tris.

At the working concentrations employed for TME, and considering the pH of the solution, 37.2 mM Tricine, and 9.3 mM glycine are calculated to be present in the anionic form. Glycine is added at nearly twice the concentration of Tricine (192 mM vs 100 mM) and yet generates only a quarter of the anions (9.2 mM) in the electrolyte solution. From the 100 mM TT buffer 58.5 mM of the Tricine component is in the anionic charge state. Tricine reportedly has a lower effective mobility than glycine, but the higher charge concentration provides a lower solution resistance.[80,188,189] By the end of TME runs using TG buffer, the voltage consistently began to continuously increase from 45-60 minutes, seen in Figure 3.2. This is indicative that the concentration of residual ionic species available in solution, and responsible to carry the current, has diminished thus increasing the total solution resistance. Adopting the TT buffer system for TME supplies a more stable

concentration of ions in solution that can be approximately maintained over the course of an AC-TME run with lower resistance facilitating operation at higher current.

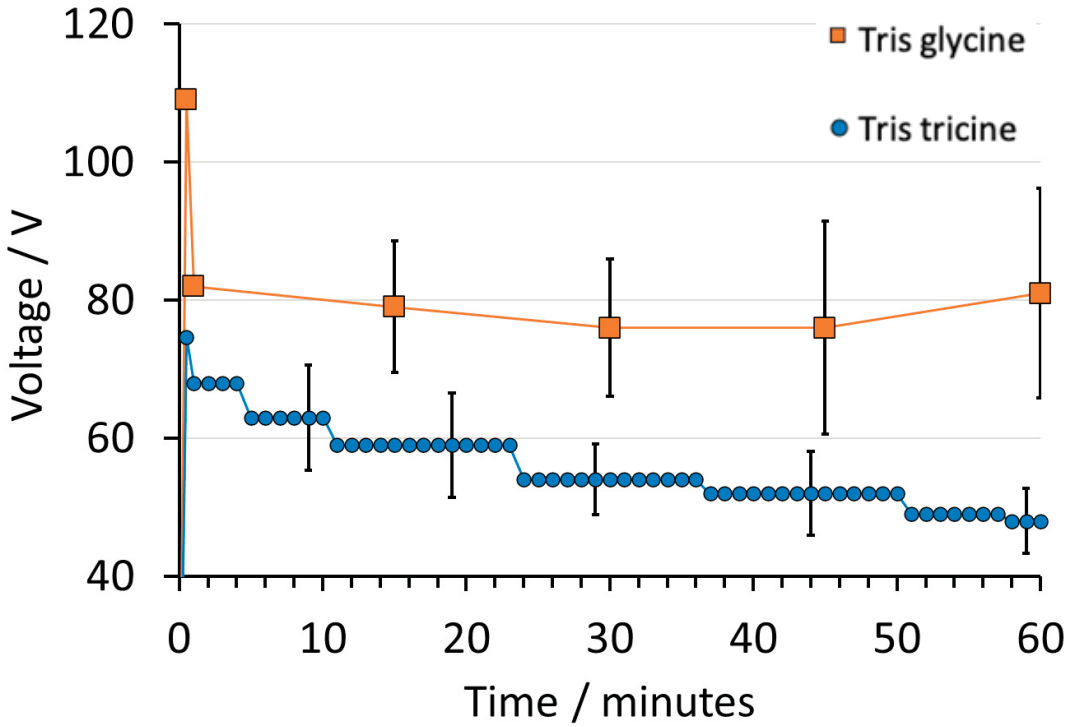

Figure 3.2 Voltage plots of TME runs operated at 50 mA with the TG and TT buffers showing the average and standard deviation (n = 3) of the voltage achieved while purifying 0.1 g×L^{-1} BSA initially prepared in 0.5% SDS.

From prior work, operating conventional-TME at an applied current of 50 mA with the TG buffer system permitted SDS depletion from 0.5% initial (5000 ppm) to a residual concentration less than 10 ppm in 1 hour.[166] The rate of SDS depletion obtained (achieving <10 ppm residual SDS) using the TT buffer was higher than that obtained with the TG buffer. The calculated half lives, from the exponential decay constants from the decay curves shown in Figure 3.3 were: TT= 5.5 ± 1 min; TG = 6.3 ± 1 min. Pairwise t-testing confirmed this to be a statistically different rate of depletion rate (t-test, $p < 0.01$) when using the glycine-based buffer. The TT buffer was employed in TME, and tested under the identical operating conditions, with results shown in Figure 3.3. The rates of SDS

depletion, reported through the decay constant with TT buffer (M = 0.11 ppm×min^{-1}, SD = 0.01) were significantly faster ($t(4) = 4.2$, $p < 0.01$) than those of the TG buffer (M = 0.13 ppm×min^{-1}, SD = 0.01).

At the low operating current of 50 mA, the final sample temperatures for the glycine and Tricine buffer systems were 54 ± 4 °C and 52 ± 2 °C, respectively. The temperatures of the sample wells were therefore not statistically different between the two buffer systems operated at 50 mA. Both buffer systems yielded the same, high recoveries (95 ± 5 %) of the BSA proteins from the TME sample cells. However, when operating TME at 100 mA for 30 minutes, the differences between the buffer systems became more pronounced. The final temperatures observed were 67 ± 1ºC and 59 ± 4ºC for TG and TT buffers respectively. In this case, the temperatures were statistically different (p = 0.02), and the protein recoveries are also reflected in these temperature differences. Owing to the lower operating temperature, the TT buffer provided a higher recovery (96 ± 2 %), relative to that obtained in the TG buffer (91 ± 5 %). The TT buffer also depleted 5000 ppm to less than 10 ppm in 50 ± 5 minutes while the TG buffer took longer at 60 ± 2 minutes.

The faster rate of SDS depletion achieved using the TT buffer, along with the published research supporting its ability to better separate SDS from smaller (1-100 kDa) protein complexes, reinforce the TT buffer system as an improvement for AC-TME. The TT buffer has a higher concentration of ionic species in solution that allowed for longer TME runs and at higher constant currents before the buffer ions were depleted. The tris

Tricine buffer system was adopted and used for all TME experiments from this section (and Section 3.4.1) onwards.

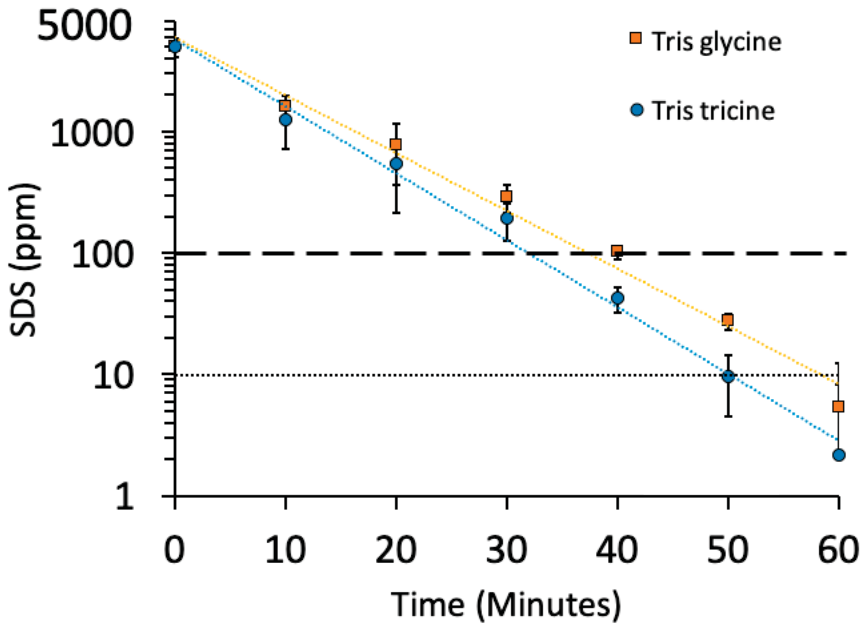

Figure 3.3 Plots of TME runs (n = 3) operated at 50 mA using 0.1 g×L^{-1} BSA initially prepared in 0.5% SDS with one of two buffer systems: 25 mM tris and 192 mM glycine or 100 mM tris 100 mM Tricine buffers. TG and TT exponential decay fit equations are $y = 5940.7e^{-0.11x}$ and $y = 5718.3e^{-0.127x}$, respectively.

3.4 Changes in Buffer pH Throughout the Course of TME Operation

The TME electrolyte buffer conducts the electric field that is generated inside the TME device between the anode and cathode buffer chambers and sample cell, but importantly it also maintains the pH of protein samples during the purification protocol. Without buffering, the pH of the cathode and anode chambers will drift, owing to the electrolysis of water. The resulting pH gradient generated across the TME device (acidic at the anode and basic at the cathode) leads to isoelectric protein precipitation which significantly reduces protein yields. The pH changes of the anodic and cathodic buffers were compared during TME operation using the TT system. As a control, measurements

of pH were conducted before and after TME runs in the absence of active cooling, using a test sample comprising 0.1 g×L^{-1} BSA contaminated with 5000 ppm SDS. TME was operated at three applied currents: 50 mA, 100 mA, and 150 mA and pH measurements were recorded following 20 min operation (Figure 3.4A) after the residual SDS dropped below 10 ppm (150 mA = 20 min; 100 mA = 40 min; 50 mA = 60 min). The difference in pH between cathode and anode buffer for the latter is shown in Figure 3.4B.

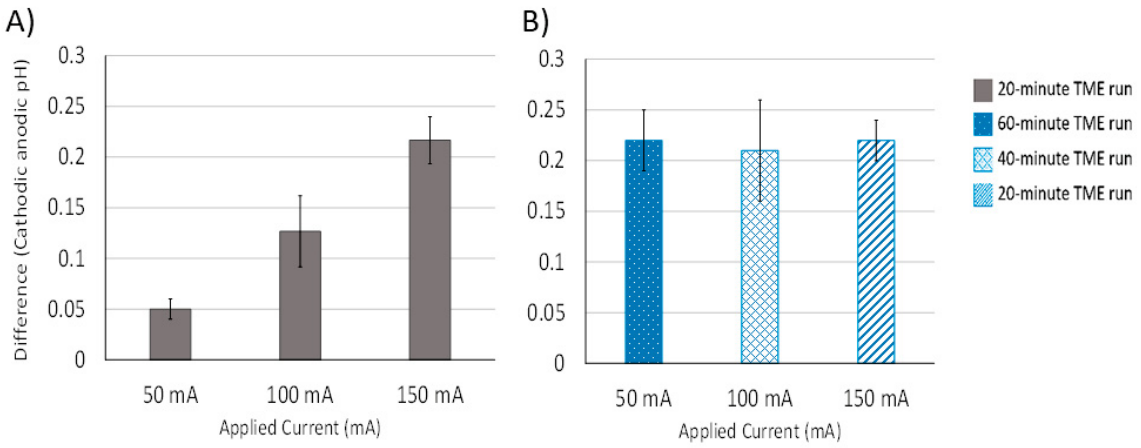

Figure 3.4 Differences in pH between the cathodic and anodic buffers following a TME run of 0.1 g×L^{-1} BSA in 5000 ppm SDS, operated at 50, 100, 150 mA. The initial TME buffer pH was 8.3. A) Shows runs depleted to <10 ppm, 50 mA stopped at 60 min, 100 mA at 40 min, and 150 mA at 20 mins and B) shows runs stopped at 20 min. Error bars represent the standard deviation of 3 replicate measurements.

It is evident from Figure 3.4A that operating TME at higher currents results in a greater change in pH, when each is confined to an equal operating time. However, TME operation at lower current requires a longer run time to purify a protein to an equivalent level of residual SDS. When the varying run times is taken into consideration for TME operated at different currents the resulting buffer pH drift was equal for each system, shown in Figure 3.4B. No significant changes to buffer pH were observed when varying the applied currents, from a one-way ANOVA ($F_{2,2} = 0.01$, $p = 0.98$, $\alpha = 0.05$). Even though the electric field is stronger with larger applied current the amount of TME operating time required to

achieve a residual SDS concentration of 10 ppm decreases. The net effect is to achieve similar amounts of ions moving through the system. It is interesting to note that the combination of a lower operating current with the proportionally longer run time required to deplete SDS to an equivalent level revealed the same pH drift. This can be explained when considering Faraday's first law of electrolysis. The amount of time and the magnitude of the applied current that TME was operated under yield the number of ions expended during TME operation. The total molar quantity of singly charged ions transported in the TME system can be calculated as the product of Faraday's constant, shown in Equation 3.2. The mass of substance liberated in grams, m, the current (amperes), *I*, and time (seconds), *t*, the species molar mass (g/mol), *M*, *F* is the Faraday constant (96,485 C), and *z* is ions valence number.

$$\mathrm{m} = \frac{MIt}{Fz} \qquad \text{Equation 3.2}$$

Theoretically the 100 mA TME runs should have shown the largest pH drifts between the anode and cathode buffer chambers because, of the three applied currents tested, it would have expended the most ions during its operating interval. The 100 mA yields approximately 2.49 mmol of ions expended compared to the 50 and 150 mA runs at 1.86 mmol, respectively. This number of ions expended represents the charge carried by both cationic and anionic species reacting at both electrodes. Therefore, the ion expenditures represent ions reacting at both the cathode and anodes. The true amount of buffer components reacting at either electrode depends on the transference number of the ions in solution. This value will change depending on the concentration and ionic mobility of every ion in solution. The concentration and mobility of tris and tricine are of a similar order of magnitude, allowing an estimated calculation that a 100-mA run yielded approximately

1.25 mmol of tricine ions expended compared to the 50 and 150 mA runs of 0.93 mmol, respectively. The amount of charge flowing through the cell is directly proportional to the amount of substance reacting at each electrode as described by Faraday's law of electrolysis.[190]

These differences were not reflected in the observed pH drift of the buffer likely because the total amount of charged ions in solution was still enough to buffer the system, so any differences were too small to measure. The TT buffer provides nearly an order of magnitude more charged ions than the amount being expended during TME operation. The drifts in buffer pH may be expected to be larger with the conventional TG TME buffer (Section 3.4.1 provides more details) because the amount of charged ions in solution is approximately five times lower.

3.4.1 Electrolyte pH changes at Low and High Buffer Volumes

A newly designed TME platform was constructed and assessed with the goal of minimizing heat sinks in non-thermally conducting materials near the sample cells and to maximize the transfer of heat to active-cooling tubes. Both aim to improve the yields of recovered samples and to push the rate of protein purification. The new design features significantly smaller buffer chambers, which contain a maximum 50 mL of buffer solution per side, compared to the original device which contains a maximum of 360 mL per side. A potential concern to moving to a smaller buffer chamber was the adequate supply of charged ions in solution to maintain current and to buffer the samples. The efficiency of TME is limited by the finite amount of charged ions contributed from both buffer species and once attracted to their respective electrodes they are not replaced (see Figure 3.2 in Section 3.3). The changes in buffer chamber pH were measured following TME runs in the

original and newly constructed devices, as a function of the buffer volume employed, with both the TT and TG buffers. The results from pH changes of TME buffers with varying volumes from a 30 min run at 100 mA (SDS concentration <100 ppm) are plotted in Figure 3.5 and shown in Table 3.1. For all the experiments in this section the conventional-TME platform, as published by Unterlander,[166] was applied except for the experiments in Table 3.1 highlighted in grey that used the new AC-TME device (described in detail in Section 3.5 and 3.6) but with the circulating-water active cooling turned off.

The magnitude of the pH drift between the two buffer chambers was largest for the lowest volumes employed (30 and 60 mL), regardless of buffer type. Similarly, the smallest shifts were seen with the largest volume of buffer (360 mL), seen in Figure 3.5. This can be attributed to the lower volume, which also means lower amount of buffer components. There is a lower buffering capacity to maintain a pH of 8.3 with smaller volumes.

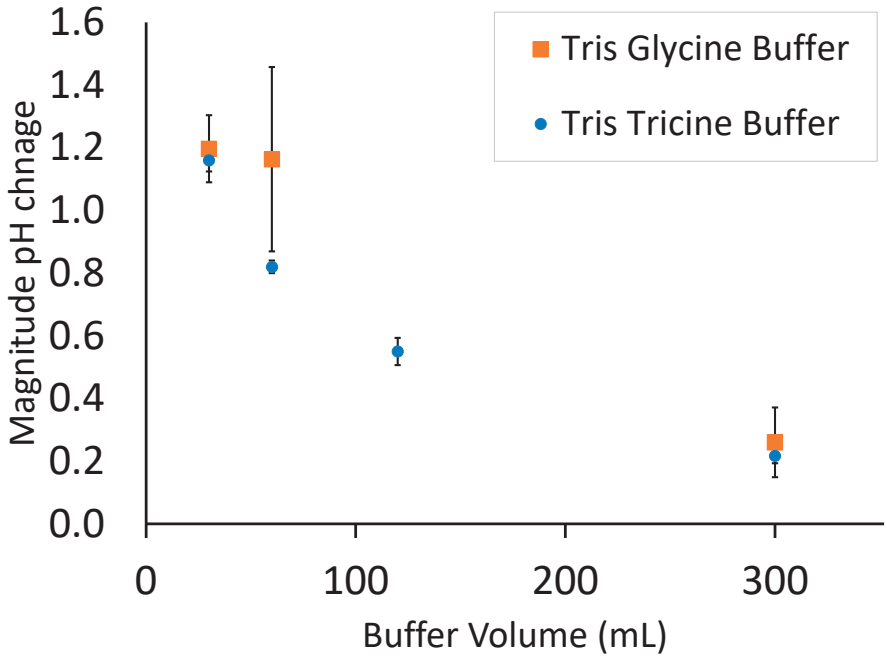

Figure 3.5 The magnitudes in pH change between the anodic and cathodic buffers as a function of their volume: 30, 60, 120, 360 mL using TG and TT buffers with TME operated at 100 mA. Error bars represent the standard deviation from 3 replicate measurements.

The larger volumes of buffer provided several benefits that included the better buffering capacity to maintain the pH of solution while also holding more charged ionic species available at disposal for electrophoresis. From Table 3.1, rows highlighted in grey are uncooled runs at full (50 mL) and half volume (25 mL) with the AC-TME (not using active-cooling) platform while the other rows represent varying volumes of buffer with the previously reported TME platform.[160]

Table 3.1 pH shifts for TME buffers using the previous conventional-TME platform and the new AC-TME (grey), but without using active cooling. Averages and standard deviations of three replicates.

Concentration	Volume of Buffer	Post-TME pH		
		Cathodic Chamber	Anodic Chamber	Difference
100 mM tris and 100 mM Tricine	360 mL	8.44 ± 0.02	8.23 ± 0.01	0.22 ± 0.02
	120 mL	8.52 ± 0.02	7.97 ± 0.06	0.55 ± 0.04
	60 mL	8.69 ± 0.02	7.87 ± 0.02	0.82 ± 0.02
	30 mL	8.80 ± 0.03	7.64 ± 0.06	1.16 ± 0.04
	50 mL	8.51 ± 0.06	8.04 ± 0.05	0.46 ± 0.08
	25 mL	8.78 ± 0.04	7.60 ± 0.06	1.18 ± 0.07
25mM tris and 192 mM glycine	360 mL	8.44 ± 0.04	8.18 ± 0.08	0.26 ± 0.11
	120 mL	8.79 ± 0.10	7.63 ± 0.21	1.16 ± 0.29
	30 mL	8.81 ± 0.01	7.62 ± 0.10	1.20 ± 0.11

3.5 AC-TME Design and Characteristics

The schematic of the basic concept of AC-TME is depicted in Figure 3.5 (see Figure 2.2 in Section 2.2 for AC-TME design and technical details). Heat is withdrawn from the buffer chambers by flowing cold water (1.0 ± 0.5°C) through borosilicate glass tubing immersed within these buffer solutions. In turn, the colder buffer draws heat from the sample cell. A 100 mM tris Tricine (pH = 8.3) buffer was adopted for the AC-TME protocol, as per Section 3.4. During a TME run, the highest temperatures are recorded

inside the sample cell, being a consequence of higher resistance, including ion passage through the MWCO membranes.

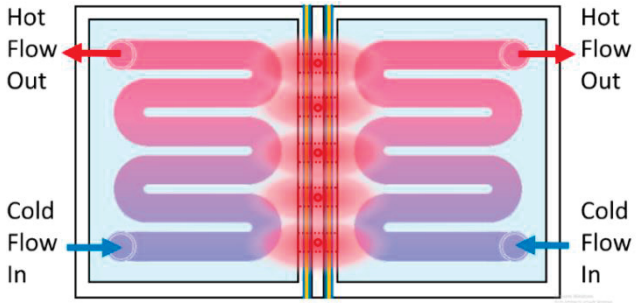

Figure 3.6 Schematic of the assembled TME device with cooling tubes in the buffer chambers. Water at 1.0 ± 0.5°C enters the tube and absorbs heat from the surrounding buffer chambers. The heat flow is depicted by the colour blue transitioning to red. The flux of ions encounters a bottleneck at the sample cartridge resulting in the highest solution temperatures at this region. The chilled buffer chambers can absorb the excess heat form the sample cartridge solution.

Unterlander and Doucette (2018) showed that stir bars placed inside the sample cells aided in the dispersion of Joule heat from the sample chamber to the surrounding buffer chambers. However, the previous conventional-TME platform could only operate at a maximum (70-100 mA) to maintain sample temperatures below a threshold temperature of 60°C.[166] Beyond these operating currents, the implementation of scheduled pauses of TME operating during the detergent removal runs was required. The power was turned off to allow the sample temperature to drop before resuming conventional-TME operation causing lengthened experiment time. More importantly, it is the applied electric field, generated when the power is turned on, that drives the anionic SDS to the anode and away from the proteins inside the sample cell. Back diffusion theoretically occurs as soon as the applied electric field is removed and the concentration gradient of high SDS-containing buffer in the anode chamber and low residual amounts of SDS drives the detergent back

through the MWCO and into the sample cell. The electromotive force from the applied electric field is the only force holding the SDS away from the proteins.

The previous iteration of the TME platform was still reliant on passive heat diffusion into the rest of the system. With most of the heat entering the electrolyte buffer and the stock Delrin® and Teflon™ materials that comprise the TME device and the pre-chilled buffer and requiring the power to be turned off to stop heat formation and allowing time for the heat to diffuse.[165] The addition of stir bars improved the passive diffusion of heat from the sample cells allowing for continuous operation without pausing intervals, but temperature regulation was still reliant on passive heat diffusion.[166] AC-TME was designed to withdraw heat from the samples allowing for operation at higher constant currents but also purifying protein samples faster than conventional TME and with less thermal denaturation to the proteins.

3.6 Sample and Buffer Temperature Control using AC-TME

The objective for the AC-TME platform was to maximize the rate of SDS removal from proteins. The parameter that influences the recovery of proteins most is the temperatures they are exposed to during duration of TME operation. It was determined that proteins exposed to temperatures exceeding 60°C showed significant thermal denaturation (see Section 1.2.1) increasing their probability to aggregate and adhere to the sample cell.[76,193,194] To evaluate the operating characteristics of the device and establish parameters for successful and controlled experimental procedures the updated AC-TME system and protocol was tested at higher operating currents than previously permitted.

To maintain the protein samples solubility during TME purification the platform was limited to passive diffusion by storing the device components at -4°C and the buffers at 4°C before each run. This worked with low constant current runs and samples that are characteristically more soluble in aqueous buffers. By actively cooling the sample the system is not limited to Joule heat passively diffusing from the sample cells. This was the reasoning behind testing the smaller volumes of buffer in Section 3.4 (see Table 3.1) as the transfer of heat between the sample cells and active cooling tubes is theoretically maximized. This is compared to the larger volumes that conduct the heat generated from Joule heating but then act as a heat sink. Buffer chambers were designed to provide volumes of buffer large enough for the adequate supply of charged ions, but small enough to not retain the heat in the solution. This is necessary for electrophoresis and to buffer the sample solution without negatively impacting the protein's recovery. Making the ratio of cooling tube surface area to volume of buffer solution largest was hypothesized to maximize the exchange of heat between buffer and cooling tubes. The extent to which the active-cooling water-cooled radiator would withdraw heat from the sample wells was tested across a range of constant current TME runs, with results summarized in Table 3.2. The data were recorded over a set time interval of 30 minutes to compare the temperatures being produced with each applied current setting. These run times and power settings would achieve varying levels of success with respect to protein purity and recovery.

Table 3.2 Temperatures recorded at the end of 30-minute TME runs on 1 g×L^{-1} whole yeast proteome in 0.5% SDS listed as averages and standard deviations, n = 3.

Applied Current (mA)	Uncooled		Active-cooled	
	Sample Temperature (°C)	Buffer Temperature (°C)	Sample Temperature (°C)	Buffer Temperature (°C)
50	43 ± 6	34 ± 4	32 ± 5	13 ± 4
100	58 ± 4	45 ± 5	35 ± 3	14 ± 5
150	66 ± 5	52 ± 5	39 ± 4	17 ± 4
200	74 ± 6	68 ± 1	42 ± 2	23 ± 2
250	96 ± 5	76 ± 7	45 ± 3	27 ± 1
300	n/a	n/a	51 ± 6	32 ± 5
350	n/a	n/a	58 ± 3	32 ± 4

At all operating currents, the sample temperatures reached by the AC-TME system were significantly lower than those in the conventional TME platform, as calculated from a two-way ANOVA ($F_{2,2}$ = 346, $p = 4.22\times10^{-14}$, $\alpha = 0.05$). Currents above 100 mA would have previously exceeded the maximum thermal limit of 60°C limit with the conventional, uncooled device. The same was seen with this platform, from Table 3.2 the updated AC-TME platform but without active cooling yielded temperatures of 66 ± 5 when using 150 mA constant current. The slightly higher temperatures with the smaller AC-TME device come from the fact the device components were not stored at -4°C as the previous systems were and the lower volumes of pre-chilled buffer used. Active-cooling the new AC-TME system allows for the applied current to be increased up to 350 mA and still maintaining sample cell temperatures of 58 ± 3°C and buffer temperatures of 32 ± 4°C.

The primary concern of a higher sample temperature is that it increases the risk of thermal aggregation of protein, particularly as the detergent (SDS) that was maintaining the proteins solubility is no longer present. The sample temperature over a range of currents with the uncooled TME system are shown in Figure 3.7. The sample cell temperatures

increased continuously throughout AC-TME runs when active-cooling was not used. It was not possible to apply greater than 350 mA to the uncooled TME system as the samples would boil inside the cell and bubble out the top of the device.

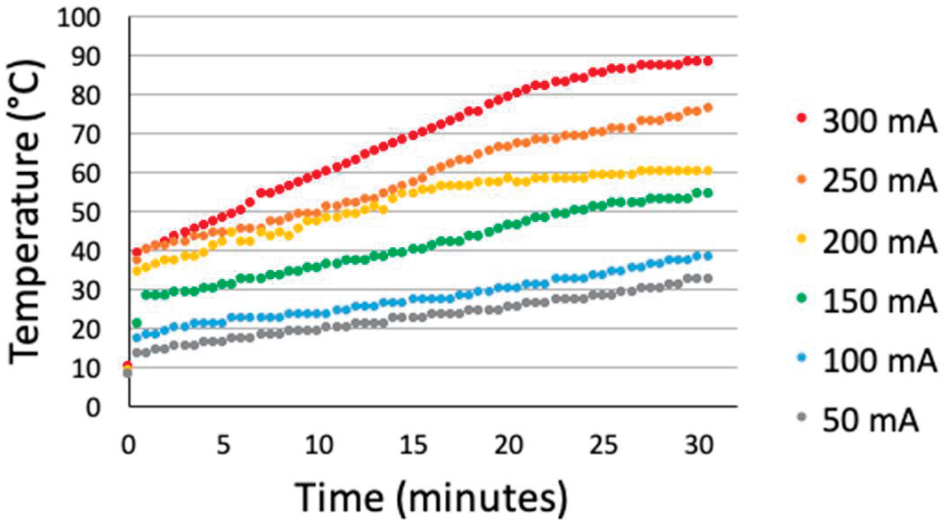

Figure 3.7 Temperatures of the sample solutions in the sample cells recorded every 60 seconds over 30-minute TME runs of 1 $g \times L^{-1}$ whole yeast proteome in 0.5% SDS without the AC water-circulating control system.

The circulating-water AC system withdraws heat from TME buffers so that the device does not retain the heat from Joule friction and instead the temperature is maintained relatively constant during the duration of the run. When no power is applied (0 mA, 30-minute TME run) the sample cell maintained 3 ± 2°C and buffers 4 ± 2°C at 0 mA, no power applied. The platform will maintain these low temperatures indefinitely if the ice bath is continuously refilled with ice and the pump keeps the flow circulating. Contrasting the increasingly higher temperatures (Figure 3.7) reached with the uncooled TME system, the AC-TME maintained sample cell temperatures below the critical 60°C thermal denaturation threshold, shown in Figure 3.8. Protein solution temperatures inside the sample cells were 35-40°C lower with the AC system when operating at 200 mA a current

that the previous TME iterations would result in diminished protein recoveries.[165,166] Maintaining sample protein temperatures below the critical denaturation temperature (60°C) was critical to accelerate the rate of detergent depletion without compromising sample recoveries.

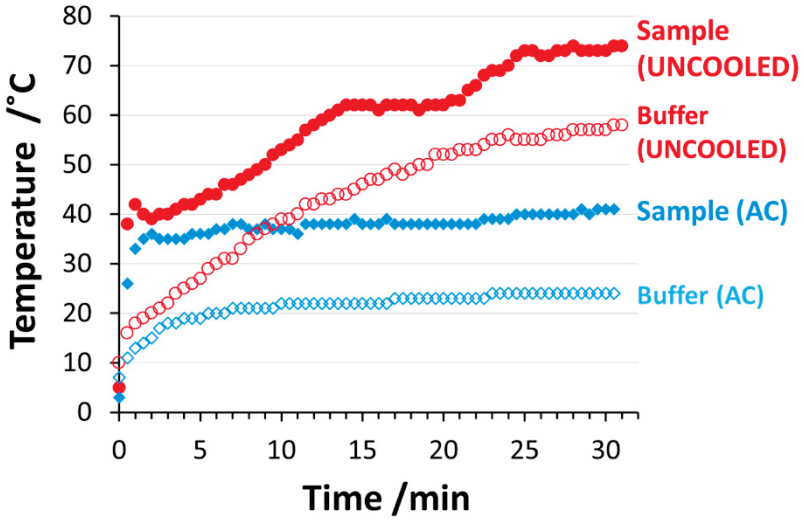

Figure 3.8 TME runs with and without the water radiator for temperature control at 200 mA. For constant current TME runs, the system temperature will increase throughout the run, owing to Joule heating. Active cooling (AC) withdraws heat from the solution in the buffer chamber, which in turn decreases the samples temperature. With a conventional, uncooled TME run, the sample cell exceeds 60°C temperatures following approximately 15 min of operation.

The AC-TME platform actively generates and continuously maintains a temperature gradient that withdraws heat produced, even the large amounts of Joule heat generated during electrophoresis. TME has been previously successful at purifying a variety of protein types with the passive methods at generating the temperature gradient from the sample cell and its surroundings for minimizing the high temperature exposure during a TME run. Now AC-TME is the next iteration with the capacity to process high throughput with maximum yields, even with proteins susceptible to thermal denaturation and aggregation (discussed in detail in Section 3.11).

3.7 Increased Protein Recovery with AC-TME versus Conventional

TME purification is beneficial as it depletes the free detergent monomers present in solution but also removes protein-bound SDS molecules while maintaining high sample recovery. The electromotive force generated by TME is sufficient to overcome the binding energy between surfactant and protein and drive the SDS detergent from the sample cell to the anode. The challenge of this process arises in maintaining protein solubility following detergent removal. The physicochemical characteristics of the proteins in the sample are expected to correlate with their recovery efficiency following AC-TME purification. The conventional-TME platform described by Unterlander was employed to deplete 5000 ppm SDS from a 1 $g \times L^{-1}$ sample of a single protein (BSA) as well as complex proteomes of varying hydrophobicity (BSA single protein < cytosolic < whole yeast proteome < membrane proteome).[195–199] TME was operated at 100 mA, after which the concentration of protein remaining in solution was measured. In general, the recoveries were seen to decrease as a function of the sample's relative hydrophobicity, as shown in Figure 3.9.

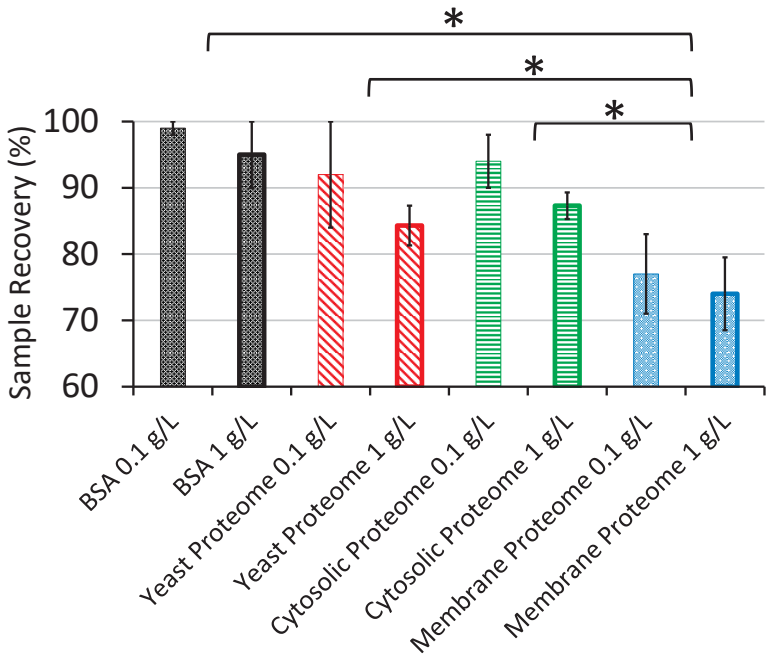

Figure 3.9 Sample recoveries for TME runs at 100 mA with the conventional TME platform as described by Unterlander (2018). The symbol * denotes statistical differences between membrane proteome recoveries and the other sample types (t-test, $p < 0.05$)

Membrane-protein enriched samples are especially susceptible to thermal aggregation. These hydrophobic proteins are expected to convey the lowest recoveries following TME purification. However, controlling the impact of Joule heating via the AC temperature gradient should hypothetically decrease the extent of protein thermal denaturation and result in the larger recoveries from the AC-TME platform compared with AC-TME with circulating water off, this is seen in Figure 3.10. Previously published TME prototypes relied on managing the heat build-up by allowing it to passively diffuse into the TME buffers and device components. At the highest operating parameters, to prevent the solution from boiling during a run, the power supply had to be intermittently turned off to allow time for heat to diffuse from the sample well. It is noted that the cumulative times refer only to when power was supplied to the TME system; the true run time is approximately

double that which was plotted. Pre-cooling the setup (-4°C) was done to maximize the temperature gradient between the sample cell and external environment to avoid high temperatures building up.[165,166] In addition to higher overall recovery, the variance in protein recovery measured between the replicate samples at each time interval (note the error bars of Figure 3.10) was lower with AC-TME compared to the uncooled platform. Increased variance is generally seen at lower recovery and is hypothesized to be a consequence of the protein aggregation, causing fouling of the MWCO membranes. This can limit the flow current through the sample cell. Membrane proteins are generally more hydrophobic because of their inherent structure and native environment.[200] Therefore, membrane-enriched protein samples are difficult to purify with high sample yields. However, AC-TME was able to deplete SDS from this sample to sufficient levels to permit LC-MS and still retained ~90% sample at this high operating parameter (250 mA).

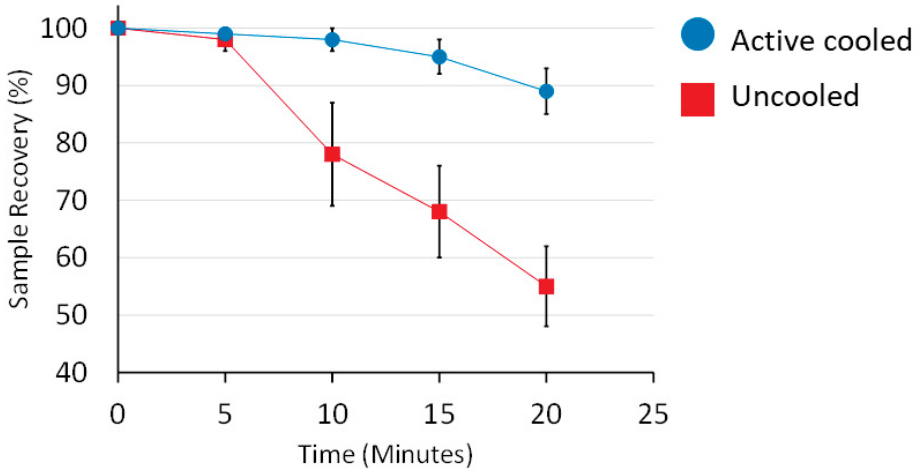

Figure 3.10 Sample recoveries for TME runs at 250 mA with (blue) and without (red) active-cooling on 1 g×L^{-1} membrane-enriched *S. cerevisiae* protein samples originally contaminated in 5000 ppm SDS and purified to a residual detergent concentration of <10 ppm.

In-gel digestion of proteins separated by SDS PAGE is a classic approach to process samples ahead of MS. Although SDS PAGE is a detergent-based workflow, proteins are physically entrapped in the gel matrix, allowing the surfactant to be extracted from the proteins prior to digestion through solvent washes of the gel slice. Thus, this technique is appropriate to manipulate membrane proteins for bottom-up MS analysis. However, the recovery of peptides following in-gel tryptic digestion was compromised. This is shown in Figure 3.11. Based on the ratio of peak area compared to the control, representing an equivalent amount of sample digested in solution, the percent recovery from in-gel digestion was 26.7 ± 9.4% (n = 3). The low yields may be due in part to proteins being released from the gel during the numerous rinsing and washing steps which the protocol incorporates.[201] Alternatively, the Doucette group has optimized an SDS-based workflow involving acetone precipitation to remove the surfactant while maintaining high protein recovery. Acetone precipitation is a robust detergent depleting method based on organic solvent protein precipitation. The method has also been applied to remove SDS with unbiased protein recoveries. Figure 3.11 demonstrates a substantial improvement in recovery relative to the in-gel digestion approach, with 90.3 ± 5.8 % yield observed. While this is considered a high yield, protein precipitation is a manual process that requires considerable user expertise to maintain high recovery. The AC-TME platform is considered a fully automated approach to protein purification. As seen in Figure 3.11, AC-TME provided yields of 93.5 ± 6.6%. Furthermore, this is nearly double the recovery of the AC-TME with water-circulating off (uncooled), that yielded only 58.9 ± 10.4%. Active-cooling of the TME platform-maintained protein recovery equivalent to acetone

precipitation and yielded over 30% more proteins than the conventional-TME iterations and over triple the amount from in-gel digestion.

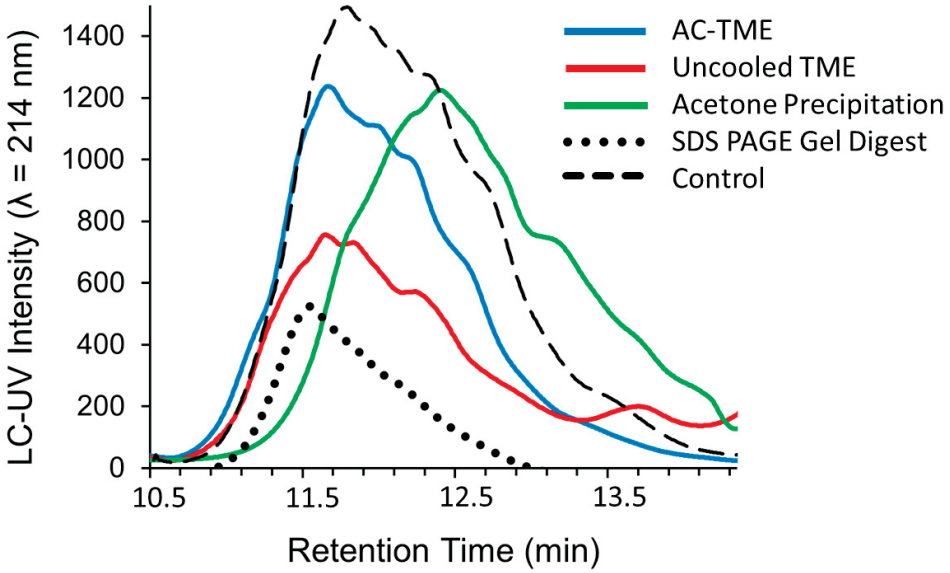

Figure 3.11 Representative LC-UV peak intensities (λ = 214 nm) as seen of *S. cerevisiae* whole proteome tryptic peptides from a control (no SDS, no AC-TME purification), and three samples depleted of 5000 ppm to below 10 ppm via either AC-TME, uncooled TME, or acetone precipitation.

The recoveries of *S. cerevisiae* cytosolic and membrane protein fractions cleaned of SDS by TME were quantified for AC-TME runs (with and without using cold water-circulating) operated from low to high current (50-350 mA), shown in Figure 3.12. SDS detergent removal with the AC-TME platform maintains yields above 80% even from the membrane-enriched proteins. Note that applying constant currents greater than 200 mA resulted in elevated temperatures above 60˚C (discussed in Section 3.6 and shown in Figure 3.7) with the potential for the sample solution to reach boiling temperatures, especially for runs conducted at 300 and 350 mA.

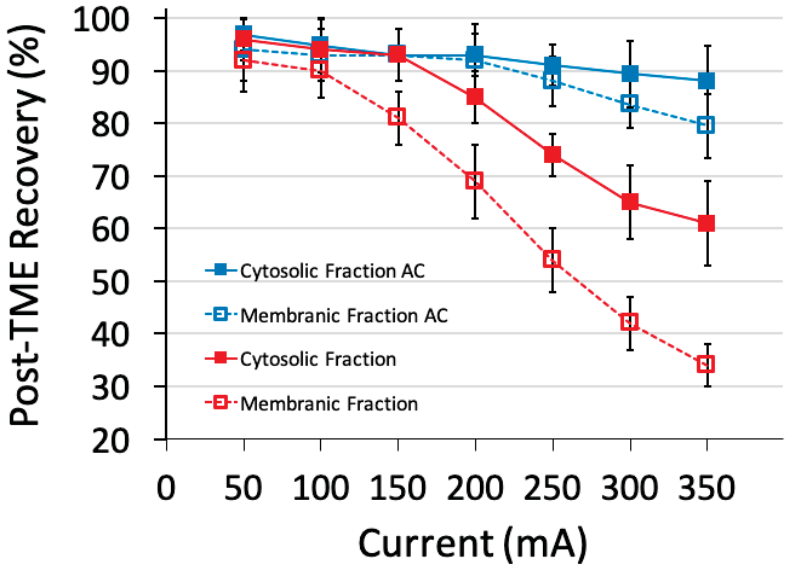

Figure 3.12 TME runs with (blue) and without (red) water circulating for AC temperature control on 1 g×L^{-1} cytosolic and membrane yeast fractions in 5,000 ppm SDS depleted to less than 10 ppm over the range of applied currents 50-350 mA.

To assess the reproducibility of TME in terms of sample recoveries using the AC system it was tested at a low and high applied currents (100 and 200 mA) and the rate of SDS depletion was monitored along with protein recovery. AC-TME operated at 100 mA and 200 mA and depleting 1 g×L^{-1} whole yeast proteome in 0.5% SDS until <10 ppm residual SDS was replicated over five experiments (n = 5). The 100 and 200 mA AC-TME purifications yielded decay constants of 0.13 ± 0.01 and 0.34 ± 0.08 min^{-1} and protein yields of 93 ± 9 and 90 ± 9%, respectively. The AC-TME platform that actively withdraws heat using a temperature gradient consistently and reliably purified protein samples to acceptable levels for LC-MS (<10 ppm) with improved yields.

3.8 SDS Depletion as a Function of Applied Current

Because AC-TME is designed to continuously remove heat (Figure 3.4) it allows for higher operating currents which result in faster rates of SDS removal from proteins while maintaining their temperature below a thermal denaturing point that would induce precipitating out of solution (previously shown in Section 3.7). The continuous removal of heat allows AC-TME to be operated at higher constant currents (>100 mA), thereby increasing the electric field strength, and increasing the rate of SDS removal. This is seen in Figure 3.13 comparing across 40 mA to 350 mA applied current. A residual level of 100 ppm is considered the maximal permissible level of SDS remaining in a sample to permit MS analysis of the proteomic mixture. However, 10 ppm is most desired as below this level is considered optimal for MS analysis.

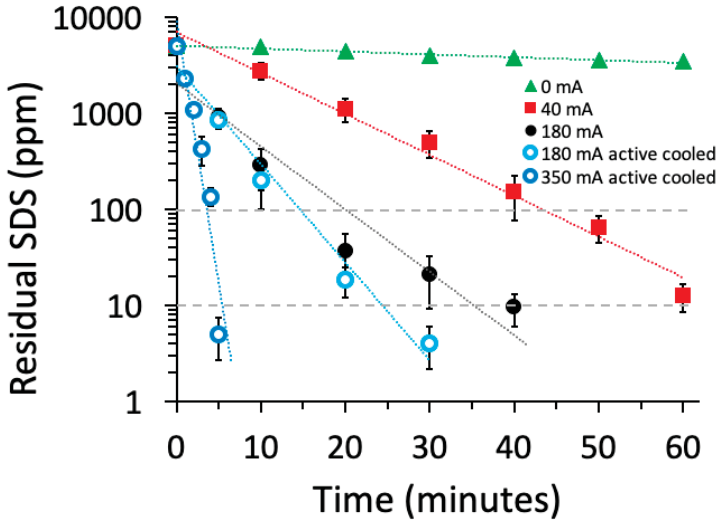

Figure 3.13 SDS depletion by TME, plotted on a logarithmic scale, shows accelerated protein purification at higher current for both conventional (uncooled) and active cooling (AC) operations.

The rate of SDS depletion was previously modelled on the assumption that voltage and temperature remained constant during TME runs. These assumptions do not hold at higher operating currents, particularly with the conventional TME system. Operating at non-constant temperature impacts the resistance and thus causes voltage to drop over the course of a TME run. Note that the active-cooling TME system showed higher voltages being used when operating compared to the uncooled system, seen in Figure 3.14. This should theoretically translate to faster SDS depletion rates, per Equation 1.1 seen in Section 1.5, as higher voltages increase the strength of the electric field which is the main factor governing electrophoresis.

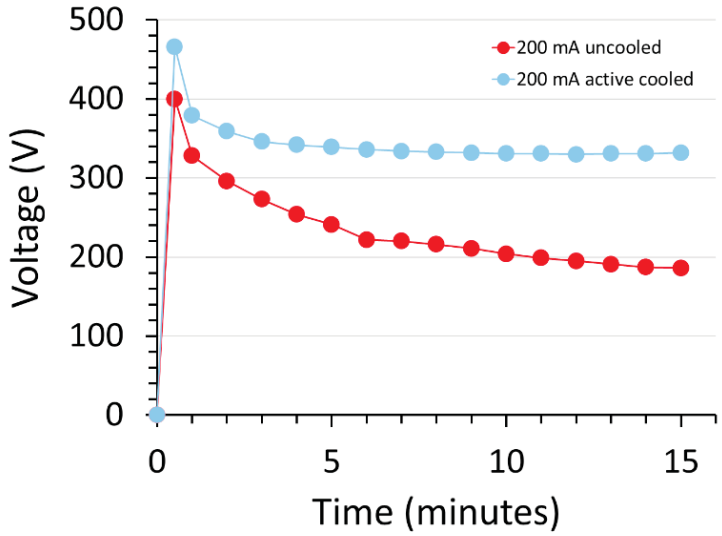

Figure 3.14 For a constant current TME run (200 mA), the voltage can change as a function of the changing solution resistance. AC-TME maintains a near constant voltage, which accelerates the purification process.

Using TME with higher constant current modes dictates faster SDS depletion times as seen in Figure 3.13 (reflected in the slope of curve). Therefore, SDS drops below 10 ppm in shorter time. However, notice the shape of an SDS depletion curve. At low current (40 mA) the depletion curve follows the predicted exponential decay (straight line on log curve)

because the temperature is approximately constant. However, when the applied current is increased to 180 mA, without using active-cooling temperature regulation, the rate of SDS decay slows with time. When AC-TME is used at 180 mA with active cooling, the initial rate of SDS depletion matches that of 180 mA uncooled. But it maintains that rate over the course of the run in a more consistent fashion therefore the voltage is higher and so the SDS depletes quicker. This is attributed to the temperature remaining constant as the active-cooling system manages to rapidly diffuse any heat generated.

A more direct comparison of the differences in SDS depletion as a function of TME cooling is provided in Figure 3.15. Currents greater than 200 mA applied to uncooled TME runs employed periodic pauses, with the time depicted in the figure corresponding to the cumulative time in which the power supply was 'on'. The true run times are approximately 50% greater than those presented in the Figure 3.15. At currents of 250 mA and above, the rate of SDS depletion continued to improve, although not to the extent seen at lower currents. Increasing the current from 50 mA to200 mA provides a ~4-fold decrease in the time required to deplete SDS to 10 ppm, and a total time reduction of nearly 1 hour. Increasing current from to 250 to 350 mA serves to double the SDS depletion rate, resulting in only approximately 10 minutes total time saved.

With the active-cooled platform, protein recovery losses due to thermal aggregation can be mitigated while applying constant currents up to 350 mA, shown in Figure 3.15. When using the active-cooled temperature regulator the speed of detergent removal was also significantly (t-test, $p < 0.05$) faster with the higher operating currents (150-300 mA) than without the AC system. No significant difference between the AC-TME and temperature unregulated system were seen at the 50 mA and 350 mA settings.

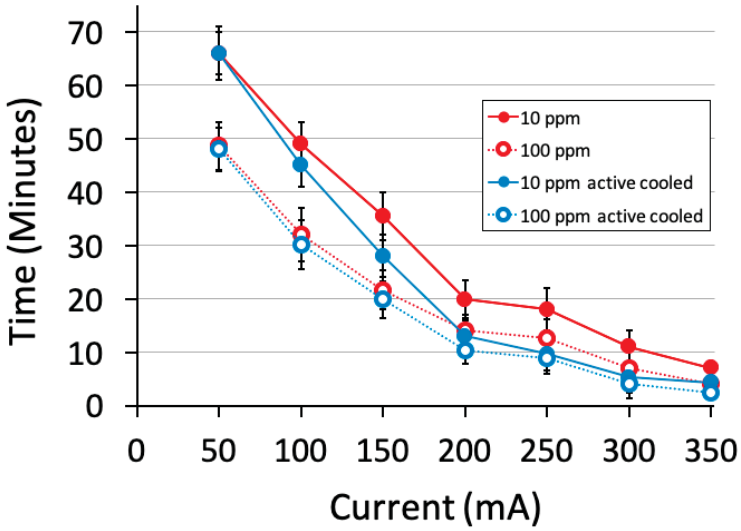

Figure 3.15 AC-TME runs with (blue) and without (red) active cooling 1 g×L^{-1} (*S. cerevisiae*) membrane proteins in 0.5% SDS displaying average rates to achieve an SDS concentration of either below 100 (open circles) or <10 ppm (filled circles).

3.9 Influence of Sample Cartridge Thickness

The AC-TME sample cells are housed in the central sample cartridge (see Figures 1.3 and 2.3) and are designed as a cylindrical chamber where the circular end constitutes a surface area of approximately 1 cm^2. The cylinder is milled out of PTFE sheets (3-, 6-, and 12-mm thickness). Previously, the conventional TME system used a 10 mm sample cartridge. The influence of cartridge thickness has not been explored. Herein, the impact of larger sample and smaller widths of sample cartridges was assessed on the efficiency of AC-TME to purify 200 µL of 5000 ppm SDS-contaminated proteins and proteomes. First, the influence of cartridge thickness on the applied voltage resulting from 120 mA constant current was examined. Figure 3.16 is a plot of voltage over a 30 min period. In this case, the water-circulating active-cooling system was off. During replicate runs (n = 3), the wider (12mm) sample cartridge consistently delivered higher voltages to yield the same current of 120 mA.

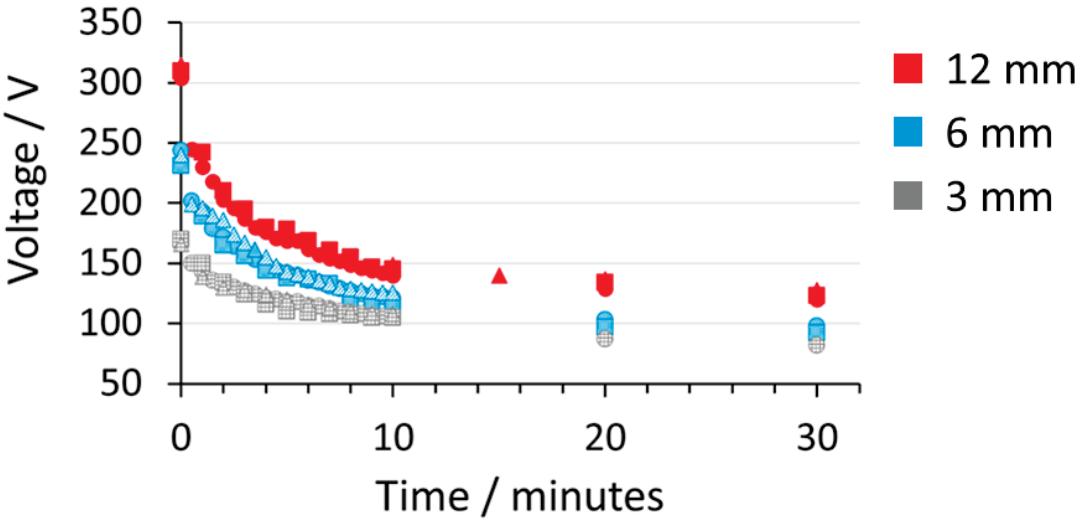

Figure 3.16 Voltage plot for TME runs without using active-cooling testing three different sample cartridge width sizes (3, 6, and 12 mm). TME operated at 120 mA constant current reached the highest voltages using the 12 mm cartridge and the lowest with the 6 mm.

With the 12 mm cartridge, the voltage reached a maximum of more than 300 V and remained above 100 V for the duration of the 30-minute run. The smallest cartridge (3 mm) did not peak above 200 V to maintain 120 mA constant current. Lengthening the sample cells theoretically weakens the strength of the electric field ($\frac{V}{cm}$) and the Coulombic force exerted onto molecules ($\frac{J}{cm}$), from Section 1.5.1, and the force driving the SDS away from proteins subsequently lower. Crucially varying the size of the sample cartridge also accommodates different volumes of sample solution. With the 3 mm the volume of sample fills the entire sample cell and subsequently covers the entire MWCO membrane. The 6 mm and 12 mm sample cartridges can accept a greater volume of sample solution. However, in these experiments, a constant volume of 200 µL per sample well was employed, inferring that the volume did not fully cover the MWCO membrane for the larger sample cells. The surface area between sample solution and the MWCO membranes

is a point of high resistance in the flux of ions. This surface area and thus contact area was maximized with the 3 mm sample cell as it fille the entire cell to the top covering the entire MWCO membranes.

The increasing lengths of sample cell (3 < 6 < 12 mm) showed an increase in the maximum temperatures recorded in the sample cells. Temperatures achieved throughout replicate runs using the varying thickness cartridges for 30-minute runs at 120 mA are shown in Figure 3.17. Note the three sizes of cartridge (3, 6, 12 mm) achieved similar final temperatures (58 ± 3, 61 ± 3, and 63 ± 4°C, respectively) but the rates at which they reached it were different. Using the AC-TME with water-circulating turned off 5000 ppm of SDS would typically be depleted to 10 ppm in 40 ± 5 min.

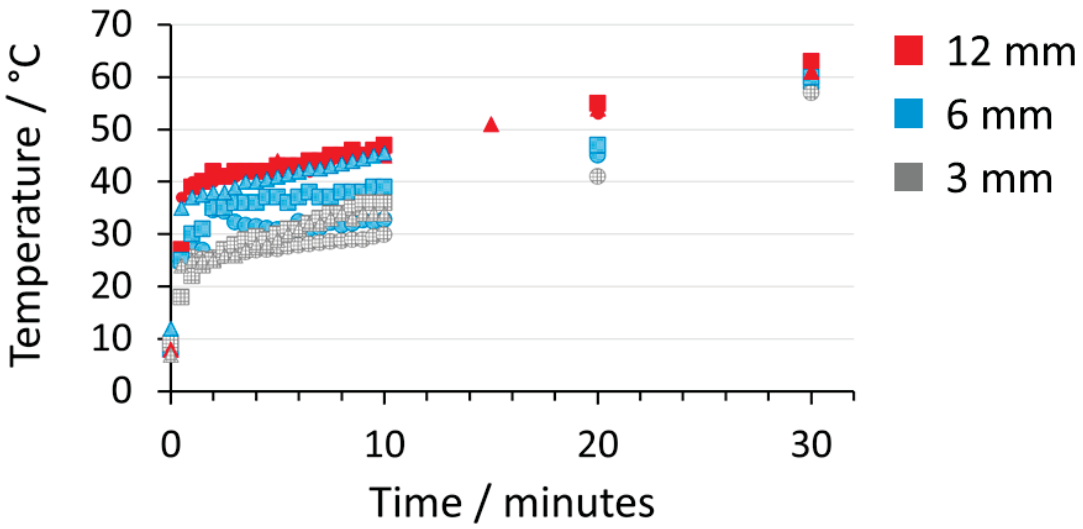

Figure 3.17: Temperature plot from replicate TME runs without active cooling at 120 mA constant current. The TME sample cell was the hottest with the 12 mm cartridge compared to the 3 mm that yielded the lowest overall temperatures.

The AC-TME platform was designed with the mission objective to maximize low temperatures in the sample cell during operation, as the conventional-TME had shown purifications that maintain lower temperatures correlate with enhanced protein recovery.

Interestingly, when the operating temperatures inside the system are lower, as was done with the thinnest sized sample cartridges, the rates of SDS depletion were also maximized and protein recovery higher, shown in Table 3.3. The smaller sample cartridge maintained a lower final temperature which correlated with increased protein yields. This supports the theory that proteins not exposed to high temperatures (40-60°C) do not undergo the same extent of structural denaturation that leads to aggregates and adhesion to the surface of materials. The increased rates of detergent removal may be because of the slightly increased Coulombic force ($\frac{J}{cm}$) the proteins in the 3 mm sample cell would experience compared to the 12 mm as the that field strength ($\frac{V}{cm}$) increases proportionally with decreases in the distance between electrodes.

Table 3.3 Influence of TME sample cartridge thickness

	Protein recovery (%)		SDS decay half-life (min^{-1})	Sample Temperature (°C), 10-12 min
Cartridge size (mm)	@ 50 mA	@ 200 mA	@ 180 mA	@ 180 Ma
12	93 ± 7	91 ± 2	2.8 ± 0.1	44 ± 2
3	98 ± 2	94 ± 8	1.49 ± 0.04	31.1 ± 0.6

The smallest sized sample cartridge (3mm) was the best choice for most efficient TME protocol for its ability to maximize the efficiency of purifying while improving the yields of proteins. Likely it would be possible to further minimize the size (and decrease volume or materials thus decreasing amount of heat sink that does not conduct heat away from sample cell) of the sample cartridge, but it becomes difficult to work with in the lab as it becomes too flexible to maintain structure and is soft enough that deformations may lead to leaks in the TME component seals. Furthermore, the updated AC-TME[188]

configuration compared to the conventional-TME, provides 5×200 µL volume capacity sample cells per single TME sample cartridge. Each of these sample cells has an approximate 1 mL of volume of space that can accommodate sample solution to be purified. The previous TME iterations had one less sample cell with four sample cells. Thus, more sample replicates are purified per run and a total of 1 mL of solution can be run at a time with this configuration of AC-TME.

3.10 AC-TME Purification of Molecular Weight Fractions of *S. cerevisiae*

Previously, it has been demonstrated that the SDS-protein binding interactions favor positively charged and hydrophobic residues of the proteins structures and so the binding-strength of different proteomes and sample systems may cause variance in the efficiency of TME purification. TME experiments have shown trends of decreasing protein recovery and rates in detergent removal efficiency correlating with the MW and relative hydrophobic characteristics of proteins.[167] Herein, it was tested with three sample types: highly soluble cytosolic, hydrophobic membrane-enriched, and a third Atlantic salmon muscular tissue sample of which the purifying characteristics were not known. AC-TME efficiency was assessed with varying MW size range fractions of Baker's yeast samples as it was hypothesized the heavier MW proteins would be harder to purify than low MW. The *S. cerevisiae* cytosol and membrane enriched proteome along with the Atlantic salmon proteome were fractionated using GELFrEE. The twelve collected fractions were grouped into three sample types based on their respective molecular weights, as is seen with the membrane enriched *S. cerevisiae* proteome in Figure 3.18. It should be noted that GELFrEE fractionated samples are collected in a glycine based running buffer (TG with

0.1% SDS) and thus contain the extra TG molecules when they undergo AC-TME purification using the adopted TT buffer. Extra ions may decrease the total resistance but extra analytes (uncharged) present in the sample, along with cellular debris (non-proteins), will add resistance to the overall system that may increase heat levels.

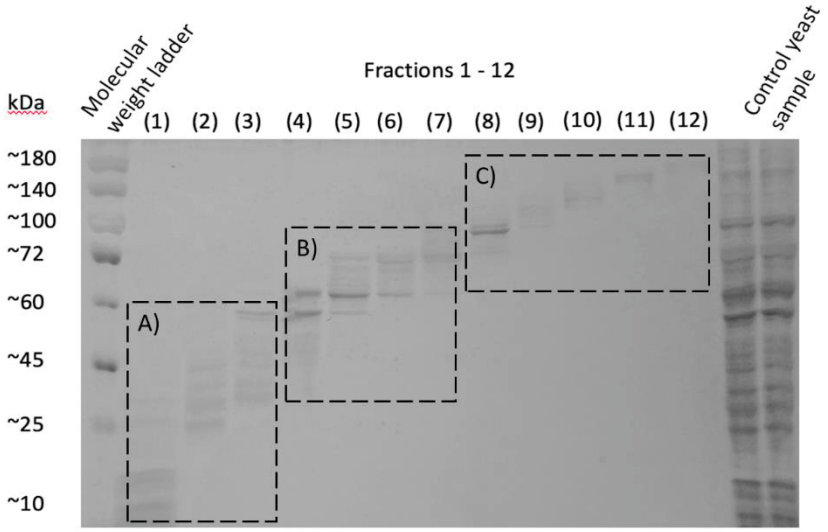

Figure 3.18 Digital image of 15%T SDS PAGE gel of 12 fractions of GELFrEE separated yeast membrane proteome. Outlined in black hashed rectangles are A) low B) medium and C) high molecular weight fractions.

Herein it was assessed how the recovery of samples was impacted when using the novel AC-TME protocol compared to the uncooled method with samples of varying molecular weights and varying aqueous solution solubility characteristics, shown in Figure 3.19. Cytosolic proteins are more water soluble than the relatively more hydrophobic membrane proteins, typically making them easier to prepare and characterise instrumentally. Yeast proteins are a common model organism for proteomics research and was selected for this study. As an independent verification, a real-world test sample, Atlantic salmon muscle tissue, was also tested on the TME system. The protein recoveries were significantly higher when the active-cooling system was implemented as opposed to relying on the conventional TME platforms passive heat diffusion techniques, as seen in

Figure 3.19A, B, C. The low MW fraction from cytosolic yeast proteome that showed smaller differences in protein recovery between the uncooled TME and AC-TME platforms were not significantly different (t-test, $p<0.05$), but still the AC-TME platforms recovery yields were higher (92 ± 12%) compared to the uncooled versions (69 ± 11%).

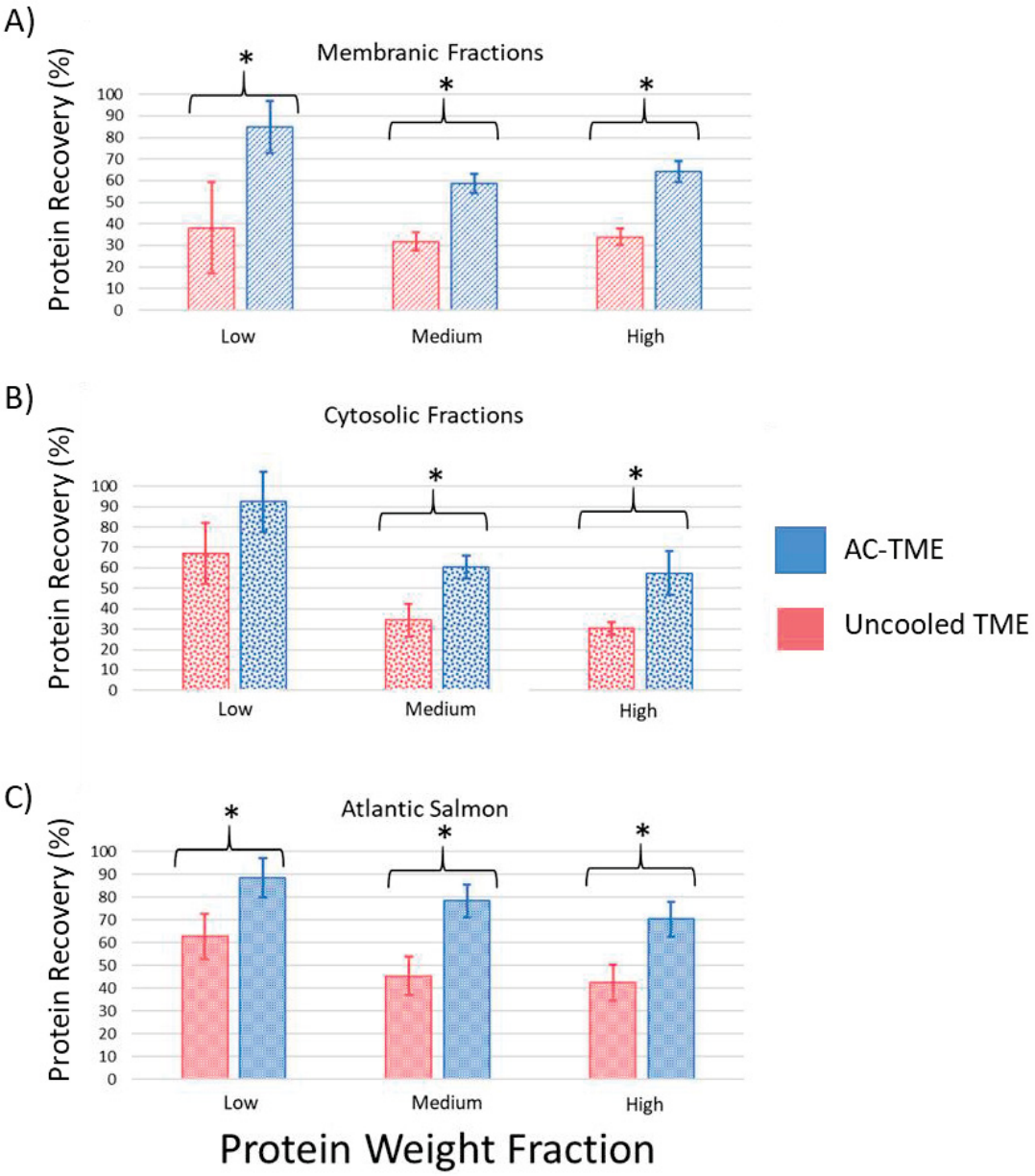

Figure 3.19 Protein recoveries of AC-TME protein purifications, with and without active-cooling implemented, on GELFrEE fractionated A) yeast (*S. cerevisiae)* cytosol and B) membrane-enriched proteins and on C) Atlantic salmon (*Salmo salar*) proteome fractions grouped by molecular weight into low, medium, and high MW samples. The symbol * denotes statistical differences between groups (t-test. $p<0.05$).

The recoveries from the Atlantic salmon proteome were greater than those of the membrane enriched yeast fraction, as was hypothesized would be the result. Muscle tissue consists of myofibrillar proteins with highly organized cells in consistent arrangement that function in contracting muscles. Typically, these are not as challenging to extract compared to membrane proteins requiring less detergent or solubilizing agents to maintain in solution.[175] It was surprising to consistently see the relatively more aqueous soluble proteins from the cytosolic fraction show comparable, or even lower recoveries to that of the membrane-enriched fractions. From these results the temperature regulation provided by AC-TME mitigated the protein aggregating effects of the Joule heat that is generated during electrophoresis. This is reflected in the higher recoveries seen with AC-TME in Figure 3.19 and Figures 3.11 and 3.12. Generally, managing the temperatures that develop from Joule heating inside the sample cell from exceeding ~60°C allows for higher recoveries from proteins, of varying MW and aqueous solubility characteristics, that were purified by TME.

3.11 *In-situ* TME Digestion Protocol of Residual Sample Pellet

Residual proteins that remain in the AC-TME sample well can result in a decrease in total protein yields. This would be particularly problematic considering that certain classes of proteins may be more susceptible to thermal aggregation. This could include larger and/or more hydrophobic proteins. However, such aggregated proteins are not lost – these proteins can be resolubilized with appropriate solvents, as has previously been demonstrated using concentrated formic acid.[201] Presented herein, an alternative strategy incorporates the trypsin enzymatic digestion protocol to work directly inside the AC-TME

sample cells, termed *in-situ* TME trypsin digestion (detailed description in Section 2.7.1). The strategy assumes that, once the thermally denatured proteins are digested, they do not aggregate as freely. The low molecular weight peptides are solubilized in aqueous buffer compared to the membrane proteins molecules that will precipitate out.

3.11.1 Protein Recovery from Supernatant versus Residual Pellet

Previous TME detergent removal protocols relied on managing the temperatures to below protein thermal denaturation levels (40-60°C)[75,77,201] otherwise the resulting protein aggregates would not be recovered. Denatured proteins are more susceptible to aggregating and adhering to sample cell walls and to the surface of the MWCO membranes. These proteins are not destroyed though. Thermal denaturation results in changes in conformational structures but it does not re-orient the peptide sequences and ultimately, for bottom-up proteomic experiments, these proteins can still be employed for sample characterization. An *in-situ* digestion protocol was therefore developed to enable aggregated proteins to be proteolyzed into peptides. The stir-bars that are used inside the AC-TME sample cells, originally to aid in heat diffusion,[166] were used as mechanical agitators and the trypsin enzymatic digestion was adapted so that reaction could take place inside the AC-TME sample wells. SDS-PAGE was used as a qualitative depiction of the protein distributions in the AC-TME supernatant and the residual pellet, this is shown in Figure 3.20. Any proteins not retrieved in the TME supernatant fraction can be seen in the residual pellet gel lanes. From this gel, some variance is seen in the distribution of protein bands between the supernatant and residual TME sample gel lanes across the triplicate runs in the individual gel lanes. This is attributed to differences between the TME sample cells

that resulted in the proteins being exposed to varying degrees of heat during the TME's operation resulting in differing amounts of residual pellet remaining.

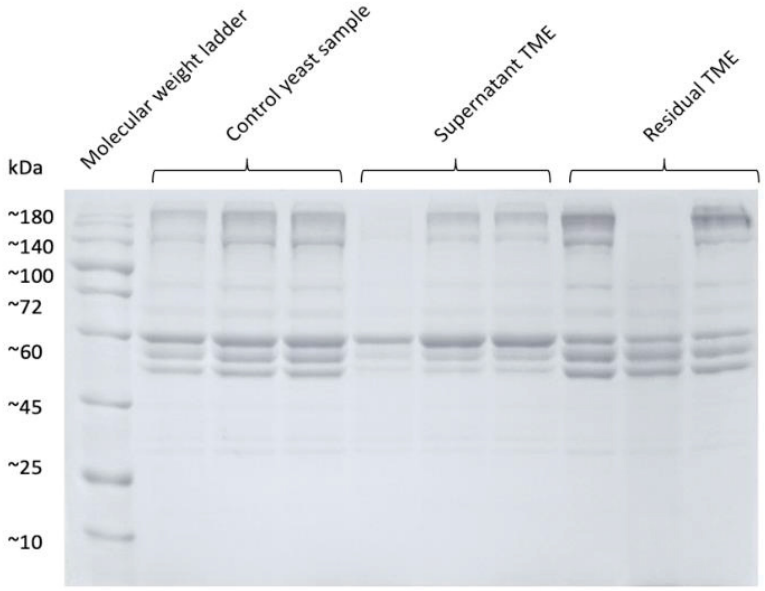

Figure 3.20 SDS PAGE of triplicate samples of TME-purified yeast membrane proteome extract, as recovered in solution (supernatant fraction) or remaining inside the AC-TME sample cell as a residual protein pellet and compared to a non-SDS contaminated control after 180 mA constant current run until the residual SDS concentration was <10 ppm.

Combining the sample recoveries from the supernatant protein solution, originally retrieved from the AC-TME sample cells by micropipette, and the *in-situ* TME trypsin digestion allows for the near total recovery of sample peptides, shown in Figure 3.21. The ability to recover the thermally denatured proteins that are retained inside the TME sample cells as aggregated residual pellets using an *in-situ* TME digestion protocol (see Section 3.11) enabled the testing of this AC-TME platform's upper limits in terms of maximizing the rate of protein purification and sample yields.

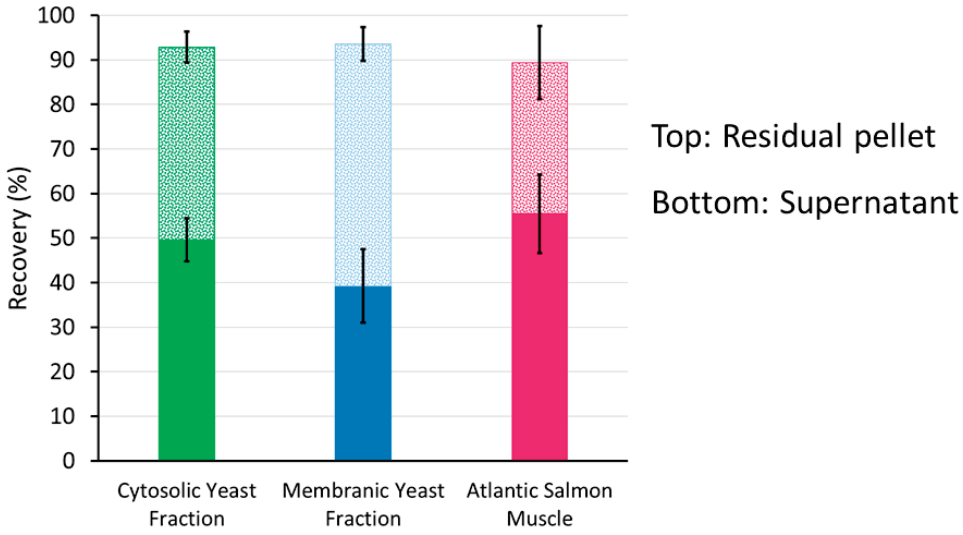

Figure 3.21 The total percent protein sample recoveries as achieved by combining the relatively low protein recoveries from AC-TME runs at 350 mA in solution as the supernatant fractions and those collected using the *in-situ* TME trypsin digestion protocol for *S. cerevisiae* cytosol- or membrane-enriched proteins and Atlantic salmon muscle tissue proteome.

The operating currents were tested up to the upper limit (350 mA) with the active-cooling temperature regulation and compared versus the uncooled platform, the recovery results discussed in Section 3.7 and seen in Figures 3.10 -3.12. SDS PAGE gels visualize the distribution of sample across the supernatant and residual pellet from the AC-TME platform and when the water-circulating temperature management is not used, shown in Figure 3.22A, B.

The protein sample distribution shifts from the supernatant that is originally retrieved from TME to the residual pellet that remains as a result of thermal induced aggregates when the water-circulating temperature management is not used. The SDS PAGE analysis of the soluble membrane proteins recovered from the AC-TME sample cells with water-circulating turned off experimental condition shows a similar pattern of proteins bands to that of the control-lanes protein bands. Both samples, the experimental

AC-TME conditions and the control (no-TME purification) used identical membrane-protein enrichment preparations. Similarly, multiple proteins are recovered from the residual insoluble proteins TME pellet but with no specificity, trends, or bias to a specific MW class of proteins can be visualized from the gel patterns. The overall resemblance in band patterns suggests that several of the same yeast proteins have partitioned between the supernatant and residual pellet phases. This implies that the thermal aggregation process impacts all the sample at the high AC-TME operating parameters and no single type or class of proteins. These results and visuals support that operating TME at high enough operating parameters may generate enough heat to thermally aggregate proteins. The mechanism behind thermal aggregation does not destroy those proteins information though and they can be retrieved and still analyzed.

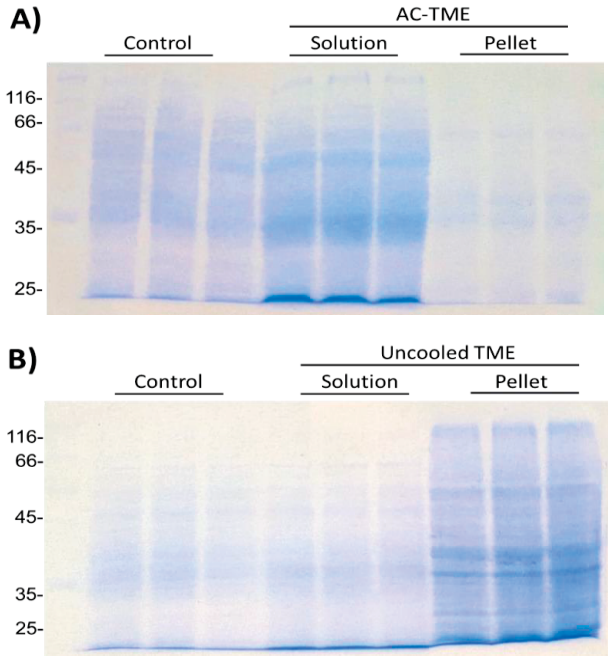

Figure 3.22 The distribution of membrane-enriched proteins from *S. cerevisiae* proteome that were purified of 5000 ppm SDS by A) AC-TME or B) conventional-TME (uncooled) runs at 200 mA constant current until a residual SDS concentration below 10 ppm was achieved (10 and 18 minutes TME operation, respectively). Majority of the proteins removed from the AC-TME platform were in the supernatant fraction compared with the conventional-TME (uncooled) where proteins were recovered mostly with the *in-situ* TME digestion of the residual pellet.

3.12 LC-MS with AC-TME versus Conventional Uncooled TME

The membrane-enriched *S. cerevisiae* proteome was characterised using MS instrumentation to assess the quality of samples generated by AC-TME purification (250 mA) versus the previously published conventional-TME. The proteins recovered from the actively cooled, temperature controlled TME system and the uncooled platform, including both the supernatant and residual protein pellets, were subject to trypsin digestion and subsequent LC-MS/MS analysis in a conventional a bottom-up proteomics MS workflow. Analysis of the membrane enriched yeast proteome following SDS depletion by AC-TME yielded more MS-identified proteins as compared to the equivalent sample purified in the uncooled platform, seen in Figure 3.23. A total of 853 proteins were confirmed by MS in the AC-TME runs compared to 701 proteins identified from the supernatant solution recovered from the uncooled TME runs.

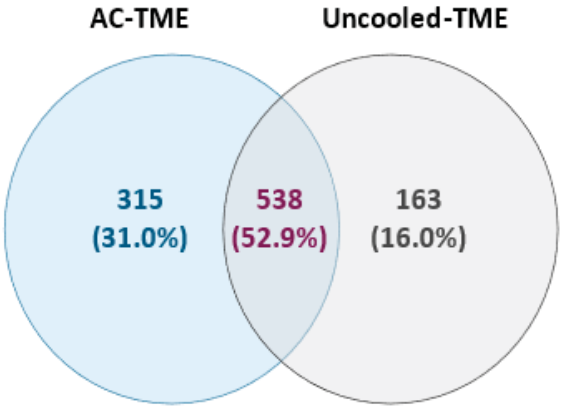

Figure 3.23 Venn diagram comparing the identified *S. cerevisiae* membrane-enriched proteins recovered from the supernatant solution that is initially retrieved from the sample cells of AC-TME or conventional-TME (uncooled) runs.

From the two TME purifications (AC-TME and uncooled-TME) the AC-TME platform yielded a greater number of unique proteins (315) recovered in the solution phase that were not isolated from the uncooled system. This is to be expected, as greater protein losses result from thermal aggregation. Nonetheless, there were still several 163 proteins that were not identified in the AC-TME solution phase. For complex proteome mixtures, the bottom-up MS analysis is unable to identify all components of the system. Comparing the residual pellets, the number of unique proteins from AC- vs uncooled-TME runs were similar (131 vs 168 unique proteins, respectively), shown below in Figure 3.24.

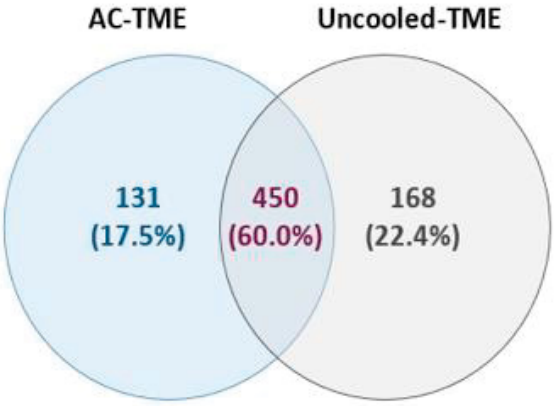

Figure 3.24 Venn diagram comparing the identified *S. cerevisiae* membrane-enriched proteins recovered from the residual pellet (complement of Figure 3.23) from an *in-situ* TME trypsin digestion from AC-TME or the conventional, uncooled TME runs.

The distribution of missed cleavage sites on identified peptides for AC-TME and conventional-TME (uncooled) are summarized in Figure 3.25. It was not surprising to confirm that the AC-TME supernatant proteins had greater fully cleaved peptides compared to the uncooled system. The digestion efficiency of proteins recovered in the pellet fraction displayed an unusual trend, with lower digestion efficiency in the AC pellet compared to the uncooled pellet. However, it is difficult to make specific comparisons between these fractions as the pellet fraction is larger for the uncooled run, and may present

a very different set of proteins across the two runs. It is clear that there are differences between the conventional solution-based trypsin digestion protocol and the *in-situ* TME trypsin digestion that has been adapted herein.

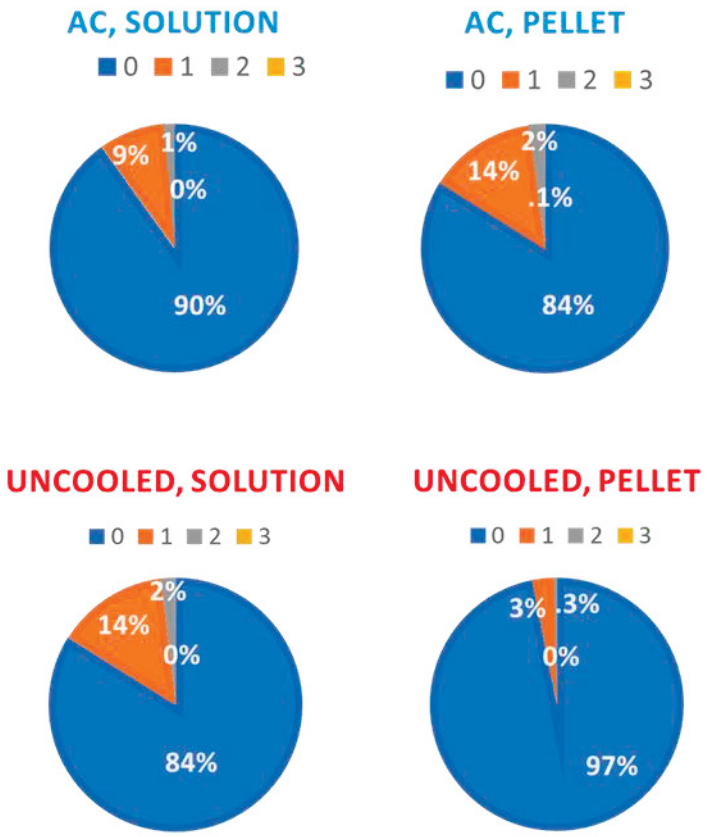

Figure 3.25 Visual representations assessing the degree of digestion for each of the four samples subject to bottom-up MS analysis. The pie charts show the percentage of identified peptides containing 0, 1, 2, or 3 missed trypsin cleavages. Over 98% of the identified peptides from each fraction contain either 0 or 1 missed cleavage sites.

It was not expected that the number and diversity of proteins identified would be larger when purifying samples through AC-TME as opposed to without water-circulating for temperature control. Combining the residual protein pellet, that was isolated by *in-situ* TME trypsin digest, with the originally retrieved supernatant solution fraction returned near quantitative recovery (>98%) with each AC-TME purification attempt. The potential of recovering aggregated proteins via direct, *in-situ* TME trypsin digestion, together with

maximizing TME efficiency by implementing active-cooling, may represent a powerful alternative frontend sample preparation platform. This is especially attractive to TDP applications that were not explored but are of high research interest (discussed in detail in Section 4.2).

Comparing the unique proteins isolated from AC-TME with those from the uncooled-TME to determine any differences or trends in sample characteristics between the two but neither the MW nor GRAVY scores were significantly different, shown in Figure 3.26. The isoelectric point of proteins recovered from the *in-situ* TME digestion was seen to be higher than that of the supernatant recovered solution phase proteins (t-test; $p = 5\times10^{-6}$). From Figure 3.26, the median pI of proteins found uniquely to the *in-situ* TME digestion was 7.9, which approaches the pH of the system (pH = 8.3). Comparatively, proteins that were uniquely identified in the supernatant solution phase had a median pI of 6.3.

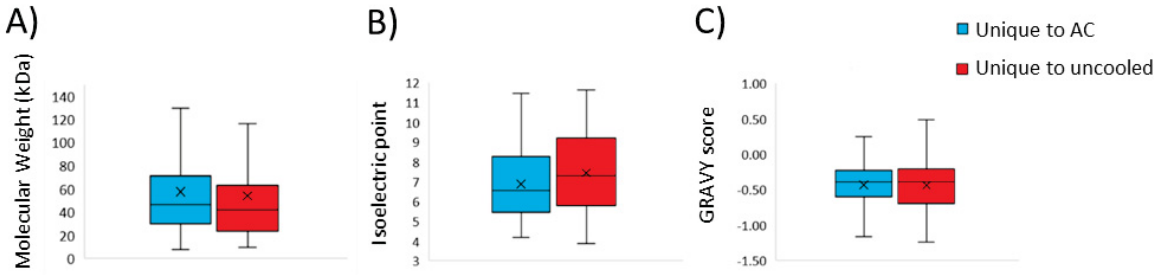

Figure 3.26 The relative distributions of the uniquely identified peptides according to their A) molecular weights, B) isoelectric points, and C) GRAVY scores, extrapolated from the unique lists of peptides identified by MS following AC-TME (red) and uncooled-TME (blue) purifications of yeast membrane proteome.

It was not surprising to see the results from MS analysis that the AC-TME platform, compared to the uncooled system, supplied more peptides that were identified by MS. The AC-TME purification led to 1434 total peptides identified (926 unique to AC-TME) compared to the 1319 from the uncooled TME (848 unique to uncooled TME), summarized in Figure 3.27. These peptides are produced from reacting the purified proteins (depleted of SDS), isolated from either AC or uncooled TME systems, with trypsin. This yields tryptic peptides that are a representation of the distribution of proteins in the sample after each sample purification procedure and experimental condition being tested. The trend that AC-TME improves the protein recoveries is seen in the relative proteins counts from the MS data, presented in Figures 3.23 and 3.24 with the resulting increases in identified peptides shown in Figure 3.27. The uncooled TME device yielded 230 peptides identified from the supernatant and 147 from the residual TME pellet (a ratio of ~1.5). The temperature regulated system yielded approximately 4.5 times more identified peptides in the supernatant as opposed to in the residual pellet. An increase in the commonly identified peptides between the supernatant (508 peptides) and the residual pellets (471 peptides) with the AC-TME platform is also seen in Figure 3.27.

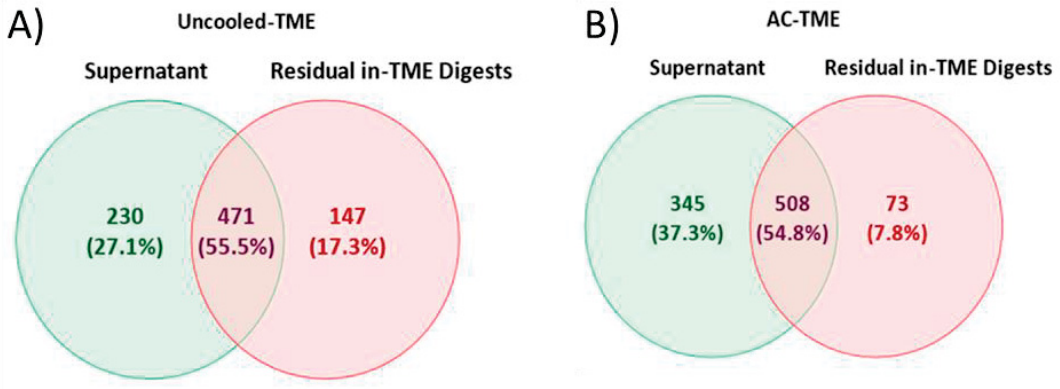

Figure 3.27 Venn diagrams showing the number of *S. cerevisiae* peptides recovered from the supernatant or the *in-situ* TME trypsin digestion of the residual pellet for both the A) uncooled- and the B) AC-TME devices.

Chapter 4 Conclusions and Future Direction

4.1 Conclusions

The effective separation of SDS detergent from proteins is critical to successful downstream characterization by LC-MS/MS. This thesis presented an updated AC-TME purification protocol. The automated platform has the capacity to deplete 99.9% SDS in 5 min, while maintaining high protein recovery, including for membrane-enriched protein samples. The desired level of protein purity (100 ppm vs 10 ppm) can be controlled by the user in choosing to operate TME at higher currents, or for a longer period of time. The limiting factor of operating TME has been the Joule heat generated at the sample wells, which causes proteins to aggregate. Incorporating active cooling into the TME platform maintains lower operating temperatures while simultaneously permitting high protein purity, high recovery, and faster processing time. Furthermore, the technique provides a fully automated format to purify multiple replicates in batch runs. Despite these improvements, protein solubility may still be compromised following SDS depletion, in TME particularly for proteins near their isoelectric point. In this case, an *in-situ* TME trypsin digestion protocol can be applied to recover these residual thermally aggregated proteins. It is expected from these results presented that AC-TME, as an optimized protein purification platform, will be beneficial and applicable for proteomics workflows involving SDS detergent and LC-MS analysis.

4.2 Future Directions

Further investigation into the effects of temperature on the mechanism of AC-TME can be performed to explore the details of how the flux of ions relates to changes in voltage

and resistance. Related to this, the impacts of membrane porosity and solution viscosity may also influence the rate of SDS depletion. A detailed theoretical approach to model the parameters governing TME could expose what is happening at the buffer-membrane-sample interface all with the aim of further achieve faster TME with higher yields.

High-throughput platforms are very attractive for proteomic LC-MS research with the ability to prepare samples rapidly, with replicates, and in batches. TME is suited to this task as it is an automatic platform working on batches of samples at a time that depends on the user loading and removing the samples and other than assembling and powering the device. Developing a flowthrough, in-line prototype of TME has potential for directly connected with LC-MS platforms with the goal of fully automated, high throughput, inline MS platform.

Pepsin is another type of protease that has been applied to proteomic workflows, similar the trypsin protocol. Pepsin preferentially cleaves peptide bonds located at the N-terminal side of hydrophobic amino acids, such as leucine and phenylalanine.[199,200] Pepsin proteolysis could be used as an alternative for residual protein recovery through *in-situ* TME digestion, presented in Section 4.3. This would make the sample amenable to formic acid protein solubilization.

Furthermore, the buffer systems used in TME may impact the protein types being purified of detergents. The electrolyte buffer is a major parameter impacting TME efficiency and its composition has not been tested. There is value in determining the concentrations, ionic conductivity, and size of the buffer and electrolyte species that would increase the mass transport of SDS detergent while minimizing Joule heat formation. The exploration of whether single or multi-component buffers improves SDS

depletion. The addition of non-buffer, charge carrying, species such as potassium chloride or sodium chloride as means of improving the conductivity of the electrolyte. Specific acidic and basic buffer systems, such as beta-alanine and formate, can be applied to accommodate proteins that require specific low or high pH environment. The impact of buffer pH among other components such as conjugate acid base pairs combinations and their effect and potential applications with the AC-TME protein purification protocol remain to be explored. The goal is still for 'real-time' SDS depletion that would allow for online coupling directly to MS platforms. TME could exist as an intermediate between detergent-based protein separations, like SDS-PAGE or GELFrEE, and an MS analysis platform as a purification technique to remove SDS from protein fractions that have been separated in a detergent buffer.

Bibliography

(1) Kahn, P. From Genome to Proteome: Looking at a Cell's Proteins. *Science* **1995**, *270(5235)*, 369–370. https://doi.org/10.1126/SCIENCE.270.5235.369.

(2) Aebersold, R.; Goodlett, D. R. Mass Spectrometry in Proteomics. *Chemical Reviews* **2001**, 101(2), 269–295. https://doi.org/10.1021/CR990076H.

(3) Aebersold, R.; Mann, M. Mass Spectrometry-Based Proteomics. *Nature* **2003**, *422*, 198–207. https://doi.org/10.1038/nature01511.

(4) Ahmed, F. E. Sample Preparation and Fractionation for Proteome Analysis and Cancer Biomarker Discovery by Mass Spectrometry. *Journal of Separation Science* **2009**, *32(5–6),* 771–798. https://doi.org/10.1002/JSSC.200800622.

(5) Nickerson, J. L.; Baghalabadi, V.; Rajendran, S. R. C. K.; Jakubec, P. J.; Said, H.; McMillen, T. S.; Dang, Z.; Doucette, A. A. Recent Advances in Top-down Proteome Sample Processing Ahead of MS Analysis. *Mass Spectrometry Reviews* **2021**, 1–39. https://doi.org/10.1002/MAS.21706.

(6) Wilkins, M. R.; Pasquali, C.; Appel, R. D.; Ou, K.; Golaz, O.; Sanchez, J. C.; Yan, J. X.; Gooley, A. A.; Hughes, G.; Humphery-Smith, I.; Williams, K. L.; Hochstrasser, D. F. From Proteins to Proteomes: Large Scale Protein Identification by Two-Dimensional Electrophoresis and Amino Acid Analysis. *Biotechnology (N Y)* **1996**, *14(1),* 61–65. https://doi.org/10.1038/NBT0196-61.

(7) Swaney, D. L.; Villén, J. Proteomic Analysis of Protein Posttranslational Modifications by Mass Spectrometry. *Cold Spring Harbor Protocols* **2016**, *2016(3),* 207–209. https://doi.org/10.1101/pdb.top077743.

(7) Licatalosi, D. D.; Darnell, R. B. RNA Processing and Its Regulation: Global Insights into Biological Networks. *Nature Reviews Genetics* **2010**, *11(1),* 75–87. https://doi.org/10.1038/nrg2673.

(9) Prabakaran, S.; Lippens, G.; Steen, H.; Gunawardena, J. Post-Translational Modification: Nature's Escape from Genetic Imprisonment and the Basis for Dynamic Information Encoding. *Wiley Interdisciplinary Reviews: Systems Biology and Medicine* **2012**, *4(6),* 565–583. https://doi.org/10.1002/wsbm.1185.

(10) Ramazi, S.; Zahiri, J. Post-Translational Modifications in Proteins: Resources, Tools and Prediction Methods. *Database* **2021**, *2021*, 1-20. https://doi.org/10.1093/database/baab012.

(11) Souda, P.; Ryan, C. M.; Cramer, W. A.; Whitelegge, J. Profiling of Integral Membrane Proteins and Their Post Translational Modifications Using High-

Resolution Mass Spectrometry. *Methods* **2011**, *55(4),* 330–336. https://doi.org/10.1016/j.ymeth.2011.09.019.

(12) Toby, T. K.; Fornelli, L.; Kelleher, N. L. Progress in Top-Down Proteomics and the Analysis of Proteoforms. *Annual Review of Analytical Chemistry* **2016**, *9 (1),* 499–519. https://doi.org/10.1146/annurev-anchem-071015-041550.

(13) Smith, L. M.; Agar, J. N.; Chamot-Rooke, J.; Danis, P. O.; Ge, Y.; Loo, J. A.; Paša-Tolić, L.; Tsybin, Y. O.; Kelleher, N. L. The Human Proteoform Project: Bringing Proteoforms to Life - A Plan to Define the Human Proteome. *Preprints* **2020**, *2020100368*, 1–18. doi: 10.20944/preprints202010.0368.v1

(14) Roth, M. J.; Forbes, A. J.; Boyne, M. T.; Kim, Y. B.; Robinson, D. E.; Kelleher, N. L. Precise and Parallel Characterization of Coding Polymorphisms, Alternative Splicing, and Modifications in Human Proteins by Mass Spectrometry. *Molecular & Cellular Proteomics* **2005**, 4 (7), 1002–1008. https://doi.org/10.1074/MCP.M500064-MCP200.

(15) Yin, H.; Flynn, A. D. Drugging Membrane Protein Interactions. *Annual Review of Biomedical Engineering* **2016**, *18,* 51–76. https://doi.org/10.1146/annurev-bioeng-092115-025322.

(16) Frantzi, M.; Latosinska, A.; Mischak, H. Proteomics in Drug Development: The Dawn of a New Era? *Proteomics - Clinical Applications* **2019**, *13 (2),* 1–13. https://doi.org/10.1002/prca.201800087.

(17) Qian, M.; Yan, F.; Yuan, T.; Yang, B.; He, Q.; Zhu, H. Targeting Post-Translational Modification of Transcription Factors as Cancer Therapy. *Drug Discovery Today* **2020**, *25 (8),* 1502–1512. https://doi.org/10.1016/j.drudis.2020.06.005.

(18) Overington, J. P.; Al-Lazikani, B.; Hopkins, A. L. How Many Drug Targets Are There? *Nature Reviews Drug Discovery* **2006**, *5 (12),* 993–996. https://doi.org/10.1038/nrd2199.

(19) Peng, L.; Cantor, D. I.; Huang, C.; Wang, K.; Baker, M. S.; Nice, E. C. Tissue and Plasma Proteomics for Early Stage Cancer Detection. *Molecular Omics* **2018**, *14 (6),* 405–423. https://doi.org/10.1039/c8mo00126j.

(20) Carlyle, B. C.; Trombetta, B. A.; Arnold, S. E. Proteomic Approaches for the Discovery of Biofluid Biomarkers of Neurodegenerative Dementias. *Proteomes* **2018**, *6 (3),* 32. https://doi.org/10.3390/proteomes6030032.

(21) Vialaret, J.; Schmit, P. O.; Lehmann, S.; Gabelle, A.; Wood, J.; Bern, M.; Paape, R.; Suckau, D.; Kruppa, G.; Hirtz, C. Identification of Multiple Proteoforms

Biomarkers on Clinical Samples by Routine Top-down Approaches. *Data in Brief* **2018**, *18*, 1013–1021. https://doi.org/10.1016/j.dib.2018.03.114.

(22) Wang, Q.; Chaerkady, R.; Wu, J.; Hwang, H. J.; Papadopoulos, N.; Kopelovich, L.; Maitra, A.; Matthaei, H.; Eshleman, J. R.; Hruban, R. H.; Kinzler, K. W.; Pandey, A.; Vogelstein, B. Mutant Proteins as Cancer-Specific Biomarkers. *Proceedings of the National Academy of Sciences of the United States of America* **2011**, *108 (6),* 2444–2449. https://doi.org/10.1073/pnas.1019203108.

(23) Lee, J.; Hang, J. J.; Altwerger, G.; Kohn, E. C. Proteomics and Biomarkers in Clinical Trials for Drug Development. *Journal of Proteomics* **2011**, *74(12)*, 2632–2641. https://doi.org/doi:10.1016/j.jprot.2011.04.023.

(24) Sobsey, C. A.; Ibrahim, S.; Richard, V. R.; Gaspar, V.; Mitsa, G.; Lacasse, V.; Zahedi, R. P.; Batist, G.; Borchers, C. H. Targeted and Untargeted Proteomics Approaches in Biomarker Development. *Proteomics* **2020**, *20 (9),* e1900029. https://doi.org/10.1002/pmic.201900029.

(25) Wang, Y. C.; Peterson, S. E.; Loring, J. F. Protein Post-Translational Modifications and Regulation of Pluripotency in Human Stem Cells. *Cell Research* **2014**, *24(2),* 143–160. https://doi.org/10.1038/cr.2013.151.

(26) Wasik, A. A.; Schiller, H. B. Functional Proteomics of Cellular Mechanosensing Mechanisms. *Seminars in Cell and Developmental Biology* **2017**, *71*, 118–128. https://doi.org/10.1016/j.semcdb.2017.06.019.

(27) Schneeweis, C.; Hassan, Z.; Schick, M.; Keller, U.; Schneider, G. The SUMO Pathway in Pancreatic Cancer: Insights and Inhibition. *British Journal of Cancer* **2021**, *124*, 531–538. https://doi.org/10.1038/s41416-020-01119-6.

(28) Han, Z. J.; Feng, Y. H.; Gu, B. H.; Li, Y. M.; Chen, H. The Post-Translational Modification, SUMOylation, and Cancer. *International Journal of Oncology* **2018**, *52 (4),* 1081–1094. https://doi.org/10.3892/ijo.2018.4280.

(29) Wu, Z.; Huang, R.; Yuan, L. Crosstalk of Intracellular Post-Translational Modifications in Cancer. *Archives of Biochemistry and Biophysics* **2019**, *676(2)*, 108138. https://doi.org/10.1016/j.abb.2019.108138.

(30) Zhang, J.; Peng, Q.; Zhao, W.; Sun, W.; Yang, J.; Liu, N. Proteomics in Influenza Research: The Emerging Role of Posttranslational Modifications. *Journal of Proteome Research* **2021**, *20*, 110–121. https://doi.org/10.1021/acs.jproteome.0c00778.

(31) Smith, L. M.; Kelleher, N. L. Proteoform: A Single Term Describing Protein Complexity. *Nature Methods* **2013**, *10(3),* 186–187. https://doi.org/10.1038/nmeth.2369.

(32) Minguez, P.; Parca, L.; Diella, F.; Mende, D. R.; Kumar, R.; Helmer-Citterich, M.; Gavin, A. C.; van Noort, V.; Bork, P. Deciphering a Global Network of Functionally Associated Post-Translational Modifications. *Molecular Systems Biology* **2012**, *8(599),* 1–14. https://doi.org/10.1038/MSB.2012.31.

(33) Spoel, S. H. Orchestrating the Proteome with Post-Translational Modifications. *Journal of Experimental Botany* **2018**, *69(19),* 4499–4503. https://doi.org/10.1093/jxb/ery295.

(34) Owen, I.; Shewmaker, F. The Role of Post-Translational Modifications in the Phase Transitions of Intrinsically Disordered Proteins. *International Journal of Molecular Sciences* **2019**, *20(21),* 1–14. https://doi.org/10.3390/ijms20215501.

(35) Bowman, G. D.; Poirier, M. G. Post-Translational Modifications of Histones That Influence Nucleosome Dynamics. *Chemical Reviews* **2014**, *115(6),* 2274–2295. https://doi.org/10.1021/CR500350X.

(36) Ponomarenko, E. A.; Poverennaya, E. V.; Ilgisonis, E. V.; Pyatnitskiy, M. A.; Kopylov, A. T.; Zgoda, V. G.; Lisitsa, A. V.; Archakov, A. I. The Size of the Human Proteome: The Width and Depth. *International Journal of Analytical Chemistry* **2016**, *2016,* 1-6. https://doi.org/10.1155/2016/7436849.

(37) Aebersold, R.; Agar, J. N.; Amster, I. J.; Baker, M. S.; Bertozzi, C. R.; Boja, E. S.; Costello, C. E.; Cravatt, B. F.; Fenselau, C.; Garcia, B. A.; Ge, Y.; Gunawardena, J.; Hendrickson, R. C.; Hergenrother, P. J.; Huber, C. G.; Ivanov, A. R.; Jensen, O. N.; Jewett, M. C.; Kelleher, N. L.; Kiessling, L. L.; Krogan, N. J.; Larsen, M. R.; Loo, J. A.; Loo, R. R. O.; Lundberg, E.; MacCoss, M. J.; Mallick, P.; Mootha, V. K.; Mrksich, M.; Muir, T. W.; Patrie, S. M.; Pesavento, J. J.; Pitteri, S. J.; Rodriguez, H.; Saghatelian, A.; Sandoval, W.; Schlüter, H.; Sechi, S.; Slavoff, S. A.; Smith, L. M.; Snyder, M. P.; Thomas, P. M.; Uhlén, M.; Eyk, J. E. Van; Vidal, M.; Walt, D. R.; White, F. M.; Williams, E. R.; Wohlschlager, T.; Wysocki, V. H.; Yates, N. A.; Young, N. L.; Zhang, B. How Many Human Proteoforms Are There? *Nature Chemical Biology* **2018**, *14(3),* 206–214. https://doi.org/10.1038/nchembio.2576.

(38) Anderson, N. L.; Anderson, N. G. The Human Plasma Proteome: History, Character, and Diagnostic Prospects. *Molecular & Cellular Proteomics* **2002**, *1(11),* 845–867. https://doi.org/10.1074/MCP.R200007-MCP200.

(39) Bowman, G. D.; Poirier, M. G. Post-Translational Modifications of Histones That Influence Nucleosome Dynamics. *Chemical Reviews* **2015**, *115(6),* 2274–2295. https://doi.org/10.1021/CR500350X.

(40) Schaffer, L. V.; Millikin, R. J.; Shortreed, M. R.; Scalf, M.; Smith, L. M. Improving Proteoform Identifications in Complex Systems through Integration of

Bottom-up and Top-down Data. *Journal of Proteome Research* **2020**, *19(8)*, 3510–3517. https://doi.org/10.1021/acs.jproteome.0c00332.

(41) Nickerson, J. L.; Doucette, A. A. Rapid and Quantitative Protein Precipitation for Proteome Analysis by Mass Spectrometry. *Journal of Proteome Research* **2020**, *19(5)*, 2035–2042. https://doi.org/10.1021/acs.jproteome.9b00867.

(42) Thomson, J. J. M. A. F. R. S. LVIII. On the Masses of the Ions in Gases at Low Pressures. *The London, Edinburgh, and Dublin Philosophical Magazine and Journal of Science* **1899**, *48(295),* 547–567. https://doi.org/10.1080/14786449908621447.

(43) Hellewell, A. L.; Rosini, S.; Adams, J. C. A Rapid, Scalable Method for the Isolation, Functional Study, and Analysis of Cell-Derived Extracellular Matrix. *Journal of Visualized Experiments* **2017**, *119,* 55051. https://doi.org/10.3791/55051.

(44) Chait, B. T. Chemistry. Mass Spectrometry: Bottom-up or Top-Down? *Science* **2006**, *314(5796),* 65–66. https://doi.org/10.1126/SCIENCE.1133987.

(45) Fenn, J. B.; Mann, M.; Meng, C. K.; Wong, S. F.; Whitehouse, C. M. Electrospray Ionization for Mass Spectrometry of Large Biomolecules. *Science* **1989**, *246(4926),* 64–71. https://doi.org/10.1126/science.2675315.

(46) Hunt, D. F.; Yates, J. R.; Shabanowitz, J.; Winston, S.; Hauer, C. R. Protein Sequencing by Tandem Mass Spectrometry. *Proceedings of the National Academy of Sciences of the United States of America* **1986**, *83(17),* 6233–6237. https://doi.org/10.1073/PNAS.83.17.6233.

(47) Eng, J. K.; Mccormack, A. L.; Yates, J. R. An Approach to Correlate Tandem Mass Spectral Data of Peptides with Amino Acid Sequences in a Protein Database. *Journal of the American Society for Mass Spectrometry* **1994**, *5(11),* 976-989. doi: 10.1016/1044-0305(94)80016-2.

(48) Wilm, M. S.; Mann, M. Electrospray and Taylor-Cone Theory, Dole's Beam of Macromolecules at Last? *International Journal of Mass Spectrometry and Ion Processes* **1994**, *136(2–3),* 167–180. https://doi.org/10.1016/0168-1176(94)04024-9.

(49) Juraschek, R.; Dülcks, T.; Karas, M. Nanoelectrospray—More than Just a Minimized-Flow Electrospray Ionization Source. *Journal of the American Society for Mass Spectrometry* **1999**, *10(4),* 300–308. https://doi.org/10.1016/S1044-0305(98)00157-3.

(50) Konermann, L.; Ahadi, E.; Rodriguez, A. D.; Vahidi, S. Unraveling the Mechanism of Electrospray Ionization. *Analytical Chemistry* **2013**, *85(1),* 2–9. https://doi.org/10.1021/ac302789c.

(51) Kebarle, P.; Tang, L. From Ions in Solution to Ions in the Gas Phase - the Mechanism of Electrospray Mass Spectrometry. *Analytical Chemistry* **1993**, *65(22),* 972A-986A. https://doi.org/10.1021/AC00070A001.

(52) Taflin, D. C.; Ward, T. L.; Davis, E. J. Electrified Droplet Fission and the Rayleigh Limit. *Langmuir* **1989**, *5(2)*, 376–384. https://doi.org/10.1021/la00086a016

(53) Kebarle, P.; Peschke, M. On the Mechanisms by Which the Charged Droplets Produced by Electrospray Lead to Gas Phase Ions. *Analytica Chimica Acta* **2000**, *406(1),* 11–35. https://doi.org/10.1016/S0003-2670(99)00598-X.

(54) Konermann, L.; Ahadi, E.; Rodriguez, A. D.; Vahidi, S. Unraveling the Mechanism of Electrospray Ionization. *Analytical Chemistry* **2012**, *85(1)*, 2–9. https://doi.org/10.1021/ac302789c.

(55) Konermann, L.; Douglas, D. J. Unfolding of Proteins Monitored by Electrospray Ionization Mass Spectrometry: A Comparison of Positive and Negative Ion Modes. *Journal of the American Society for Mass Spectrometry* **1998**, *9(12),* 1248–1254. https://doi.org/10.1016/S1044-0305(98)00103-2.

(56) Meyer, J. G.; Komives, E. A. Charge State Coalescence During Electrospray Ionization Improves Peptide Identification by Tandem Mass Spectrometry. *Journal of The American Society for Mass Spectrometry* **2012**, *23(8),* 1390–1399. https://doi.org/10.1007/S13361-012-0404-0.

(57) Loo, R. R. O.; Dales, N.; Andrews, P. C. The Effect of Detergents on Proteins Analyzed by Electrospray Ionization. *Methods in Molecular Biology* **1996**, *61*, 141–160. https://doi.org/10.1385/0-89603-345-7:141.

(58) Rundlett, K. L.; Armstrong, D. W. Mechanism of Signal Suppression by Anionic Surfactants in Capillary Electrophoresis-Electrospray Ionization Mass Spectrometry. *Rapid Communications in Mass Spectrometry* **1996**, *68(19),* 3493-3497. doi:10.1021/ac960472p.

(59) Permentier, H. P.; Bruins, A. P. Electrochemical Oxidation and Cleavage of Proteins with On-Line Mass Spectrometric Detection: Development of an Instrumental Alternative to Enzymatic Protein Digestion. *Journal of the American Society for Mass Spectrometry* **2004**, *15(12),* 1707–1716. https://doi.org/10.1016/J.JASMS.2004.09.003.

(60) Basile, F.; Hauser, N. Rapid Online Nonenzymatic Protein Digestion Combining Microwave Heating Acid Hydrolysis and Electrochemical Oxidation. *Analytical Chemistry* **2011**, *83(1),* 359–367. https://doi.org/10.1021/AC1024705.

(61) Dupree, E. J.; Jayathirtha, M.; Yorkey, H.; Mihasan, M.; Petre, B. A.; Darie, C. C. A Critical Review of Bottom-Up Proteomics: The Good, the Bad, and the Future of This Field. *Proteomes* **2020**, *8(3),* 14. https://doi.org/10.3390/PROTEOMES8030014.

(62) Kelleher, N. L. Top-Down Proteomics. *Analytical Chemistry* **2004**, *76(11),* 196A-203A. https://doi.org/10.1021/AC0415657.

(63) Toby, T. K.; Fornelli, L.; Kelleher, N. L. Progress in Top-down Proteomics and the Analysis of Proteoforms. *Annual Review of Analytical Chemistry* **2016**, *9*, 499–519. https://doi.org/10.1146/annurev-anchem-071015-041550.

(64) Doucette, A. A.; Tran, J. C.; Wall, M. J.; Fitzsimmons, S. Intact Proteome Fractionation Strategies Compatible with Mass Spectrometry. *Expert Review of Proteomics* **2011**, *8(6)*, 787–800. doi: 10.1586/epr.11.67.

(65) Ball, P. Water as an Active Constituent in Cell Biology. *Chemical Reviews* **2007**, *108(1),* 74–108. https://doi.org/10.1021/CR068037A.

(66) Jafari, M.; Mehrnejad, F.; Rahimi, F.; Asghari, S. M. The Molecular Basis of the Sodium Dodecyl Sulfate Effect on Human Ubiquitin Structure: A Molecular Dynamics Simulation Study. *Scientific Reports* **2018**, *8(1)*, 2150. https://doi.org/10.1038/s41598-018-20669-7.

(67) Dahanayake, J. N.; Mitchell-Koch, K. R. How Does Solvation Layer Mobility Affect Protein Structural Dynamics? *Frontiers in Molecular Biosciences* **2018**, *5* (JUL), 65. https://doi.org/10.3389/FMOLB.2018.00065.

(68) Shaw, K. L.; Grimsley, G. R.; Yakovlev, G. I.; Makarov, A. A.; Pace, C. N. The Effect of Net Charge on the Solubility, Activity, and Stability of Ribonuclease Sa. *Protein Science* **2001**, *10(6),* 1206–1215. https://doi.org/10.1110/ps.440101.

(69) Kramer, R. M.; Shende, V. R.; Motl, N.; Pace, C. N.; Scholtz, J. M. Toward a Molecular Understanding of Protein Solubility: Increased Negative Surface Charge Correlates with Increased Solubility. *Biophysical Journal* **2012**, *102(8),* 1907. https://doi.org/10.1016/J.BPJ.2012.01.060.

(70) Kastelic, M.; Kalyuzhnyi, Y. V; Hribar-Lee, B.; Dill, K. A.; Vlachy, V. Protein Aggregation in Salt Solutions. *Proceedings of the National Academy of Sciences of the United States of America* **2015**, *112(21).* 6766-6770. https://doi.org/10.1073/pnas.1507303112.

(71) Li, R.; Wu, Z.; Wangb, Y.; Ding, L.; Wang, Y. Role of PH-Induced Structural Change in Protein Aggregation in Foam Fractionation of Bovine Serum Albumin. *Biotechnology Reports* **2016**, *9*, 46-52. https://doi.org/10.1016/J.BTRE.2016.01.002.

(72) Otzen, D. E. Protein Unfolding in Detergents: Effect of Micelle Structure, Ionic Strength, PH, and Temperature, *Biophysical Journal* **2002**, *83(4)*, 2219–2230. https://doi.org/10.1016/S0006-3495(02)73982-9.

(73) Park, Z.-Y.; Russell, D. H. Thermal Denaturation: A Useful Technique in Peptide Mass Mapping. *Analytical Chemistry* **2000**, *72(11)*, 2667–2670. https://doi.org/10.1021/ac991444k.

(74) Yan, Y. Bin; Wang, Q.; He, H. W.; Zhou, H. M. Protein Thermal Aggregation Involves Distinct Regions: Sequential Events in the Heat-Induced Unfolding and Aggregation of Hemoglobin. *Biophysical Journal* **2004***, 86(3),* 1682–1690. https://doi.org/10.1016/S0006-3495(04)74237-X.

(75) Markossian, K. A.; Golub, N. V.; Khanova, H. A.; Levitsky, D. I.; Poliansky, N. B.; Muranov, K. O.; Kurganov, B. I. Mechanism of Thermal Aggregation of Yeast Alcohol Dehydrogenase I: Role of Intramolecular Chaperone. *Biochimica et Biophysica Acta* **2008**, *1784(9),* 1286–1293. https://doi.org/10.1016/j.bbapap.2008.04.030.

(76) Wang, X.; Wang, H.; Wang, D.; Wang, D.; Han, B.; Tian, W.; Guo, A. Thermal Denaturation Produced Degenerative Proteins and Interfered with MS for Proteins Dissolved in Lysis Buffer in Proteomic Analysis. *Electrophoresis* **2011**, *32(3–4),* 348–356. https://doi.org/10.1002/elps.201000496.

(77) Borzova, V. A.; Markossian, K. A.; Chebotareva, N. A.; Kleymenov, S. Yu.; Poliansky, N. B.; Muranov, K. O.; Stein-Margolina, V. A.; Shubin, V. V.; Markov, D. I.; Kurganov, B. I. Kinetics of Thermal Denaturation and Aggregation of Bovine Serum Albumin. *Plos One* **2016**, *11(4),* e0153495. https://doi.org/10.1371/journal.pone.0153495.

(78) Dong, A.; Randolph, T. W.; Carpenter, J. F. Entrapping Intermediates of Thermal Aggregation in α-Helical Proteins with Low Concentration of Guanidine Hydrochloride. *Journal of Biological Chemistry* **2000**, *275(36),* 27689–27693. https://doi.org/10.1074/jbc.M005374200.

(79) Laemmli, U. K. Cleavage of Structural Proteins during the Assembly of the Head of Bacteriophage T4. *Nature* **1970**, *227(5259),* 680–685. https://doi.org/10.1038/227680a0.

(80) Haider, S. R.; Sharp, B. L.; Reid, H. J. A Comparison of Tris-Glycine and Tris-Tricine Buffers for the Electrophoretic Separation of Major Serum Proteins.

Journal of Separation Science **2011**, *34(18),* 2463–2467. doi:10.1002/jssc.201100315.

(81) Nowakowski, A. B.; Wobig, W. J.; Petering, D. H. Native SDS-PAGE: High Resolution Electrophoretic Separation of Proteins with Retention of Native Properties Including Bound Metal Ions. *Metallomics* **2014**, *6(5),* 1068–1078. https://doi.org/10.1039/c4mt00033a.

(82) Sharma, R.; Deka, B.; Mandal, A.; Mahto, V. Study the Influence of Sodium Dodecyl Sulfate on Emulsification of Heavy and Waxy Crude Oils to Improve Their Flow Ability in Low Temperature Conditions. *Asia-Pacific Journal of Chemical Engineering* **2019**, *14(1),* e2279. https://doi.org/10.1002/apj.2279.

(83) Bondi, C. A. M.; Marks, J. L.; Wroblewski, L. B.; Raatikainen, H. S.; Lenox, S. R.; Gebhardt, K. E. Human and Environmental Toxicity of Sodium Lauryl Sulfate (SLS): Evidence for Safe Use in Household Cleaning Products. *Environmental Health Insights* **2015**, *9,* 27-32. https://doi.org/10.4137/EHI.S31765.

(84) Privé, G. G. Detergents for the Stabilization and Crystallization of Membrane Proteins. *Methods* **2007**, *41(4),* 388–397. https://doi.org/10.1016/j.ymeth.2007.01.007.

(85) Walker, C.H. *The Hydrophobic Effect: Formation of Micelles and Biological Membranes*; Wiley: New York, **1981**.

(86) Rharbi, Y.; Chen, L.; Winnik, M. A. Exchange Mechanisms for Sodium Dodecyl Sulfate Micelles: High Salt Concentration. *Journal of the American Chemical Society* **2004**, *126(19),* 6025–6034. https://doi.org/10.1021/ja0304805.

(87) Andersen, K. K.; Oliveira, C. L.; Larsen, K. L.; Poulsen, F. M.; Callisen, T. H.; Westh, P.; Pedersen, J. S.; Otzen, D. The Role of Decorated SDS Micelles in Sub-CMC Protein Denaturation and Association. *Journal of Molecular Biology* **2009**, *391(1),* 207–226. https://doi.org/10.1016/j.jmb.2009.06.019.

(88) Otzen, D. E. Proteins in a Brave New Surfactant World. *Current Opinion in Colloid and Interface Science* **2015**, *20(3),* 161–169. https://doi.org/10.1016/j.cocis.2015.07.003.

(89) Jones, M. N. Surfactant Interactions with Biomembranes and Proteins. *Chemical Society Reviews* **1992**, *21(2),* 127–136. https://doi.org/10.1039/CS9922100127.

(90) Wang, G.; Treleaven, W. D.; Cushley, R. J. Conformation of Human Serum Apolipoprotein A-I(166-185) in the Presence of Sodium Dodecyl Sulfate or Dodecylphosphocholine by 1H-NMR and CD. Evidence for Specific Peptide-SDS Interactions. *Biochimica et Biophysica Acta* **1996**, *1301(3),* 174–184. https://doi.org/10.1016/0005-2760(96)00037-9.

(91) Reynolds, J. A.; Tanford, C. Binding of Dodecyl Sulfate to Proteins at High Binding Ratios. Possible Implications for the State of Proteins in Biological Membranes. *Proceedings of the National Academy of Sciences of the United States of America* **1970**, *66(3),* 1002-1007. https://doi.org/10.1073/PNAS.66.3.1002.

(92) Hammouda, B. Temperature Effect on the Nanostructure of SDS Micelles in Water. *Journal of Research of the National Institute of Standards and Technology* **2013**, *118*, 151–167. https://doi.org/10.6028/JRES.118.008.

(93) Bhuyan, A. K. On the Mechanism of SDS-Induced Protein Denaturation. *Biopolymers* **2010**, *93(2),* 186–199. https://doi.org/10.1002/BIP.21318.

(94) Samsó, M.; Daban, J.-R.; Hansen, S.; Jones, G. R. Evidence for Sodium Dodecyl Sulfate/Protein Complexes Adopting a Necklace Structure. *European Journal of Biochemistry* **1995**, *232(3),* 818–824. https://doi.org/10.1111/J.1432-1033.1995.0818A.X.

(95) Nelson, C. A. The Binding of Detergents to Proteins. *Journal of Biological Chemistry* **1971**, *246(12),* 3895–3901. https://doi.org/10.1016/s0021-9258(18)62118-0.

(96) Tran, J. C.; Doucette, A. A. Gel-Eluted Liquid Fraction Entrapment Electrophoresis: An Electrophoretic Method for Broad Molecular Weight Range Proteome Separation. *Analytical Chemistry* **2008**, *80(5),* 1568–1573. https://doi.org/10.1021/ac702197w.

(97) Tanca, A.; Biosa, G.; Pagnozzi, D.; Addis, M. F.; Uzzau, S. Comparison of Detergent-Based Sample Preparation Workflows for LTQ-Orbitrap Analysis of the Escherichia Coli Proteome. *Proteomics* **2013**, *13(17),* 2597–2607. https://doi.org/10.1002/pmic.201200478.

(98) Chang, Y.-H.; Gregorich, Z. R.; Chen, A. J.; Hwang, L.; Guner, H.; Yu, D.; Zhang, J.; Ge, Y. A New Mass Spectrometry-Compatible Degradable Surfactant for Tissue Proteomics. *Journal of Proteome Research* **2015**, *14(3),* 1587-1599. https://doi.org/10.1021/PR5012679.

(99) Schüpbach, J.; Ammann, R.; Freiburghaus, A. A Universal Method for Two-Dimensional Polyacrylamide Gel Electrophoresis of Membrane Proteins Using Isoelectric Focusing on Immobilized PH Gradients in the First Dimension. *Analytical Biochemistry* **1991**, *196(2),* 337–343. https://doi.org/10.1016/0003-2697(91)90475-9.

(100) Botelho, D.; Wall, M. J.; Vieira, D. B.; Fitzsimmons, S.; Liu, F.; Doucette, A. Top-Down and Bottom-Up Proteomics of SDS Containing Solutions Following Mass-

Based Separation Research Articles. *Journal of Proteome Research* **2010**, *9(6),* 2863–2870. doi: 10.1021/pr900949p.

(101) Kachuk, C.; Doucette, A. A. The Benefits (and Misfortunes) of SDS in Top-down Proteomics. *Journal of Proteomics* **2018**, *175*, 75–86. https://doi.org/10.1016/j.jprot.2017.03.002.

(102) Arribas, J.; Castaño, J. G. Kinetic Studies of the Differential Effect of Detergents on the Peptidase Activities of the Multicatalytic Proteinase from Rat Liver. *Journal of Biological Chemistry* **1990**, *265(23),* 13969–13973. DOI:https://doi.org/10.1016/S0021-9258(18)77443-7

(103) Lin, Y.; Zhou, J.; Bi, D.; Chen, P.; Wang, X.; Liang, S. Sodium-Deoxycholate-Assisted Tryptic Digestion and Identification of Proteolytically Resistant Proteins. *Analytical Biochemistry* **2008**, *377(2),* 259–266. https://doi.org/10.1016/j.ab.2008.03.009.

(104) Leon, I. R.; Schwammle, V.; Jensen, O. N.; Sprenger, R. R. Quantitative Assessment of In-Solution Digestion Efficiency Identifies Optimal Protocols for Unbiased Protein Analysis. *Molecular and Cellular Proteomics* **2013**, *12(10),* 2992–3005. https://doi.org/10.1074/mcp.M112.025585.

(105) Choi, N. S.; Hahm, J. H.; Pil, J. M.; Kim, S. H. Comparative Study of Enzyme Activity and Stability of Bovine and Human Plasmins in Electrophoretic Reagents, β-Mercaptoethanol, DTT, SDS, Triton X-100, and Urea. *Journal of Biochemistry and Molecular Biology* **2005**, *38(2),* 177–181. https://doi.org/10.5483/bmbrep.2005.38.2.177.

(106) Ghosh, S. Interaction of Trypsin with Sodium Dodecyl Sulfate in Aqueous Medium: A Conformational View. *Colloids and Surfaces. B, Biointerfaces* **2008**, *66(2),* 178–186. https://doi.org/10.1016/J.COLSURFB.2008.06.011.

(107) Kawasaki, H.; Suzuki, K. Separation of Peptides Dissolved in a Sodium Dodecyl Sulfate Solution by Reversed-Phase Liquid Chromatography: Removal of Sodium Dodecyl Sulfate from Peptides Using an Ion-Exchange Precolumn. *Analytical Biochemistry* **1990**, *186(2),* 264–268. https://doi.org/10.1016/0003-2697(90)90077-M.

(108) Bosserhoff, A.; Wallach, J.; Frank, R. Micropreparative Separation of Peptides Derived from Sodium Dodecyl Sulphate-Solubilized Proteins. *Journal of Chromatography* **1989**, *473(1),* 71–77. https://doi.org/10.1016/S0021-9673(00)91291-3.

(109) Ortiz-Bolsico, C.; Ruiz-Angel, M. J.; García-Alvarez-Coque, M. C. Adsorption of the Anionic Surfactant Sodium Dodecyl Sulfate on a C18 Column under Micellar and High Submicellar Conditions in Reversed-Phase Liquid Chromatography.

Journal of Separation Science **2015**, *38(4),* 550–555. https://doi.org/10.1002/JSSC.201401059.

(110) Loo, R. R. O.; Dales, N.; Andrews, P. C. Surfactant Effects on Protein Structure Examined by Electrospray Ionization Mass Spectrometry. *Protein Science* **1994**, *3(11),* 1975–1983. https://doi.org/10.1002/pro.5560031109.

(111) Schindler, P. A.; Van Dorsselaer, A.; Falick, A. M. Analysis of Hydrophobic Proteins and Peptides by Electrospray Ionization Mass Spectrometry. *Analytical Biochemistry* **1993**, *213(2),* 256–263. https://doi.org/10.1006/abio.1993.1418.

(112) Lu, X.; Zhu, H. Tube-Gel Digestion: A Novel Proteomic Approach for High Throughput Analysis of Membrane Proteins. *Molecular & Cellular Proteomics* **2005**, *4(12)*, 1948–1958. https://doi.org/10.1074/mcp.M500138-MCP200.

(113) Doucette, A.; Craft, D.; Li, L. Protein Concentration and Enzyme Digestion on Microbeads for MALDI-TOF Peptide Mass Mapping of Proteins from Dilute Solutions. *Analytical Chemistry* **2000**, *72(14),* 3355–3362. https://doi.org/10.1021/ac000176j.

(114) Kim, K. H.; Compton, P. D.; Tran, J. C.; Kelleher, N. L. Online Matrix Removal Platform for Coupling Gel-Based Separations to Whole Protein Electrospray Ionization Mass Spectrometry. *Journal of Proteome Research* **2015**, *14(5),* 2199–2206. https://doi.org/10.1021/pr501331q.

(115) Loo, R. R.; Dales, N.; Andrews, P. C. The Effect of Detergents on Proteins Analyzed by Electrospray Ionization. *In:Chapman J.R. (eds) Protein and Peptide Analysis by Mass Spectrometry. Methods in Molecular Biology* **1996**, *61*, 141–160. https://doi.org/10.1385/0-89603-345-7:141.

(116) Lin, Y.; Zhou, J.; Bi, D.; Chen, P.; Wang, X.; Liang, S. Sodium-Deoxycholate-Assisted Tryptic Digestion and Identification of Proteolytically Resistant Proteins. *Analytical Biochemistry* **2008**, *377(2),* 259–266. https://doi.org/10.1016/J.AB.2008.03.009.

(117) Wu, F.; Sun, D.; Wang, N.; Gong, Y.; Li, L. Comparison of Surfactant-Assisted Shotgun Methods Using Acid-Labile Surfactants and Sodium Dodecyl Sulfate for Membrane Proteome Analysis. *Analytica Chimica Acta* **2011**, *698(1–2),* 36–43. https://doi.org/10.1016/j.aca.2011.04.039.

(118) Lehner, I.; Niehof, M.; Borlak, J. An Optimized Method for the Isolation and Identification of Membrane Proteins. *Electrophoresis* **2003**, *24(11),* 1795–1808. https://doi.org/10.1002/elps.200305387.

(119) Lai, X. Reproducible Method to Enrich Membrane Proteins with High Purity and High Yield for an LC-MS/MS Approach in Quantitative Membrane Proteomics. *Electrophoresis* **2013**, *34(6),* 809–817. https://doi.org/10.1002/elps.201200503.

(120) Kuljanin, M.; Dieters-Castator, D. Z.; Hess, D. A.; Postovit, L.-M. M.; Lajoie, G. A. Comparison of Sample Preparation Techniques for Large-Scale Proteomics. *Proteomics* **2017**, *17(1–2),* 1600337. https://doi.org/10.1002/pmic.201600337.

(121) Kachuk, C.; Stephen, K.; Doucette, A. Comparison of Sodium Dodecyl Sulfate Depletion Techniques for Proteome Analysis by Mass Spectrometry. *Journal of Chromatography A* **2015**, *1418*, 158–166. https://doi.org/10.1016/j.chroma.2015.09.042.

(122) Tubaon, R. M.; Haddad, P. R.; Quirino, J. P. Sample Clean-up Strategies for ESI Mass Spectrometry Applications in Bottom-up Proteomics: Trends from 2012 to 2016. *Proteomics* **2017**, *17(20),* 1–8. https://doi.org/10.1002/pmic.201700011.

(123) Žilionis, A. Removal of Sodium Dodecyl Sulfate from Protein Samples. *Chemija* **2018**, *29(4),* 199–208. DOI: https://doi.org/10.6001/chemija.v29i4.3835

(124) Kawasaki, H.; Suzuki, K. Separation of Peptides Dissolved in a Sodium Dodecyl Sulfate Solution by Reversed-Phase Liquid Chromatography: Removal of Sodium Dodecyl Sulfate from Peptides Using an Lon-Exchange Precolumn. *Analytical Biochemistry* **1990**, *186(2),* 264–268. https://doi.org/10.1016/0003-2697(90)90077-M.

(125) Zhu, Z.; Chen, H.; Ren, J.; Lu, J. J.; Gu, C.; Lynch, K. B.; Wu, S.; Wang, Z.; Cao, C.; Liu, S. Two-Dimensional Chromatographic Analysis Using Three Second-Dimension Columns for Continuous Comprehensive Analysis of Intact Proteins. *Talanta* **2018**, *179*, 588–593. https://doi.org/10.1016/j.talanta.2017.11.060.

(126) Swiderek, K. M.; Klein, M. L.; Hefta, S. A.; Shively, J. E. Strategies for the Removal of Ionic and Non-Ionic Detergents from Protein and Peptide Mixtures for on- and off-Line Liquid Chromatography Mass Spectrometry (LCMS). *Techniques in Protein Chemistry* **1995**, *6* (C), 267–275. https://doi.org/10.1016/S1080-8914(06)80034-7.

(127) Berridge, G.; Chalk, R.; D'Avanzo, N.; Dong, L.; Doyle, D.; Kim, J. I.; Xia, X.; Burgess-Brown, N.; Deriso, A.; Carpenter, E. P.; Gileadi, O. High-Performance Liquid Chromatography Separation and Intact Mass Analysis of Detergent-Solubilized Integral Membrane Proteins. *Analytical Biochemistry* **2011**, *410(2),* 272–280. https://doi.org/10.1016/j.ab.2010.11.008.

(128) Jenö, P.; Scherer, P. E.; Manning-Krieg, U.; Horst, M. Desalting Electroeluted Proteins with Hydrophilic Interaction Chromatography. *Analytical Biochemistry* **1993**, *215(2),* 292–298. https://doi.org/10.1006/abio.1993.1589.

(129) Boersema, P. J.; Mohammed, S.; Heck, A. J. R. Hydrophilic Interaction Liquid Chromatography (HILIC) in Proteomics. *Analytical and Bioanalytical Chemistry* **2008**, *391(1),* 151–159. https://doi.org/10.1007/s00216-008-1865-7.

(130) Bensaddek, D.; Nicolas, A.; Lamond, A. I. Evaluating the Use of HILIC in Large-Scale, Multi Dimensional Proteomics: Horses for Courses? *International Journal of Mass Spectrometry* **2015**, *391*, 105–114. https://doi.org/10.1016/j.ijms.2015.07.029

(131) Serra, A.; Gallart-Palau, X.; Dutta, B.; Sze, S. K. Online Removal of Sodium Dodecyl Sulfate via Weak Cation Exchange in Liquid Chromatography-Mass Spectrometry Based Proteomics. *Journal of Proteome Research* **2018**, *17(7),* 2390–2400. https://doi.org/10.1021/acs.jproteome.8b00156.

(132) Antharavally, B. S.; Mallia, K. A.; Rosenblatt, M. M.; Salunkhe, A. M.; Rogers, J. C.; Haney, P.; Haghdoost, N. Efficient Removal of Detergents from Proteins and Peptides in a Spin Column Format. *Analytical Biochemistry* **2011**, *416(1),* 39–44. https://doi.org/10.1016/j.ab.2011.05.013.

(133) Ilavenil, S.; Al-Dhabi, N. A.; Srigopalram, S.; Kim, Y. O.; Agastian, P.; Baaru, R.; Choi, K. C.; Arasu, M. V.; Park, C. G.; Park, K. H. Removal of SDS from Biological Protein Digests for Proteomic Analysis by Mass Spectrometry. *Proteome Science* **2016**, *14(1),* 1–6. https://doi.org/10.1186/s12953-016-0098-5.

(134) Shami, S.; Dash, R. R.; Verma, A. K.; Dash, A. K.; Pradhan, A. Adsorptive Removal of Surfactant Using Dolochar: A Kinetic and Statistical Modeling Approach. *Water Environment Research* **2020**, *92(2),* 222–235. https://doi.org/10.1002/wer.1193.

(135) Palanirajan, S. K.; Govindasamy, P.; Gummadi, S. N. Polystyrene Adsorbents: Rapid and Efficient Surrogate for Dialysis in Membrane Protein Purification. *Scientific Reports* **2020**, *10(1),* 16334. https://doi.org/10.1038/s41598-020-73522-1.

(136) Brown, W.; Zhao, J. Adsorption of Sodium Dodecyl Sulfate on Polystyrene Latex Particles Using Dynamic Light Scattering and Zeta Potential Measurements. *Macromolecules* **1993**, *26(11),* 2711–2715. https://doi.org/10.1021/ma00063a012.

(137) Quirino, J. P. Sodium Dodecyl Sulfate Removal during Electrospray Ionization Using Cyclodextrins as Simple Sample Solution Additive for Improved Mass Spectrometric Detection of Peptides. *Analytica Chimica Acta* **2018**, *1005*, 54–60. https://doi.org/10.1016/j.aca.2017.12.012.

(138) Tuszynski, G. P.; Warren, L. Removal of Sodium Dodecyl Sulfate from Proteins. *Analytical Biochemistry* **1975**, *67(1),* 55–65. https://doi.org/10.1016/0003-2697(75)90271-7.

(139) Wiśniewski, J. R.; Zougman, A.; Nagaraj, N.; Mann, M. Universal Sample Preparation Method for Proteome Analysis. *Nature Methods* **2009**, *6(5),* 359–362. https://doi.org/10.1038/nmeth.1322.

(140) Wiśniewski, J. R. Filter Aided Sample Preparation – A Tutorial. *Analytica Chimica Acta* **2019**, *1090*, 23–30. https://doi.org/10.1016/j.aca.2019.08.032.

(141) Wiśniewski, J. R. Filter-Aided Sample Preparation: The Versatile and Efficient Method for Proteomic Analysis. In *Methods in Enzymology*, **2017**, *585*, 15–27. https://doi.org/10.1016/bs.mie.2016.09.013.

(142) Hughes, C. S.; Moggridge, S.; Müller, T.; Sorensen, P. H.; Morin, G. B.; Krijgsveld, J. Single-Pot, Solid-Phase-Enhanced Sample Preparation for Proteomics Experiments. *Nature Protocols* **2019**, *14(1),* 68–85. https://doi.org/10.1038/s41596-018-0082-x.

(143) Mikulášek, K.; Konečná, H.; Potěšil, D.; Holánková, R.; Havliš, J.; Zdráhal, Z. SP3 Protocol for Proteomic Plant Sample Preparation Prior LC-MS/MS. *Frontiers in Plant Science* **2021**, *12*, 635550. https://doi.org/10.3389/fpls.2021.635550.

(144) Dagley, L. F.; Infusini, G.; Larsen, R. H.; Sandow, J. J.; Webb, A. I. Universal Solid-Phase Protein Preparation (USP3) for Bottom-up and Top-down Proteomics. *Journal of Proteome Research* **2019**, *18(7),* 2915–2924. https://doi.org/10.1021/acs.jproteome.9b00217.

(145) Zougman, A.; Selby, P. J.; Banks, R. E. Suspension Trapping (STrap) Sample Preparation Method for Bottom-up Proteomics Analysis. *Proteomics* **2014**, *14(9),* 1006–1000. https://doi.org/10.1002/PMIC.201300553.

(146) Carraro, U.; Rizzi, C.; Sandri, M. Effective Recovery by KCl Precipitation of Highly Diluted Muscle Proteins Solubilized with Sodium Dodecyl Sulfate. *Electrophoresis* **1991**, *12(12),* 1005–1010. https://doi.org/10.1002/elps.1150121203.

(147) Zhou, J. Y.; Dann, G. P.; Shi, T.; Wang, L.; Gao, X.; Su, D.; Nicora, C. D.; Shukla, A. K.; Moore, R. J.; Liu, T.; Camp, D. G.; Smith, R. D.; Qian, W. J. Simple Sodium Dodecyl Sulfate-Assisted Sample Preparation Method for LC-MS-Based Proteomics Applications. *Analytical Chemistry* **2012**, *84(6),* 2862–2867. https://doi.org/10.1021/ac203394r.

(148) Sandri, M.; Rizzi, C.; Catani, C.; Carraro, U. Selective Removal of Free Dodecyl Sulfate from 2-Mercaptoethanol-SDS-Solubilized Proteins before KDS-Protein

Precipitation. *Analytical Biochemistry* **1993**, *213* (1), 34–39. https://doi.org/10.1006/abio.1993.1382.

(149) Santa, C.; Anjo, S. I.; Manadas, B. Protein Precipitation of Diluted Samples in SDS-Containing Buffer with Acetone Leads to Higher Protein Recovery and Reproducibility in Comparison with TCA/Acetone Approach. *Proteomics* **2016**, *16(13),* 1847–1851. https://doi.org/10.1002/pmic.201600024.

(150) Jiang, L.; He, L.; Fountoulakis, M. Comparison of Protein Precipitation Methods for Sample Preparation Prior to Proteomic Analysis. *Journal of Chromatography A* **2004**, *1023(2),* 317–320. https://doi.org/10.1016/j.chroma.2003.10.029.

(151) Fic, E.; Kedracka-Krok, S.; Jankowska, U.; Pirog, A.; Dziedzicka-Wasylewska, M. Comparison of Protein Precipitation Methods for Various Rat Brain Structures Prior to Proteomic Analysis. *Electrophoresis* **2010**, *31(21),* 3573–3579. https://doi.org/10.1002/elps.201000197.

(152) Doucette, A.; Crowell, A. Precipitation of Detergent-Containing Samples for Top-Down and Bottom-Up Proteomics. *Proteomics Technologies and Applications* **2019**. https://doi.org/10.5772/intechopen.85547.

(153) Crowell, A.; Wall, M.; Doucette, A. Maximizing Recovery of Water-Soluble Proteins through Acetone Precipitation. *Analytica Chimica Acta* **2013**, *796*, 48–54. https://doi.org/10.1016/J.ACA.2013.08.005.

(154) Crowell, A. M. J.; MacLellan, D. L.; Doucette, A. A. A Two-Stage Spin Cartridge for Integrated Protein Precipitation, Digestion and SDS Removal in a Comparative Bottom-up Proteomics Workflow. *Journal of Proteomics* **2015**, *118*, 140–150. https://doi.org/10.1016/j.jprot.2014.09.030.

(155) Shevchenko, A.; Tomas, H.; Havliš, J.; Olsen, J. V.; Mann, M. In-Gel Digestion for Mass Spectrometric Characterization of Proteins and Proteomes. *Nature Protocols* **2007**, *1(6),* 2856–2860. https://doi.org/10.1038/nprot.2006.468.

(156) Quirino, J. P. Electrokinetic Removal of Charged Species from Small Sample Volumes. *Journal of Chromatography A* **2013**, *1299*, 131–135. https://doi.org/10.1016/j.chroma.2013.05.055.

(157) Tubaon, R. M.; Haddad, P. R.; Quirino, J. P. Membrane-Free Electrokinetic Device Integrated to Electrospray-Ionization Mass Spectrometry for the Simultaneous Removal of Sodium Dodecyl Sulfate and Enrichment of Peptides. *Analytical Chemistry* **2018**, *90(17),* 10122–10127. https://doi.org/10.1021/acs.analchem.8b01707.

(158) Pandigamage, P.; Wilson, R.; Quirino, J. P. A Simple Apparatus for Electrokinetic Removal of Sodium Dodecyl Sulfate from Protein Digests. *Journal of*

Chromatography A **2020**, *1628,* 1-19. https://doi.org/10.1016/j.chroma.2020.461443.

(159) Kachuk, C.; Faulkner, M.; Liu, F.; Doucette, A. A. Automated SDS Depletion for Mass Spectrometry of Intact Membrane Proteins Though Transmembrane Electrophoresis. *Journal of Proteome Research* **2016**, *15(8),* 2634–2642. https://doi.org/10.1021/acs.jproteome.6b00199.

(160) Unterlander, N.; Doucette, A. A. Accelerated SDS Depletion from Proteins by Transmembrane Electrophoresis: Impacts of Joule Heating. *Electrophoresis* **2018**, *39(11),* 1349–1356. https://doi.org/10.1002/elps.201700410.

(161) Unterlander, N.; Doucette, A. A. Membrane-Based SDS Depletion Ahead of Peptide and Protein Analysis by Mass Spectrometry. *Proteomics* **2018**, *18(9),* 1–8. https://doi.org/10.1002/pmic.201700025.

(162) Xixi, E.; Dimitraki, P.; Vougas, K.; Kossida, S.; Lubec, G.; Fountoulakis, M. Proteomic Analysis of the Mouse Brain Following Protein Enrichment by Preparative Electrophoresis. *Electrophoresis* **2006**, *27(7),* 1424–1431. https://doi.org/10.1002/elps.200500562.

(163) Pottiez, G.; Deracinois, B.; Duban-Deweer, S.; Cecchelli, R.; Fenart, L.; Karamanos, Y.; Flahaut, C. A Large-Scale Electrophoresis- and Chromatography-Based Determination of Gene Expression Profiles in Bovine Brain Capillary Endothelial Cells after the Re-Induction of Blood-Brain Barrier Properties. *Proteome Science* **2010**, *8(57),* 1–11. https://doi.org/10.1186/1477-5956-8-57.

(164) Hao, F.; Li, J.; Zhai, R.; Jiao, F.; Zhang, Y.; Qian, X. A Novel Microscale Preparative Gel Electrophoresis System. *Analyst* **2016**, *141(16),* 4953–4960. https://doi.org/10.1039/c6an00780e.

(165) Jenkins, M. A. Clinical Applications of Capillary Electrophoresis: Status at the New Millennium. *Molecular Biotechnology* **2000**, *15(3),* 201–209. https://doi.org/10.1385/mb:15:3:201.

(166) Lin, C.-Y.; Lee, C.-H.; Chuang, Y.-H.; Lee, J.-Y.; Chiu, Y.-Y.; Wu Lee, Y.-H.; Jong, Y.-J.; Hwang, J.-K.; Huang, S.-H.; Chen, L.-C.; Wu, C.-H.; Tu, S.-H.; Ho, Y.-S.; Yang, J.-M. Membrane Protein-Regulated Networks across Human Cancers. *Nature Communications 10,* **2019**, *10(1),* 1–17. https://doi.org/10.1038/s41467-019-10920-8.

(167) Kai, F.; Drain, A. P.; Weaver, V. M. The Extracellular Matrix Modulates the Metastatic Journey. *Developmental Cell* **2019**, *49*(3), 332-346. https://doi.org/10.1016/J.DEVCEL.2019.03.026.

(168) Zhao, J. Q.; Sun, F. J.; Liu, S. S.; Yang, J.; Wu, Y. Q.; Li, G. S.; Chen, Q. Y.; Wang, J. X. Expression of Connexin 43 and E-Cadherin Protein and MRNA in Non-Small Cell Lung Cancers in Chinese Patients. *Asian Pacific Journal of Cancer Prevention* **2013**, *14(2),* 639–643. https://doi.org/10.7314/APJCP.2013.14.2.639.

(169) Samaeekia, R.; Adorno-Cruz, V.; Bockhorn, J.; Chang, Y. F.; Huang, S.; Prat, A.; Ha, N.; Kibria, G.; Huo, D.; Zheng, H.; Dalton, R.; Wang, Y.; Moskalenko, G. Y.; Liu, H. MiR-206 Inhibits Stemness and Metastasis of Breast Cancer by Targeting MKL1/IL11 Pathway. *Clinical Cancer Research* **2017**, *23(4),* 1091–1103. https://doi.org/10.1158/1078-0432.CCR-16-0943.

(170) Kong, Y.; Qiao, Z.; Ren, Y.; Genchev, G. Z.; Ge, M.; Xiao, H.; Zhao, H.; Lu, H. Integrative Analysis of Membrane Proteome and MicroRNA Reveals Novel Lung Cancer Metastasis Biomarkers. *Frontiers in Genetics* **2020**, *11*, 1023. https://doi.org/10.3389/FGENE.2020.01023.

(171) Du, H.; Chen, Y.; Hou, X.; Huang, Y.; Wei, X.; Yu, X.; Feng, S.; Wu, Y.; Zhan, M.; Shi, X.; Lin, S.; Lu, L.; Yuan, S.; Sun, L. PLOD2 Regulated by Transcription Factor FOXA1 Promotes Metastasis in NSCLC. *Cell Death & Disease* **2017**, *8(10),* e3143–e3143. https://doi.org/10.1038/cddis.2017.553.

(172) Unterlander, N.; Doucette, A. A. Membrane-Based SDS Depletion Ahead of Peptide and Protein Analysis by Mass Spectrometry. *Proteomics* **2018**, *18(9),* 1700025. https://doi.org/10.1002/pmic.20170002

(173) Haider, S. R.; Sharp, B. L.; Reid, H. J. A Comparison of Tris-Glycine and Tris-Tricine Buffers for the Electrophoretic Separation of Major Serum Proteins. *Journal of Separation Science* **2011**, *34(18),* 2463–2467. https://doi.org/10.1002/jssc.201100315.

(174) Dennison, C. *A Guide to Protein Isolation*; Kluwer Academic Publishers: PIetermaritszburg, South Africa, **2002**. https://doi.org/10.1007/0-306-46868-9.

(175) Malva, A. della; Albenzio, M.; Santillo, A.; Russo, D.; Figliola, L.; Caroprese, M.; Marino, R.; Díaz-Cruz, J. M. Methods for Extraction of Muscle Proteins from Meat and Fish Using Denaturing and Nondenaturing Solutions. *Journal of Food Quality* **2018**, 1–9. https://doi.org/10.1155/2018/8478471.

(176) George, A. L.; White, G. F. Optimization of the Methylene Blue Assay for Anionic Surfactants Added to Estuarine and Marine Water. *Environmental Toxicology and Chemistry* **1999**, *18(10),* 2232–2236. https://doi.org/10.1002/etc.5620181016.

(177) Arand, M.; Friedberg, T.; Oesch, F. Colorimetric Quantitation of Trace Amounts of Sodium Lauryl Sulfate in the Presence of Nucleic Acids and Proteins.

Analytical Biochemistry **1992**, *207(1),* 73–75. https://doi.org/10.1016/0003-2697(92)90502-X.

(178) Smith, P. K.; Krohn, R. I.; Hermanson, G. T.; Mallia, A. K.; Gartner, F. H.; Provenzano, M. D.; Fujimoto, E. K.; Goeke, N. M.; Olson, B. J.; Klenk, D. C. Measurement of Protein Using Bicinchoninic Acid. *Analytical Biochemistry* **1985**, *150(1),* 76–85. https://doi.org/10.1016/0003-2697(85)90442-7.

(179) Bainor, A.; Chang, L.; McQuade, T. J.; Webb, B.; Gestwicki, J. E. Bicinchoninic Acid (BCA) Assay in Low Volume. *Analytical Biochemistry* **2011**, *410(2),* 310–312. https://doi.org/10.1016/j.ab.2010.11.015.

(180) Richards, A. L.; Hebert, A. S.; Ulbrich, A.; Bailey, D. J.; Coughlin, E. E.; Westphall, M. S.; Coon, J. J. One-Hour Proteome Analysis in Yeast. *Nature Protocols* **2015**, *10(5),* 701–714. https://doi.org/10.1038/nprot.2015.040.

(181) Shevchenko, A.; Wilm, M.; Vorm, O.; Mann, M. Mass Spectrometric Sequencing of Proteins from Silver-Stained Polyacrylamide Gels. *Analytical Chemistry* **1996**, *68(5),* 850–858. https://doi.org/10.1021/ac950914h.

(182) Orton, D. J.; Doucette, A. A. A Universal, High Recovery Assay for Protein Quantitation through Temperature Programmed Liquid Chromatography (TPLC). *Journal of Chromatography B* **2013**, *921–922*, 75–80. https://doi.org/10.1016/j.jchromb.2013.01.021.

(183) Chevallet, M.; Luche, S.; Rabilloud, T. Silver Staining of Proteins in Polyacrylamide Gels. *Nature Protocols* **2006**, *1(4),* 1852–1858. https://doi.org/10.1038/nprot.2006.288.

(184) Steinberg, T. H. Protein Gel Staining Methods. An Introduction and Overview. In *Methods in Enzymology*; Burgess, Richard R., Deutscher, M. P., Ed.; Elsevier Inc., **2009**; *463*, 541–563. https://doi.org/10.1016/S0076-6879(09)63031-7.

(185) Tran, J. C.; Doucette, A. A. Gel-Eluted Liquid Fraction Entrapment Electrophoresis: An Electrophoretic Method for Broad Molecular Weight Range Proteome Separation. *Analytical Chemistry* **2008**, *80(5),* 1568–1573. https://doi.org/10.1021/ac702197w.

(186) Kachuk, C.; Stephen, K.; Doucette, A. Comparison of Sodium Dodecyl Sulfate Depletion Techniques for Proteome Analysis by Mass Spectrometry. *Journal of Chromatography A* **2015**, *1418*, 158–166. https://doi.org/10.1016/j.chroma.2015.09.042.

(187) Oliveros, J. C. Venny. An interactive tool for comparing lists with Venn's diagrams. https://bioinfogp.cnb.csic.es/tools/venny/ (accessed 2021 -07 -10).

(188) Jakubec, P. J.; Doucette, A. A. Automated Electrokinetic Platform for High-Throughput Sodium Dodecyl Sulfate Depletion Ahead of Proteome Analysis by Mass Spectrometry. *Analytical Chemistry* **2021**, *93* (42), 14042–14047. https://doi.org/10.1021/ACS.ANALCHEM.1C03549.

(189) Laemmli, U. K. Cleavage of Structural Proteins During the Assembly of the Head of Bacteriophage T4. *Nature* **1970**, *227(5259),* 680–685. https://doi.org/10.1038/227680a0.

(190) Schägger, H.; von Jagow, G. Tricine-Sodium Dodecyl Sulfate-Polyacrylamide Gel Electrophoresis for the Separation of Proteins in the Range from 1 to 100 KDa. *Analytical Biochemistry* **1987**, *166(2),* 368–379. https://doi.org/10.1016/0003-2697(87)90587-2.

(191) Schägger, H. Tricine-SDS-PAGE. *Nature Protocols* **2006**, *1(1),* 16–22. https://doi.org/10.1038/nprot.2006.4.

(192) Kachuk, C.; Faulkner, M.; Liu, F.; Doucette, A. A. Automated SDS Depletion for Mass Spectrometry of Intact Membrane Proteins Though Transmembrane Electrophoresis. *Journal of Proteome Research* **2016**, *15(8),* 2634–2642. https://doi.org/10.1021/acs.jproteome.6b00199.

(193) Borzova, V. A.; Markossian, K. A.; Chebotareva, N. A.; Kleymenov, S. Yu.; Poliansky, N. B.; Muranov, K. O.; Stein-Margolina, V. A.; Shubin, V. V.; Markov, D. I.; Kurganov, B. I. Kinetics of Thermal Denaturation and Aggregation of Bovine Serum Albumin. *Plos One* **2016**, *11(4),* e0153495. https://doi.org/10.1371/journal.pone.0153495.

(194) Kishore, D.; Kundu, S.; Kayastha, A. M. Thermal, Chemical and PH Induced Denaturation of a Multimeric β-Galactosidase Reveals Multiple Unfolding Pathways. *Plos One* **2012**, *7(11),* e50380. https://doi.org/10.1371/JOURNAL.PONE.0050380.

(195) Rawlings, A. E. Membrane Proteins: Always an Insoluble Problem? *Biochemical Society Transactions* **2016**, *44(3),* 790–795. https://doi.org/10.1042/BST20160025.

(196) Choksawangkarn, W.; Edwards, N.; Wang, Y.; Gutierrez, P.; Fenselau, C. A Comparative Study of Workflows Optimized for In-Gel, In-Solution and On-Filter Proteolysis in the Analysis of Plasma Membrane Proteins. *Journal of Proteome Research* **2012**, *11(5),* 3030. https://doi.org/10.1021/PR300188B.

(197) Plucinsky, S. M.; Root, K. T.; Glover, K. J. Efficient Solubilization and Purification of Highly Insoluble Membrane Proteins Expressed as Inclusion Bodies Using Perfluorooctanoic Acid. *Protein Expression and Purification* **2018**, *143*, 34–37. https://doi.org/10.1016/J.PEP.2017.10.012.

(198) Ma, J.; Hou, C.; Sun, L.; Tao, D.; Zhang, Y.; Shan, Y.; Liang, Z.; Zhang, L.; Yang, L.; Zhang, Y. Coupling Formic Acid Assisted Solubilization and Online Immobilized Pepsin Digestion with Strong Cation Exchange and Microflow Reversed-Phase Liquid Chromatography with Electrospray Ionization Tandem Mass Spectrometry for Integral Membrane Proteome Analys. *Analytical Chemistry* **2010**, *82(23),* 9622–9625. https://doi.org/10.1021/AC1023099.

(199) Rondeau, P.; Navarra, G.; Cacciabaudo, F.; Leone, M.; Bourdon, E.; Militello, V. Thermal Aggregation of Glycated Bovine Serum Albumin. *Biochimica et Biophysica Acta - Proteins and Proteomics* **2010**, *1804(4),* 789–798. https://doi.org/10.1016/j.bbapap.2009.12.003.

(200) Palmblad, M. Theoretical Considerations for Next-Generation Proteomics. *Journal of Proteome Research* **2021**, *20*, 3395–3399. https://doi.org/10.1021/acs.jproteome.1c00136.

(201) Timp, W.; Timp, G. Beyond Mass Spectrometry, the Next Step in Proteomics. *Science Advances* **2020**, *6*(2). https://doi.org/10.1126/sciadv.aax8978.

(202) Jones, R. G. A.; Landon, J. A Protocol for 'Enhanced Pepsin Digestion': A Step by Step Method for Obtaining Pure Antibody Fragments in High Yield from Serum. *Journal of Immunological Methods* **2003**, *275(1–2),* 239–250. https://doi.org/10.1016/S0022-1759(03)00005-X.

Appendices

File S1: Complete list, saved as XLSX format, of proteins identified from *S. cerevisiae* membrane-enriched proteome from AC-TME supernatant collected sample.

File S2: Complete list, saved as XLSX format, of proteins identified from *S. cerevisiae* membrane-enriched proteome from AC-TME residual pellet collected sample.

File S3: Complete list, saved as XLSX format, of proteins identified from *S. cerevisiae* membrane-enriched proteome from uncooled TME supernatant collected sample.

File S4: Complete list, saved as XLSX format, of proteins identified from *S. cerevisiae* membrane-enriched proteome from uncooled TME residual pellet collected sample.